U.PORTO

UNIVERSIDADE DO PORTO

2.º CICLO

FCUP
2014

M 2014

U.PORTO

Spatial analysis applied to the Barroso-Alvão rare-elements pegmatite field (Northern Portugal)

DAVID BARBOSA DA SILVA

U.PORTO

FACULDADE DE CIÊNCIAS
UNIVERSIDADE DO PORTO

Spatial analysis applied to the Barroso-Alvão rare-elements pegmatite field (Northern Portugal)

DAVID BARBOSA DA SILVA

DISSERTAÇÃO DE MESTRADO APRESENTADA
À FACULDADE DE CIÊNCIAS DA UNIVERSIDADE DO PORTO
PARA OBTENÇÃO DO GRAU DE MESTRE EM GEOLOGIA

U.PORTO

FACULDADE DE CIÊNCIAS
UNIVERSIDADE DO PORTO

Spatial analysis applied to the Barroso-Alvão rare-elements pegmatite field (Northern Portugal)

DAVID BARBOSA DA SILVA

Mestrado em Geologia
Departamento de Geociências, Ambiente e Ordenamento do Território
2014

ORIENTADOR
Alexandre Martins Campos de Lima
Faculdade de Ciências da Universidade do Porto

Todas as correcções determinadas pelo júri, e só essas, foram efectuadas.

O Presidente do Júri,

Porto, _____ /_____ /_____

AGRADECIMENTOS / ACKNOWLEDGMENTS

Terminada esta importante etapa da minha vida académica, gostaria de aproveitar para agradecer a todos aqueles que contribuíram e me acompanharam nesta aventura.

Agradeço ao Doutor Alexandre Lima por ter aceite a orientação desta dissertação, pelo apoio e interesse demonstrado ao longo de todo o processo de investigação, mesmo nos momentos em que milhares de quilômetros interferiam nesta dinâmica de trabalho.

I would like to express my gratitude to Eric Gloaguen, Sarah Deveaud, Laurent Guillou-Frottier and Jérémie Melleton from the Bureau de Recherches Géologiques et Minières, and Charles Gumiaux from Orléans University for their scientific mentoring and the good moments lived in Orléans during my internship at BRGM.

Gostaria de agradecer a todos os meus amigos pelos inúmeros momentos de descontração e boa disposição, e sem os quais este trabalho teria sido terminado bem mais rapidamente.

Por ultimo, quero agradecer aos meus pais por todo o apoio fornecido, e sem os quais a realização desta dissertação e de todo o meu percurso académico não teria sido possível.

ABSTRACT

In this study, statistical spatial analyses were performed for the LCT-type pegmatites belonging to the Barroso-Alvão aplitopegmatitic field (Northern Portugal), to highlight any possible relationship, or lack of it, between the pegmatites and the surrounding granitic plutons, faults or schistose foliations. Distance to nearest neighbors, Ripley´s L´-function and pegmatites orientations families were employed to study the spatial distribution pattern of the LCT-pegmatites, whereas Euclidean distance and Kernel density distributions aimed the spatial association between these same pegmatites to the various geological features within the study area. The results show that the pegmatites spatial distribution follows clearly a clustering pattern, presenting the Li-enriched pegmatites a higher rate and extent compared to the total pegmatites, as well as a spatial association with high pegmatites density. Three families of pegmatites orientation were obtained: i) A family from N0º to N63º (max at N24º); ii) B family from N64º to N113º (max at N92º), and iii) C family from N114º to N179º (max at N156º). No statistically significant spatial relationship were observed for the total pegmatites or Li-enriched relatively to the Cabeceiras de Basto and Barroso granitic plutons, moreover the Li-enriched pegmatites showed an inverted distance fractionation from the two granites and overlapped distribution of the spodumene, petalite and lepidolite-enriched pegmatites. The total pegmatites and, in a higher grade, the Li-enriched pegmatites showed a preferential association with fault-strikes densities compared to the moderate pegmatite relationship observed concerning the distance to faults-strikes. Computed modeling of regional schistosity highlighted a regime of deformation within the study area, suggesting the presence of corridors of dextral deformation with NW to NNW orientations. Altogether, these results suggests that the pegmatites spatial emplacement followed dextral shear-zones, interpreted using ASTER imagery. These shear zones and associated corridors of deformation probably created channel-ways within the metasedimentary units that permitted the ascent and emplacement, following the Riedel model of fracturation, of the pegmatitic melts precursor of the pegmatites bodies.

RESUMO

Neste estudo, analises estatísticas espaciais foram aplicadas em pegmatitos do tipo LCT localizados no campo aplitopegmatítico do Barroso-Alvão (Norte Portugal), no intuito de sobressair possíveis relações espaciais entre os pegmatitos e os plutões graníticos, falhas ou foliações metasedimentares envolventes. Análises de distância ao vizinho mais próximo, função-L´de Ripley e famílias de orientações de pegmatitos foram utilizados com o objetivo de estudar os padrões de distribuição espacial dos pegmatitos, ao passo que análises de distância Euclidiana e distribuição de densidade Kernel visaram compreender a associação espacial entre os pegmatitos e as supracitadas estruturas geológicas. Os resultados evidenciaram que a distribuição espacial dos pegmatitos segue claramente um padrão de aglomeração, apresentando os pegmatitos enriquecidos em Li uma maior extensão e taxa de aglomeração comparada com a totalidade dos pegmatitos, bem como uma associação espacial com altas densidades de pegmatitos. Foram obtidas três famílias de orientação de pegmatitos: i) família A desde N0º até N63º (max em N24º); ii) família B desde N64º até N113º (max N92º); iii) família C desde N114º até N179º (max N156º). Análises de distância Euclidiana demonstraram não existir qualquer relação espacial estatisticamente relevante entre os pegmatitos na sua totalidade ou enriquecidos em Li e os plutões graníticos envolventes de Cabeceiras de Basto e do Barroso. Além disso, os pegmatitos enriquecidos em Li evidenciaram na maioria dos casos um fracionamento espacial invertido a partir dos dois plutões graníticos, bem como uma distribuição parcialmente sobreposta dos pegmatitos enriquecidos em espodumena, petalite e lepidolite. A totalidade dos pegmatitos, bem como dos pegmatitos enriquecidos em Li, estes últimos em maior grau, apresentam uma associação preferencial com densidades de falhas, comparado com as relações moderadas observadas relativamente à distância às falhas. Modelações computadorizadas da xistosidade regional permitiram por em evidência um regime de deformação presente na área de estudo, sugerindo a presença de corredores de deformação de rotação destra com orientações compreendidas entre NW até NNW. Estes resultados sugerem que a instalação dos pegmatitos no terreno foi possível através da utilização de zonas de cisalhamento dextrogiros, interpretados utilizando imagens de satélite ASTER. Estas zonas de cisalhamento, e corredores de deformação associados, criaram provavelmente canais de ascensão magmática nos terrenos metasedimentares que permitiram a instalação, seguindo o modelo de fraturação de Riedel, de magma especializado precursor dos corpos pegmatíticos.

LIST OF FIGURES

LIST OF TABLES

TABLE OF CONTENTS

INTRODUCTION

INTRODUCTION

Granitic pegmatites rich in rare elements are currently recognized for their concentration and diversity in ore minerals, both in metallic and industrial minerals (Glover et al., 2012; Linnen et al., 2012). The importance of pegmatites in our actual society, regarding to the provision in certain types of elements [e.g. tantalum (Ta), niobium (Nb) and lithium (Li)], was recognized by the European Union (EU), identifying these elements as "Critical raw materials" or "Strategic resources", in part because of the risk of provision or their economic and/or military importance for some European countries. As an example, one of the issues that triggered the necessity to develop a working group for defining critical materials inside the EU was the difficulty to obtain rare earths elements (REE) for industries when China applied export restrictions and quota for these elements. The importance of the quotas applied by China, which accounted for 97% of the world production of REE in 2009, was inflated due to the inexistence of REE production inside EU (EC Critical Raw Materials Report, 2010). Western countries have also put in action measures to fight the dependence for foreign rare-elements supply. One important aspect is the decision of the US government to face the finance of civil war, in particular the interdiction to trade conflicting mineral ores (Columbite-Tantalite or coltan, the colloquial African term, cassiterite, wolframite and gold) from unreliable destinations, like the Democratic Republic of the Congo, with the Dodd-Frank Act signed into law by the US president in 2010 (Drajem et al., 2011).

The most common critical elements found in pegmatites are Li, Ta, Nb, Be, Sn and the aforementioned REE. The rare-elements class pegmatites, which is the most economically important and best studied class to date, is normally enriched with incompatible elements (i.e. High Field Strength and Large Ion Lithophile Elements), in which a large number of them are strategic and critical metals. In recent years, the majority of worldwide provisions in Ta comes from Greenbushes' granitic pegmatites (also the world's largest estimated primary Li resource, with 0.85 Mt) or Tanco, in Canada (world's almost exclusive supplier in Cs, with resources of primary Li estimated in 0.14 Mt; British Geological Survey, 2011; Kesler et al., 2012). The Nb concentrates provision comes from Brazil (92% in 2009) and Chilean brine deposits dominate the Li's market (47% in 2009). These rare elements' use in industrial processes is not very well known by the public in general, but it is of substantial importance in electronic, automobile, aerospatial or traditional industries (EC Critical Raw Materials Report, 2010).

For the Portuguese case, respecting to Li's mineral exploitation in granitic pegmatites, at this moment, the only pegmatites that are in production provide for industrial minerals, used in ceramic and glass industries [approx. 38 000 t in 2011 (Direcção-Geral de Energia e

Geologia, 2014)]. These pegmatites are of small dimension if we compare them with world's major producers, but the geological context of Portugal gives a considerable potential in Li mineralization, associated with pegmatites (Farinha Ramos, 2000; Lima et al., 2011). One of the finest examples of Li's mineral concentration zone in Portugal is the Barroso-Alvão aplitopegmatitic field, located in the northwestern portion of the Iberian Peninsula, north of Portugal, in the Trás-os-Montes e Alto Douro region. This portion of Portugal is recognized for its numerous (~2000) outcropping aplitopegmatites (Noronha, 1987; Charoy et al., 1992, 2001; Lima, 2000; Lima et al., 2003a,b,c; Martins, 2009; Martins et al., 2011, 2012), hundreds of them mineralized in Sn and Li, giving the Barroso-Alvão aplitopegmatitic field a considerable potential for extraction of Li mineral associated with pegmatites.

The purpose of this study is based on the premise that pegmatites in the Barroso-Alvão region were not extensively studied, regarding their field scale emplacement or the relationship between pegmatites and surrounding geological structures (fragile/ductile tectonics and granitic lithologies). The previous studies for this area were more focused in a mineralogical and petrographical description of the pegmatites, sometimes containing explanations about the Li mineralized pegmatites' localization and emplacement within the Barroso-Alvão pegmatitic field. The comprehension of the relationship between pegmatites and surrounding geological structures is necessary to better understand some processes regarding the pegmatite's emplacement model, differentiation trends and conception of a genetic model. To achieve these objectives, we apply a spatial statistical analysis using geocomputational techniques, especially the geographic information system (GIS) technology, to the pegmatites in general and, in more focus, to the mineralized ones. The results are posteriorly interpreted and discussed, to elaborate the most accurate genetical model possible for the regional emplacement of Barroso-Alvão pegmatites.

CHAPTER 1

PEGMATITES COMPREHENSION: GENERALITIES

CHAPTER 1 - PEGMATITES COMPREHENSION: GENERALITIES

1. 1. INTRODUCTORY FACTS AND CLASSIFICATION

The definition of the term "pegmatite" was originally proposed by the French mineralogist R. J. Haüy in 1801 (Brongniart, 1813) and refers to an intergrowth of quartz visually similar to ancient cuneiform writings and pertitic microcline called "graphic granite" (Fig. 1). It is because of this complex geometrical fabric that the pegmatites have garnered attention in the primordial years of pegmatite studies. Years later, and until recently, the term was broadened to include very coarse grained granitic segregation that normally tends to be enriched in rare elements (e.g. Jackson, 1997; Clark and Steigeler, 2000), but these definitions failed to address the full spectrum of pegmatitic textures. London (2008) propose the following definition for pegmatites, in an attempt to fully describe them in all their complexity: "an essentially igneous rock, commonly of granitic composition, that is distinguished from other igneous rocks by its extremely coarse but variable grain-size, or by an abundance of crystals with skeletal, graphic, or other strongly directional growth-habits. Pegmatites occur as sharply bounded homogeneous to zoned bodies within igneous or metamorphic host-rocks".

Fig. 1 Macroscopic aspect of graphic granite, an intergrowth of skeletal quartz (gray) in perthitic microcline (beige). (From London, 2008).

It is clear now that the pegmatites have intrigued the scientist since early 19th century with particular attention to the exotic mineralogy. This interest has provided elaboration of early empirical models, at first by Lindgren (1913), linking pegmatites as an evolutionary process from granite to hydrothermal quartz veins. Later, Landes (1933) advocated a magmatic origin for "simples" pegmatites with igneous composition. Inevitably, the need for scientists to classify all the natural creations has also reached the pegmatites community. The early classifications of pegmatites are pronouncedly influenced by classification of granitic

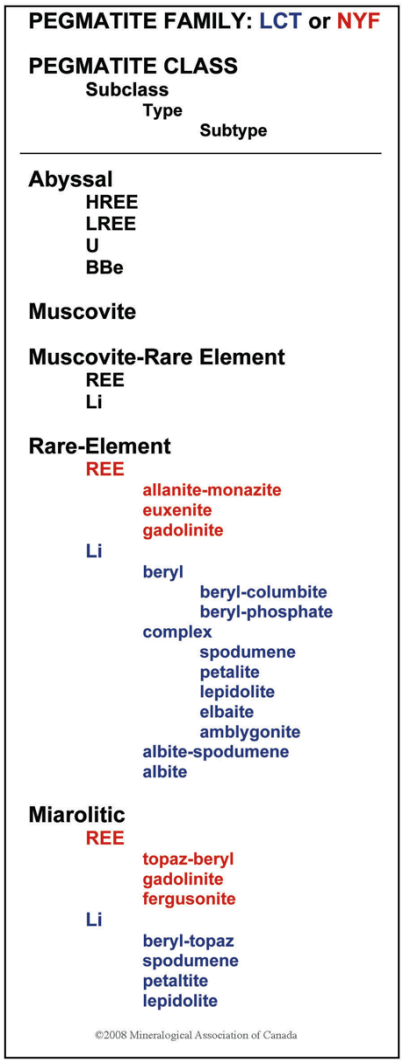

Fig. 2 The pegmatite classification scheme adopted by Černý and Ercit (2005). (From London, 2008).

rocks relatively to their emplacement depth (Buddington, 1959; Ginsburg *et al.*, 1979). Repeated revisions of these contemporaneous classifications, more recently by Petr Černý, culminated in the published paper and classification of Černý and Ercit (2005), which is currently the most used to classify pegmatites (Fig. 2). Their classification is the combination of different criteria's for the pegmatites bodies, which are, depth of emplacement, metamorphic environment, minor element content, and mineralogy. This classification has five main categories or classes: i) abyssal, ii) muscovite, iii) muscovite – rare-element, iv) rare-element, and v) miarolitic pegmatite class. The rare-element class is subdivided according to their composition in **LCT-type** (Lithium, Cesium and Tantalum), mostly needed for Nb-Ta oxides and Li, and **NYF-type** (Niobium, Yttrium and Fluor), a highly important REE provider. These two subclasses are then subdivided in types and subtypes according to their mineralogical and/or geochemical characteristics. Moreover, within this classification, a petrogenetic classification of pegmatites derived from plutons was proposed. This petrological classification is a "family system" of classifying granitic pegmatites of plutonic derivation, linking the LCT family to orogenic peraluminous granitic type protoliths [major S, I or mixed S+I-type; after Chappell and White (1974)], NYF family to anorogenic depleted mantelic granitoides protoliths with a wide range of alumina composition (A and I-types) and a mixed LCT+NYF family essentially subaluminous with a source lithology from mixed protoliths (Černý *et al.*, 2005) However, during the last decade various studies revealed pegmatites and even pegmatites field that do not fit inside the classification presented above. One of the principal problems is that the Černý and Ercit (2005) classification is primarily a depth-zone classification that requires a previous knowledge of pegmatite formation pressure (P) and temperature (T) mixing mineralogy (Muscovite class), geochemistry (Rare-element class) and structural criteria's (Miarolitic class). This diversity of criteria makes the classification slightly confusing. Given that this current pegmatite classification presents some ambiguities, some scientists (*e.g.* Simmons, 2005; Martin and De Vito, 2005) tends to propose alternative new petrogenetic classification related to i) tectonic regimes and ii) associated magma generating processes. These two main considerations are necessary to better understand the pegmatite genesis within the larger-

scale earth processes.

In this study, we do not tackle directly this issue about pegmatite classification, but our approach consists in the understanding of some relation between tectonics features and LCT pegmatites families.

1. 2. UNDERSTANDING FIELD–SCALE PEGMATITES

1. 2. 1. A REGIONAL ZONING CONTINUUM

Various authors (*e.g.* Cameron *et al.*, 1949; Heinrich, 1953; Vlasov, 1961; Trueman and Černý, 1982) observed in similar pegmatites the existence of variation in chemical content with the distance of pegmatites to the melt source. These groups of pegmatites exhibit most often a structural, igneous and geochemical liaison between them. Pegmatite groups constitute the basic component within a population of pegmatites that possess a structural, igneous and geochemical link. The diversity in various attributes that pegmatites are recognized was simply classified by Černý (1991) from a lower to higher scale-order in **pegmatitic fields** (usually not superior to 10000 Km^2), **pegmatitic belts** (various pegmatitic fields linked to a regional linear structure) and **pegmatitic provinces** (sum of pegmatitic belt and field within a single metallogenic province).

Černý (1989, 1991) also proposed a more detailed concept of regional zonation for pegmatites, particularly for the rare-element class with igneous origins (Fig. 3). In this regional zonation, the author proposes a categorization in types and subtypes sequentially more fractionated and distant to the parental pluton: i) barren, ii) beryl type, with beryl-columbite and beryl-columbite-phosphate subtypes, iii) complex type, including spodumene, petalite and amblygonite subtypes, iv) complex type, lepidolite subtype, v) albite-spodumene type, and vi) albite type. With the distal distance to the parental pluton, the pegmatites increase their fractionation, volatile enrichment, complexity of zoning and extent of emplacement. However, the concentric zonation around the parental pluton proposed in the Černý's model is rarely observed, mainly because of the influence of potential pre-intrusive host structures by the exposed erosional level and, to a lesser extent, by the lack of granitic pluton. This model implies the liaison of pegmatites to large igneous bodies with acidic

composition and does not approach in large extent to the anatectic model proposed by some authors (*e.g.* Norton and Redden, 1990; Simmons *et al.*, 1995; Roda-Robles *et al.*, 1999; Simmons and Webber, 2008; Demartis *et al.*, 2011). This issue between magmatic or anatectic origin for the pegmatites is a highly debated theme within the pegmatology community and is discussed below.

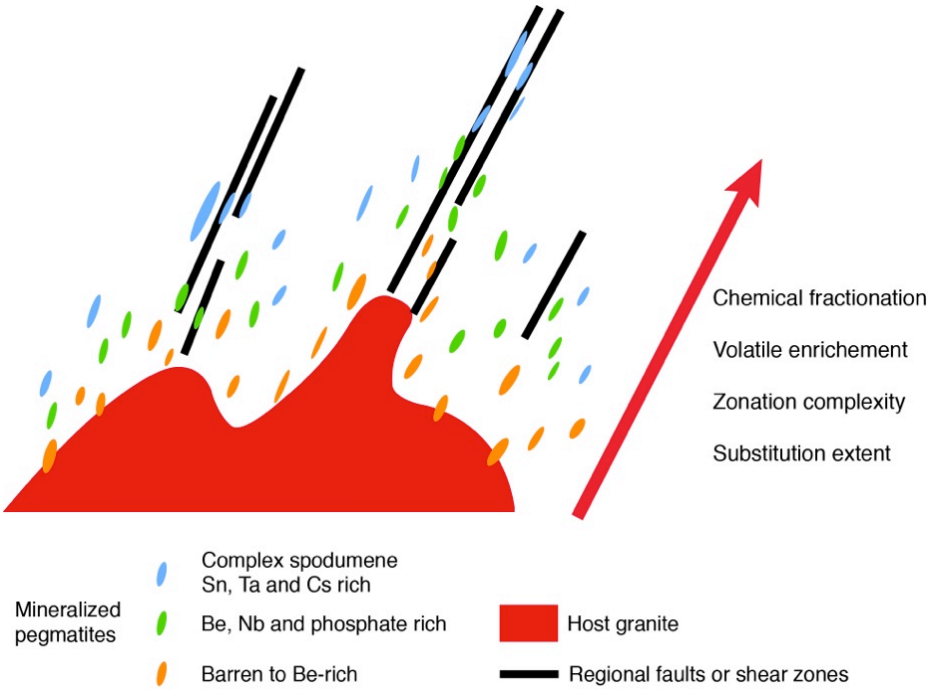

Fig. 3 Schematic representation of a vertical section trough a zoned granite-pegmatite system. (Adapted from Černý, 1989).

1. 2. 2. PETROGENESIS MODELS: GRANITE RELATED, ANATECTIC OR BOTH?

As the title implies, the most popular models for the pegmatites genesis are the granitic parental magma model and the anatectic model. These models usually propose to explain the parental protolith and the most peculiar pegmatites characteristics, which are the presence of exotic minerals side-by-side with common minerals, the grain size variability, internal textural differences and the pegmatites spatial distribution. Until now, none of the models have obtained consensus from the scientific community, but the granitic parental magma model is by far the best studied and the most applied model to date. It is nowadays, practically without any doubt, admitted the relation between pegmatites and granitic melts

source. The granitic parental magma model proposes that the pegmatites are formed by segregation of extremely fractionated residual magma, rich in rare and volatile element from the parental granite. The major arguments for this model are: i) the spatial relationship between pegmatites and the parental pluton, ii) age determination, iii) mineral, geochemical and textural evolution from parental pluton to pegmatites (Černý, 1991). Considering the granitic parental magma model, London (2014) illustrates the P-T path forming environment and emplacement process within an LCT-type pegmatite group (Fig. 4). In this scheme, the pegmatites only emanates from the roof-ward contacts of their source granite, since volatile and rare-elements are concentrated in the upper part of the granitic cupola. The regional zonation is in concordance with the aforementioned model of Černý (1989).

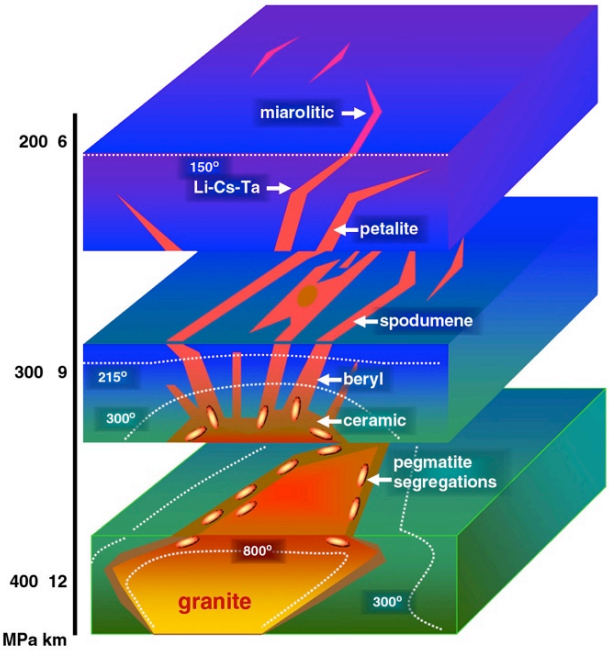

Fig. 4 P-T forming environment and emplacement processes within a pegmatite group of the LCT family for the magmatic model. (From London, 2014).

Unlike the granitic parental magma model, the anatectic model propose that it may be possible to form a pegmatitic melt of the same composition as that formed by protracted fractional crystallization, if a low-rate anatexic crustal-melting of rocks with the appropriate composition is present (Simmons and Webber, 2008). This model was suggested in response to problems in fitting some pegmatites and pegmatites field within the magmatic model. The main arguments to support the anatectic model were the difficulty in trying to relate extremely evolved pegmatitic compositions with their primitive parental granite (Stewart, 1978; Norton and Redden, 1990) and the existence of groups of pegmatites with no apparent relation with any granitic source (Simmons *et al.*, 1995). The difficulty to prove a magmatic liaison to pegmatites is enhanced if we think that a low viscous magma rich in fluxing agents (*i.e.* Li, P, F, and B elements that reduce the viscosity of the melt) and stable at low T can migrate up to 10 Km if the pluton have sufficient dimension to emanate pegmatitic melt (Baker, 1998). Simmons and Webber (2008) proposes that low-degree anatexis produced around plutons in orogenic environment could form pegmatitic melts, and Simmons *et al.* (1995) theorize that perhaps, in some case, the pegmatite farthest from the pluton are a consequence of a very-low degree partial melts generated in the thermal halo of the pluton. Roda-Robles *et al.* (1999) in a study of pegmatites in the Fregeneda area, Spain, proposed that regionally zoned pegmatites are a combination between the magmatic and anatectic model, in which the pegmatites are a

conjunction of different percentage of anatexis followed by the fractional crystallization of that same anatectic melt.

1. 2. 3. MODELS OF PEGMATITES EMPLACEMENT

In recent years, various authors (*e.g.* Partington, 1990; Araújo *et al.,* 2001; Henderson and Ihlen, 2004; Demartis *et al.*, 2011) demonstrated the existence of a correlation between sites of concentrated magmatism precursor of pegmatites occurrences and crustal deformation zones. One of the former studies about the mechanism of pegmatites emplacement was realized by Brisbin (1986). In this study, W. Brisbin pretended to summarize the geological factors that interacts in the control of position, shape, size and orientation of pegmatites at different crustal levels. To do so, he based is model of pegmatites emplacement in previous concepts of structural geology not integrated to date in the study of pegmatites. Brisbin proposes that the pegmatites emplacement are characterized by a complex interplay between pegmatites fluid pressure, host rock (rheological state, anisotropies) and stresses conditions. In the upper crust, the lithostatic and directed-stresses combined with the rock anisotropies prevails, controlling the emplacement in tabular shape and with preferential orientation of the pegmatites. Lower crustal levels present pegmatites with lensoid to irregular shape due to the prevailing hydrostatic conditions.

Some years later, Partington (1990) aimed the Greenbushes giant pegmatite to describe the environment, timing and preferred model of intrusion for this world Li producer pegmatite. Partington (1990) proposed that the Greenbushes pegmatite magma was controlled by the nearby crustal-scale shear-zone, where the intrusive rocks in the Greenbushes pegmatite district are concentrated. This crustal-scale shear-zone acted as a channel for the melts or fluid to ascent, leading to the intrusion of the pegmatite. Partington concludes that giant rare metal pegmatites can occur in high grade metamorphic terrains and that this type of pegmatites does not need to present an obvious parental granitoid, which they are likely to be associated with tectonism along crustal-scale fault systems. Araújo *et al.* (2001) described a similar association of pegmatites emplacement with a crustal-scale shear-zone in the Seridó belt, NE of Brazil. In this pegmatitic filed, the pegmatites swarms are located near to the transpressive strike-slip shear-zone and presents two stages of pegmatites emplacement during the strike-slip event. The older stage of pegmatite emplacement, synchronous and homeneous with the last deformational phase, intruded mostly along lithological and structural discontinuities. The younger stage of pegmatites emplacement intruded the host

rock using *échelon* tension gashes and other dilation structures following the Riedel (1929) model of fracturation (Fig. 5a), promoting a heterogeneous orientation emplacement relatively to the regional schistosity. More recently, Demartis *et al.* (2011) observed that the pegmatites melts ascent and emplacement in the Comechingones pegmatitic field in Argentina were associated with a major reverse shear-zone. The Comechingones pegmatitic field present two different strain gradient domain related to the crustal-scale shear-zone, dividing in two the pegmatitic field in domains with high and low deformation. The pegmatites are emplaced within the two deformational domains, however they show a higher preference to intrude the high deformation domain. Demartis *et al.* (2011) recognizes two mechanism for the ascent and emplacement of pegmatitic melt, one similar to the fracture-controlled observed in Araújo *et al.* (2001) where the pegmatites present high-dip, and a second mechanism associated with C´-shear zones or T-fractures similar to magma pumping (Fig. 5b). They contend that this mechanism promote a negative pressure gradient that induce the ascent of buoyant pegmatitic melt from low crustal levels.

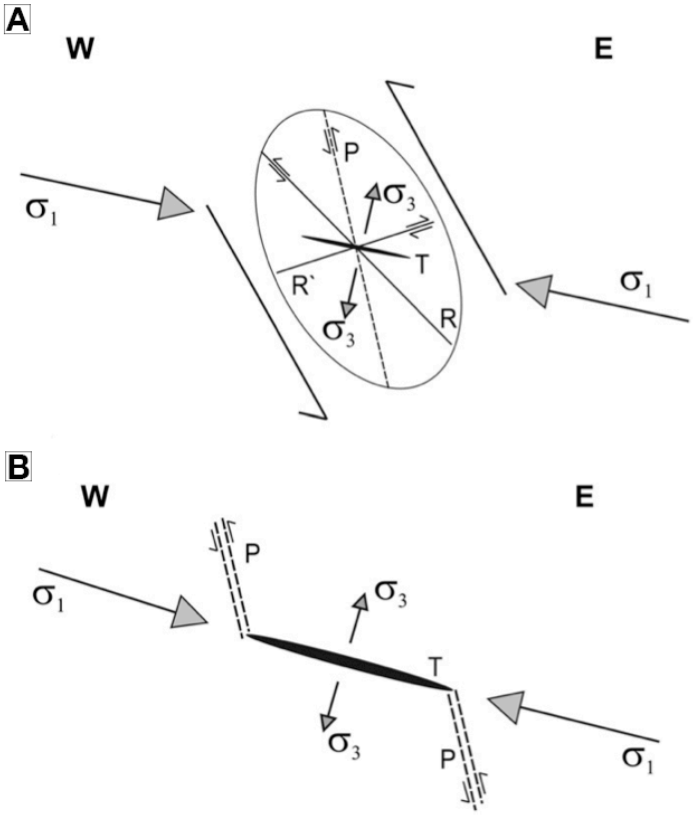

Fig. 5 Schematic model for space generation. a) Spaces develop in a shear zone according to the Riedel (1929) model of fracturation. b) Highly dipping pegmatites are consistent with P-shear fractures. These fractures were able to act as feeding channels for low-dipping and thicker pegmatites emplaced along extensional T-fractures (From Demartis *et al.*, 2011).

CHAPTER 2

GEOLOGIC DESCRIPTION OF BARROSO-ALVÃO APLITOPEGMATITE FIELD

CHAPTER 2 - GEOLOGIC DESCRIPTION OF BARROSO-ALVÃO APLITOPEGMATITE FIELD

The Barroso-Alvão aplitopegmatitic field is situated in the northwestern portion of the Iberian Peninsula at north of Portugal, in the Trás-os-Montes e Alto Douro region. This pegmatitic field is recognized for its large number of outcropping aplitopegmatites (~2000) (Noronha, 1987; Charoy *et al.*, 1992, 2001; Lima, 2000; Lima *et al.*, 2003a,b,c; Martins, 2009; Martins *et al.*, 2011, 2012), from poorly mineralized to geochemically evolved and sometimes with low grades of Sn mineralization. The pegmatitic field area covers partially four 1:50.000 geological maps of Portugal, which are 6A-Montalegre, 6B-Chaves, 6C-Cabeceiras de Basto, and 6D-Vila Pouca de Aguiar (Fig. 6 and 7).

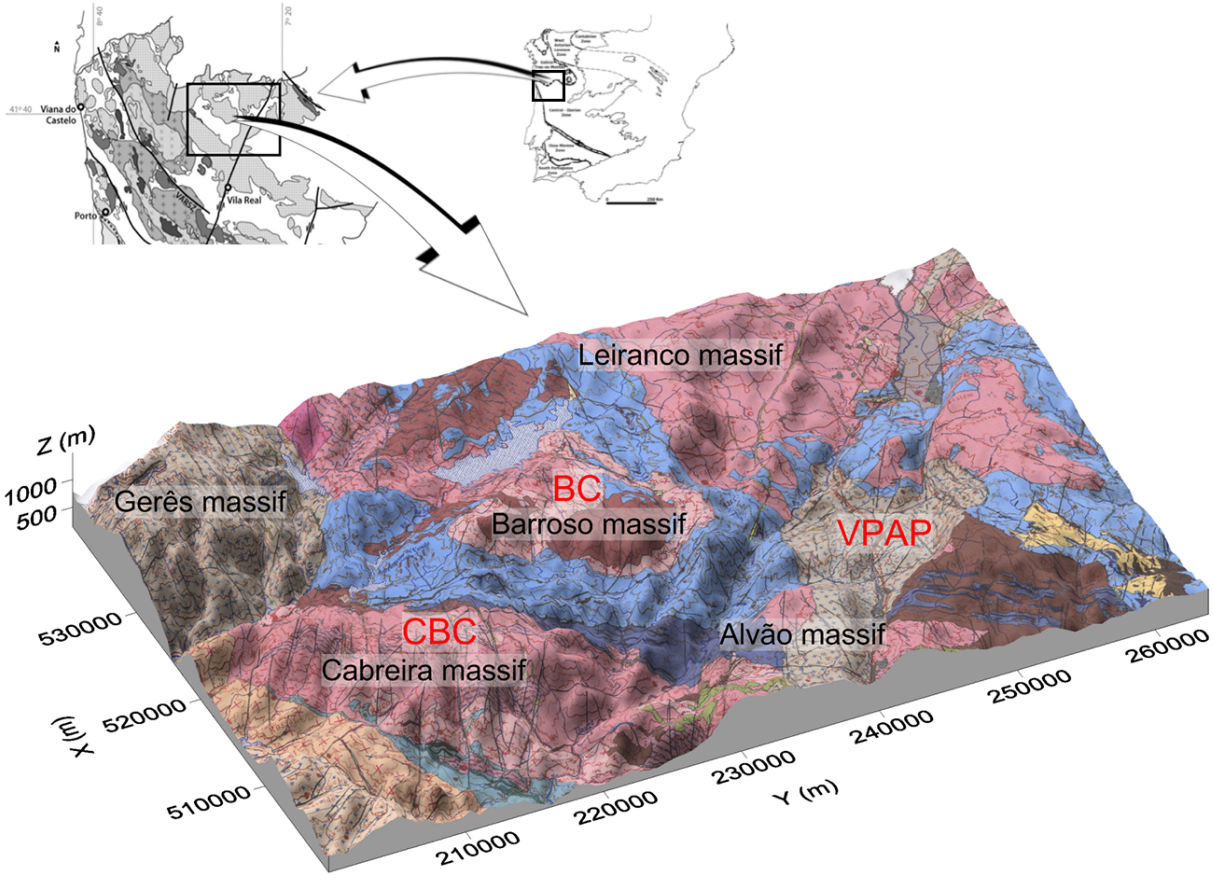

Fig. 6 3-Dimensional map from a portion of the sheet nº2 of the 1:200.000 geological map of Portugal made by the Instituto Geológico e Mineiro. The map edges are equivalent with the limits of the four maps from the nº6 series of 1:50.000 geological maps of Portugal. CBC – Cabeceiras de Basto granitic complex; BC – Barroso granitic complex; VPAP – Vila Pouca de Aguiar pluton.

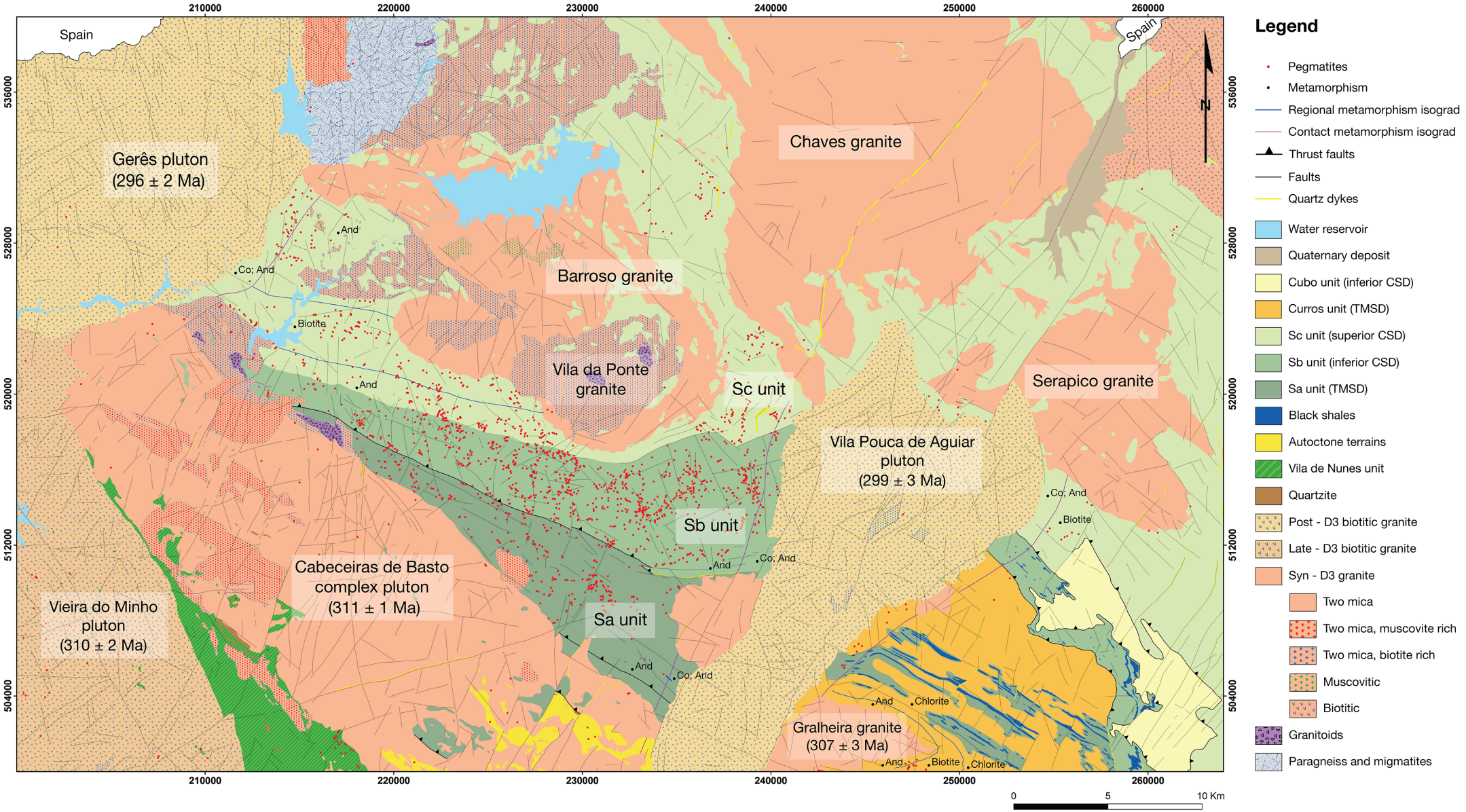

Fig. 7 Simplified geology of the Barroso-Alvão region based on 1:50.000 scale regional geological maps. UTM coordinates acording to Lisbon Hayford-Gauss IGeoE datum. Displayed emplacement ages for the various granitic rocks from Almeida *et al.,* 1998; Dias *et al.,* 1998; Martins, H. *et al.,* 2009, 2013; Priem and den Tex, 1984.

The potential for spodumene exploration was discovered in 1987 during the geological acquisition for the 6C-Cabeceiras de Basto geological map mentioned before (Noronha, 1987), although, abundant artisanal exploration for tin in weathered pegmatites was already done in this area. Some years later, due to is large potential in exploring industrial minerals and metallic elements, the former IGM (Instituto Geológico e Mineiro) initiated mineralogical, petrological, geochemical and explorational studies in these Li-rich intrusions. In the new millennium, Lima *et al.* (2003 a,b,c) identified a new set of pegmatites with petalite as the dominant phase. Recently, Martins (2009) studied more profoundly the pegmatitic field in terms of genesis, petrology and distribution of different intrusive phases, where several new pegmatites were found, especially mineralized in petalite. Up to date, the assigned mining concession within Barroso-Alvão pegmatitic field involving granitic pegmatites are property of Felmica, S.A. (Adagoi pegmatite) and Imerys Ceramics Portugal, S.A. (Mina do Barroso) for quartz, feldspar and Li exploitation, and José Aldeia Lagoa & Filhos, S.A. (Veral and Alijó pegmatites) for quartz and feldspar exploitation. All the mining concessions mentioned above are for non-metallic production (Direcção Geral Energia e Geologia, 2014).

2. 1. LARGE-SCALE TECTONICS OF NORTHERN PORTUGAL

The aplitopegmatite field is localized on the occidental portion of the Iberian part of the so-called Ibero-Armorican arc. The Iberian Peninsula is affected by the Variscan orogeny starting in the Devonian and continuing into the Carboniferous up to early Permian time. Its structural organization results from three main deformation phases that acted during the Variscan orogeny as proposed by Ribeiro, A., (1974, 2013). The 1st phase (D1), compressive, originates folds with NW-SE axis with vertical axial plan in the Central Iberian Zone (CIZ), and differentiated vergence in parautochthonous grounds. The 2nd phase (D2), tangential, induces subhorizontal displacement with mantels-fold formation in the parautochthonous grounds, and the 3rd phase (D3) covers all the zones developing folds with subvertical axial planes. The pegmatite field is emplaced inside the Galicia Trás-os-Montes Zone (GTMZ), an essentially parautochthonous geotectonic zone using the classification proposed by Julivert *et al.* (1974) for the Iberian Massif, but very close at south to the boundary (the basal thrust) between GTMZ and CIZ. In the oriental sector of the study area is localized the regional fault Régua-Verin, a late-D3 mega scalar shear zone structure with polyphasic reactivation and NNE-SSW trend. This regional fault controls the emplacement of the post-tectonic Vila Pouca de Aguiar massif (Martins, 1998; Sant'Ovaia *et al.,* 2000).

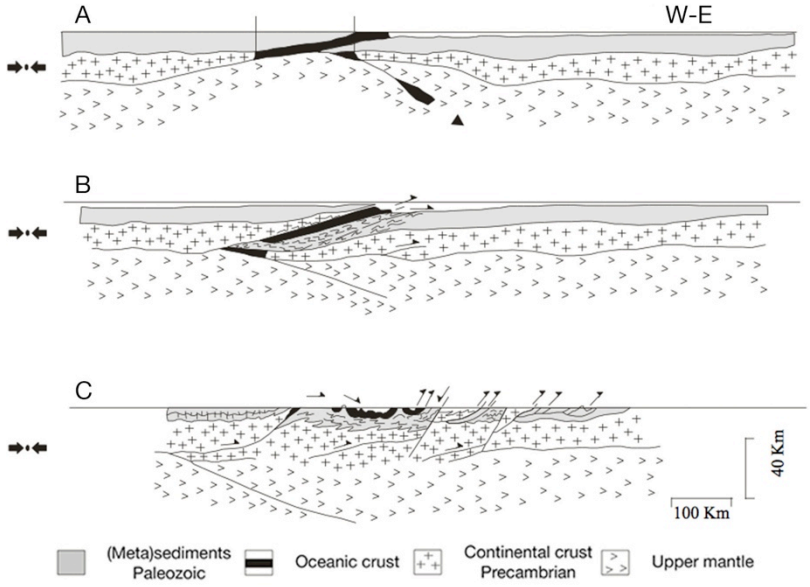

Fig. 8 Simplified scheme of the Variscan geodynamic evolution for the northwestern Iberian Peninsula. A- Middle Devonian; B- Late Devonian (A and B represents the D1 and D2 phases); C- Late Carboniferous (wrenched D3 phase). (Adapted from Iglesias *et al.,* 1983).

2. 2. METASEDIMENTS

The aplitopegmatites belonging to the Barroso-Alvão field intrude mainly parautochthonous terrains. This one is made of early-Paleozoic metasedimentary and volcano-sedimentary metapelitic, micaschist, and rarely carbonaceous or graphitic schist (Ribeiro, M. A. *et al.*, 2003). The overlapping and piling of contrasting paleogeographic units, separated by tangential D2 thrusts, forms the structural domains observed in the GTMZ (Ribeiro, A., 2013). Ribeiro, M. A. (1998) and Rodrigues *et al.*, (2005) subdivides these parautochthonous sequences in Lower Parautochthonous or Três Minas Structural Domain (TMSD) and the Upper Parautochthonous or Carrazedo Structural Domain (CSD) for the oriental sector relatively to the Régua-Verin fault. This sector is later correlated with the occidental sector in which the metasediments are subdivided in Sa, Sb and Sc units (Ribeiro M. A. *et al.*, 2007).

Table 1 Structural and lithological correlation between metasedimentary rocks from western and eastern sectors within Barroso-Alvão study area.

Structural domain	*West sector*	*East sector*	*Lithology*
Três Minas Structural Domain (TMSD)	Sa unit	Fragas Negras unit (S_{FN})	Phyllites and micaschists interlayed with black schists, lydites and some quartzphyllites and calcossilicated rocks
Carrazedo Structural Domain (CSD)	Sb unit	Rancho sub unit (S_{RA})	Quartzites and quartz-phyllites interlayered with phyllites and some lydites and black schists but in less proportion than Sa/S_{FN}
	Sc unit	Santa Maria de Émeres unit (S_{SE})	Relatively monotonous sequence of phyllites, micaschists and quartzgreywacke with rare calcosilicated rocks

2. 2. 1. DEFORMATION

Three superimposed schistosities (S1, S2 and S3) are observed in the metasedimentary rocks consequence of also three deformational phases (D1, D2, D3) originated during the Variscan orogeny that characterizes this zone. The 1st phase (D1) originated an axial planar foliation (S1) parallel with the mainly N120º stratifications (S1//S0). The 2nd phase (D2) generated a subhorizontal shear cleavage (S2) locally verticalized by D3. The S1=S2 foliations are well preserved near the Covas do Barroso batholith. The last, late Variscan phase (D3), originated a locally strong, penetrative crenulation cleavage (S3), preferentially associated with ductile shear zones (Fig. 9), that overprints structures from the firsts phases of ductile deformation with N120º trending folds (Fig. 10). Finished the D3 phase, a significant fragile deformational regime generated important faults that includes Régua-Verin fault, which varies from N30º to N-S, and E-W to ENE-WSW (Noronha *et al.*, 1981; Pereira *et al.*, 1993; Dias and Ribeiro, A., 1995).

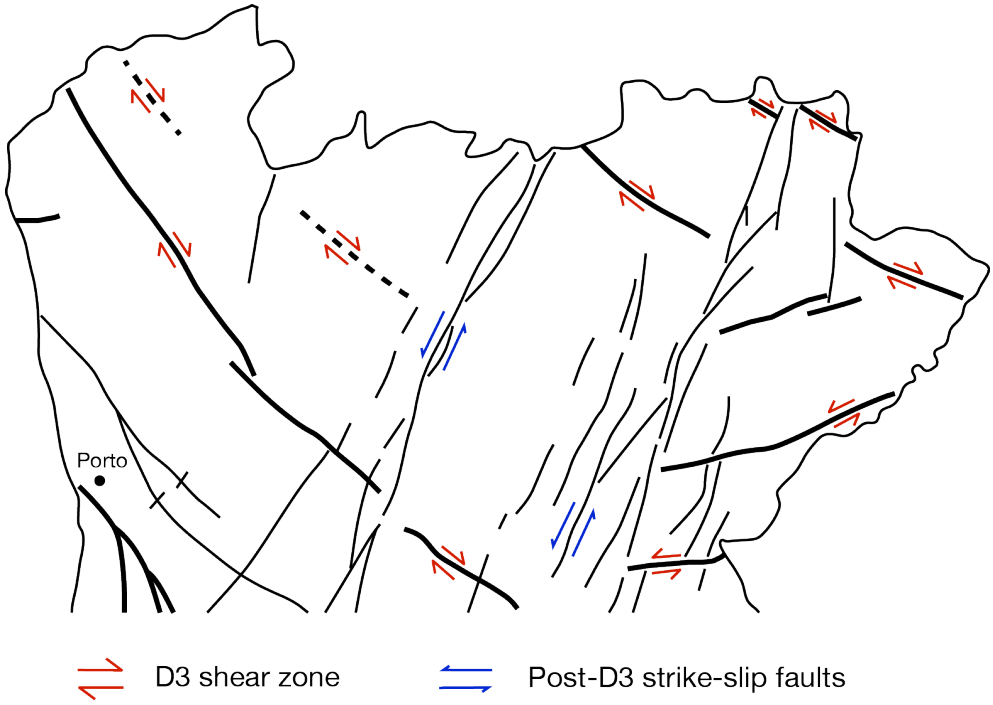

Fig. 9 North of Portugal shear-zones and faults originated during the D3 and post-D3 Variscan deformational phase (Adapted from Pereira *et al.*, 1993).

Fig. 10 Observed crenulation cleavage planar fabric in metassedimentary rock from Barroso-Alvão pegmatite field, resulting of superimposed S3 foliation originated during D3 late Variscan phase. Picture taken from a horizontal outcrop.

2. 2. 2. METAMORPHISM

The metasedimentary sequence that constitutes the host of the Barroso-Alvão aplitopegmatitic field experienced a marked prograde metamorphism, analogous to the metamorphic conditions defined by Miyashiro (1961) as Abukuma-type [Low pressure (P), High temperature (T)] and Barrovian-type (Medium P, High T). This metamorphism resulted in isograds parallels to the syn-tectonic Cabeceiras de Basto massif and to the lithostratigraphics contacts (see Fig. 7). The isograds results from the pre- to syn-D3 thermal peak, subsequent to a prograde dinamothermal evolution expressed by the occurrence of staurolite, premature relatively to the andalusite and to the cordierite (Noronha and Ribeiro, M. L., 1983; Noronha, 1983; Ribeiro, M. A., 2000; Ribeiro, M. A. *et al.*, 2000). Close to the contact with the syn-D3 Cabeceiras de Basto granite there was described two different mineralogical associations that defines the andalusite isograd: i) quartz + muscovite + biotite +/- andalusite +/- staurolite; ii) quartz + muscovite + biotite +/- andalusite +/- staurolite +/- garnet +/- plagioclase. Parallel to the andalusite isograd was also identified a biotite isograd with different mineralogical association: i) quartz + muscovite + biotite; ii) quartz + muscovite + biotite + chlorite; iii) quartz + muscovite + biotite + albite +/- chlorite +/- garnet. It is observed as well a post-kinematic contact metamorphism crosscutting the regional metamorphism, inferred by the development of aluminosilicate porphyroblasts of andalusite and fibolitic sillimanite related with Gerês and Vila Pouca de Aguiar post-D3 magmatism. Local hydrothermal alteration related to aplite-pegmatite or quartz veins is sometimes observed (Ribeiro, M. A. *et al.*, 2007).

2. 3. GRANITIC ROCKS

The septentrional region of Portugal presents a large diversity of granitoids rocks intruding mainly thick autochthonous and parautochthonous metasedimentary rocks. Following the work and classification proposed by Ferreira *et al.* (1987) for orogenic granitic magmatism, two main large groups of granitoides are considered (Fig. 11): i) Peraluminous

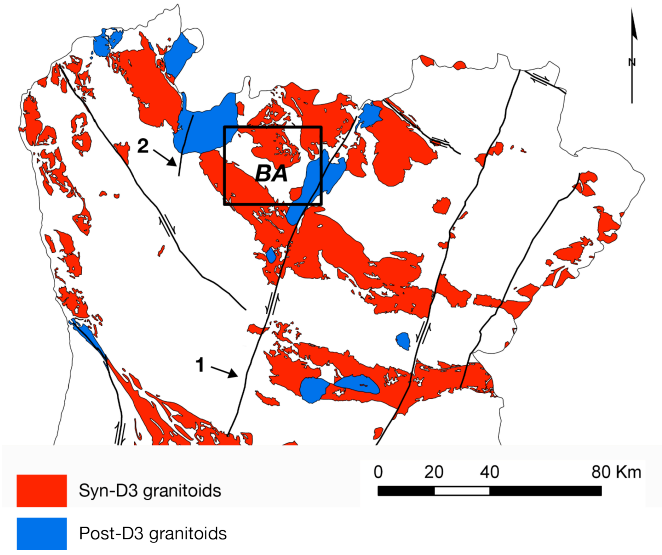

Fig. 11 Schematic representation of the different types of granitic rocks encountered at the Barroso- Alvão pegmatite field (BA). 1- Régua-Verin fault; 2- Gerês-Lovios fault.

granites or "two-mica granites with dominant muscovite"; and ii) Monzonitic granites and granodiorites or "biotitic granitoids with calcic plagioclase". The granites belonging to the first group are "mesocrustal granites", generated by wet anatexis controlled by the regional metamorphism and aged as post-crustal thickening (*i.e.* the crustal thickening happened during D1 and D2 phases) and was accentuated by the emplacement of thrusting terrains. These peraluminous intruding granites were emplaced simultaneously with D3 folding and associated ductile shear zones, inside elongated D3 regional antiforms. The granitoids that belong to the second group are "infracrustal granitoids" with facies that can vary from tonalites to granodiorites with hornfels and/or biotite, to biotitic granites and even to leucogranites. These granitoids are post-collisional emplaced, taking advantage of late-D3 deep fractures. According to a temporal evolution and concordant with D3, we evolve from syn- to late-tectonic peraluminous magmatism, to a post-tectonic subalkaline magmatism. Taking account the relationship between granitic rocks and the Variscan orogeny, we can divide the granitoids belonging to the Barroso-Alvão aplitopegmatitic field as syn- to late-D3 granitoids (Syn-D3) defining the pegmatitc field to the north and southwest and post-tectonic granitoids (Post-D3) defining the east and in small amount the northwest limit.

2. 3. 1. SYN-D3 GRANITES

The more relevant Syn-D3 granitoids can be individualized in Barroso and Cabeceiras de Basto complex plutons. The Barroso complex it is constituted in is majority by the Barroso granite and the Vila da Ponte granite. The Barroso granite is a two-mica granite, medium-grained to porphyritic tendency. Petrographic study (Noronha and Ribeiro, M. L., 1983) describes deformation especially apparent when the granite is weathered and close to the contact with the metasedimentary rocks. The major mineral phases are orthoclase, albite-

oligoclase, biotite and less abundant late muscovite. Accessory apatite, tourmaline and opaques are described. The Vila da Ponte granite is a two-mica granite, medium grained to porphyritic tendency, biotite rich with depletion in muscovite. The geochemical data for the Barroso complex is not abundant, but seems that its composition is apparently similar to the Cabeceiras de Basto peraluminous two-mica granite. Moreover, due to the lack of systematic trace element analysis for the Barroso granite, it is difficult to assess the metallogenic specialization for the trace elements (*e.g.* Li, Nb, Ta) usually found in pegmatites (Noronha and Ribeiro, M. L., 1983; Ferreira *et al.*, 1987).

The Cabeceiras de Basto complex pluton is localized in the southwest limit of the pegmatitic field and it is considered the most probable parental intrusion for the Barroso-Alvão pegmatites, and also the regional metamorphism enhancer (Lima, 2000). The pluton is a peraluminous two-mica granitoid that intruded lower Silurian metasediments along the core of a regional N130º antiform concomitant with D3 deformational phase (Ferreira *et al.*, 1987), dated as 311 ± 1 Ma (U-Pb method on monazite and zircon (Almeida *et al.*, 1998). The mineral association described by Almeida (1994) for the three series of granites (G'f, G'm and G'g) for the granitic complex is quartz, albite (An_1-An_6), perthitic K-feldspar (orthoclase to microcline), biotite and muscovite. Apatite, monazite, zircon, ilmenite, rutile, rare sillimanite and tourmaline occur as accessory minerals. It is observed late- to post-tectonic alteration favored by large corridors as shear zones and different levels of hydrothermal alteration essentially sericitization, muscovitization and albitization. The geochemistry for the three series indicates also a similar composition resembling to peraluminous granites (1,2 < A/KCN <1,4).

Using the model of magmatic differentiation, Lima (2000) suggests that the Cabeceiras de Basto granite is the possible parental source for the pegmatites from the Barroso-Alvão pegmatitic field. The suggestion was funded in the metallogenic specialization in Li, Sn and W for the Cabeceiras de Basto granite (Almeida, 1994), the high content in P_2O_5 for the granite that, according to London (1998), is the result of S-type granite and sources high fractionation, and also in the pegmatites alignment and distance from the granitic complex.

2. 3. 2. POST-D3 GRANITOIDS

The more relevant Post-D3 granitoids can be individualized in Vila Pouca de Aguiar (VPA) and Gerês plutons. The VPA pluton is a non-deformed and zoned composite massif elongated according to NNE-SSW direction, dated as 299 ± 3 Ma (U-Pb method on zircon; Martins, 1998). Two main types of granites compose the VPA pluton, the VPA granite that

represents approximately 70% of the massif and the Pedras Salgadas granite. The granites composing the pluton are classified as biotitic monzogranites with granular hypidiomorphic porphyroidal texture. The major mineral phases are quartz, pertitic K-feldspar, plagioclase and biotite as the only ferromagnesian phase. Zircon, apatite, alanite, ilmenite and monazite occur as accessory minerals. The pluton emplacement was controlled by the regional Régua-Verin tectonic structure (Fig. 11; Martins, 1998; Sant'Ovaia *et al.,* 2000), reason why is discordant relatively to the syn-tectonic two-mica granite and to the D3 structure observed in the metasedimentary rocks from inferior Paleozoic, in which the VPA pluton marked an aureole of contact metamorphism (Ribeiro, M. A., 2000; Ribeiro, M. A. *et al.*, 2007).

According to Ferreira *et al.* (1987) the Gerês pluton is composed by non-deformed granite and is spatially related to the Gerês-Lovios fragile fracture system from the late Variscan orogeny. The major mineral phases are quartz, K-feldspar, plagioclase and biotite (partial or completely chloritised). Allanite, zircon, apatite, epidote, chlorite, muscovite, fluorite (related with chlorite) and Fe-rich chlorite occur as accessory phases.

2. 4. BARROSO-ALVÃO PEGMATITES

The aplitopegmatitic field from Barroso-Alvão region is an appreciated object of study by several authors (*e.g.* Charoy *et al.*, 1992; Lima, 2000; Martins, 2009) and it is described by all as containing hundreds of pegmatitic bodies, from barren to intrusions highly concentrated in rare elements. The aforementioned recent work of Martins (2009) allowed the pegmatite division inside the pegmatitic field in five different groups, as a result of field observations, pegmatite relationships with the host rocks, pegmatites internal structures and mineral geochemistry (Table 2). This division followed the classification of Černý and Ercit (2005) and allowed the elaboration of an incipient and spatially imperfect regional zoning concordant with Černý (1989, 1991) involving the Cabeceiras de Basto granitic complex and the Barroso batholith.

Table 2 Pegmatite type classification and respective mineralogy inside the Barroso-Alvão pegmatitic field.

Pegmatite type	*Mineralogy*
Intragranitic	Mainly quartz, feldspar, muscovite, biotite and minor tourmaline, beryl and garnet
Barren	The more primitive group; quartz, feldspar, muscovite and minor biotite, apatite, beryl, tourmaline, chlorite, zircon, pyrite and (Ce)-monazite)
Spodumene	Spodumene, Nb-Ta minerals, (F)-apatite, montebrasite, phosphoferite, chlorite, tourmaline, uraninite and spharelite
Petalite	Petalite, cassiterite, Nb-Ta minerals, (F)-apatite, montebrasite, pyrite, uraninite, spharelite and (Ce)-monazite
Lepidolite	Albite, lepidolite, cassiterite and phosphate minerals with Sr-A

However, Martins (2009) also mention two exceptions not consistent with the theoretical genesis model and associated regional zonation of Černý and Ercit (2005): i) barren pegmatites outcrops intruding the same structural levels as Li-bearing pegmatites and ii) spodumene and petalite pegmatites frequently emplaced in similar metamorphic terrains. According to Lima (2000) and Martins (2009) the Barroso-Alvão pegmatites are generally non-zoned (Fig. 12), except for the intragranitic pegmatites, and were affected by the D3 deformational phase. The deformations are visible in macroscopic to microscopic scale and the "pinch and swell" ductile deformation is observed in several outcrops (Martins, 2009).

Fig. 12 Example of a spodumene-rich outcropping pegmatite from Barroso-Alvão region (Eric Gloaguen for scale).

Regarding the Li-enriched pegmatites bodies emplacement, all of them are emplaced in metassediment terrain where some are concordant with D2 structures and others discordant but, in both cases, deformed by the D3 ductile phase. The variations in the intrusions behavior are probably due to pre-existent heterogeneities accentuated by a non-coaxial terrain deformation (Martins, 2009). The pressure and depth emplacement for the pegmatitic bodies were obtained with the utilization of the thermobaric petrogenetic grid for Li-aluminosilicates (petalite-spodumene-eucryptite) proposed in London (1984).

In this petrogenetic grid it is possible to visualize five different evolutionary paths for the pegmatites belonging to the Barroso-Alvão pegmatitic field (Fig. 13-B) (Martins, 2009). The more simple to analyze are the paths where only one Li-mineral phase prevail (spodumene or petalite). In these paths the thermobaric condition for the pegmatites remained inside each respective stability field. In one other path, the spodumene and petalite are co-existent probably because the P-T evolution for these pegmatites was in equilibrium with the univariant curve between spodumene and petalite fields (Fig. 13-A). The last two evolutionary paths show a crosscut between the stability field of spodumene and petalite, where in one case the spodumene is the first to crystalize and later modification in P-T condition allows petalite crystallization inside the same pegmatite. The other path shows as the first phase the petalite crystallization followed by the break down by isochemical reaction of the same petalite minerals to petalite → spodumene + 2 quartz usually named SQI *i.e.* Spodumene Quartz Intergrowth (London, 1984). These discoveries seem to imply a thermobaric variation in the pegmatites emplacement terrains to the Régua-Verin shear zone (Charoy *et al.,* 2001; Martins, 2009) and/or uplift process during the pegmatitic evolutionary paths (Noronha *et al.,* 2013).

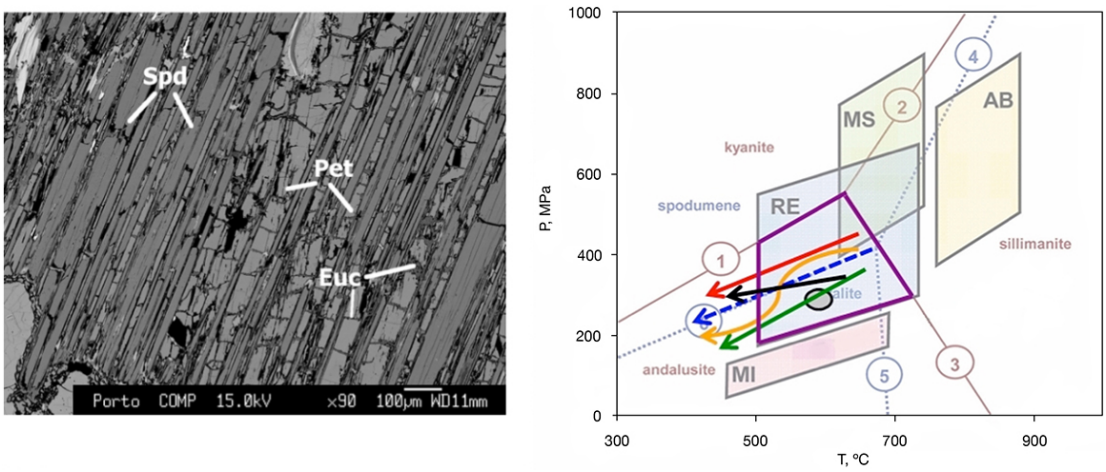

Fig. 13 (A) BSE imaging of spodumene (Spd), petalite (Pet) and eucryptite (Euc) from a spodumene pegmatite where is visible an intimate intergrowth of Spd and Pet. Euc is replacing Pet in the fractures; (B) Thermobaric constrain for Li-bearing pegmatites of the Barroso-Alvão taking into account the London's petrogenetic grid, regional metamorphism of the study area (reaction boundaries kyanite, andalusite, and sillimanite according to Pattison, 2001), Černý (1991) classification and petrographic study. Arrows of different colors define the possible P-T paths for the different case studies. (From Martins, 2009).

Geochemical studies from Martins *et al.* (2011, 2012) involving Ta-Nb oxides fractionation in Li-bearing pegmatites and micas trace elements chemical evolution from intragranitic to lepidolite pegmatites provided a new perception in the parental source for the Barroso-Alvão pegmatites. In these studies the micas and Ta-Nb chemical evolution do not show a trend from a single parental melt source, but instead they evidence an origin from different batches of melts, in the sequence barren to spodumene, petalite and finally to lepidolite. Field relationship between Cabeceiras de Basto granitic body and the Li-bearing pegmatites are not clear or easy to establish, in part because of: i) the difficulty to evidence the same petrogenetic process and path of crystallization in all the pegmatites extension, ii) a discontinuous increase in the content of incompatible elements (*e.g.* Li, F, Sn, Rb) from the granite to the most evolved pegmatites, and iii) a not elucidative regional zoning relatively to Cabeceiras de Basto complex. As a conclusion remark in the end of the studies, Martins *et al.* (2011, 2012) propose that the parental source for the pegmatites within the Barroso-Alvão region could be related to other two-mica granites bodies or, even, some other granite body that does not outcrop.

CHAPTER 3

SPATIAL STATISTICAL ANALYSES

CHAPTER 3 - SPATIAL STATISTICAL ANALYSES

3. 1. CONSIDERATIONS ABOUT SPATIAL ANALYSES MODELING

The geoscientist community fairly agrees that some mineral deposits present a non-random spatial pattern, mainly because the geneses of those mineral deposits are controlled by the combination of some known geological processes. Another fact that strengthens the non-random spatial pattern is the evident spatial association from several mineral deposits around the globe with certain geologic characteristics, but definitively not with all of them (Carranza, 2009a). It is precisely because of these observed interrelations between the mineral deposits and certain geological features, that the analysis of spatial pattern can provide empirical spatial geo-information that potentially improves our conceptual understanding of mineral systems (Carranza, 2009b).

Until recently, mineralogical and geochemical studies of granitic pegmatites have been the principal methods to determine the genesis of pegmatites, especially the LCT-type, and to establish the relationships between pegmatites and the host rock (*e.g.* London, 1986a,b; Černý, 1991; Roda-Robles *et al.*, 2004). In contrast, conceptual models proposing to explain the control of intrusion and emplacement of pegmatites sets exploring kinematics relations were poorly studied (*e.g.* Černý and Brisbin, 1982; Brisbin, 1986; Partington, 1990; Demartis *et al.*, 2011). This structural control of intrusion and emplacement are of high importance, because of specific common features of pegmatites fields to be clustered in swarms, and in a large number of cases, associated to regional shear zone systems [*e.g.* Black Hills, USA (Norton and Redden, 1990); Fregeneda-Almendra, Portugal/Spain (Vieira, 2010); Comechingones, Argentina (Demartis *et al.*, 2011); Monts d'Ambazac, France (Deveaud *et al.*, 2013)]. If these two large forms of studying the pegmatites (kinematic and petrogenetic relations) possess intrinsic coherence and reproducibility, they convert into indicators of great efficiency and application in prospecting programs. However, these two-forms of studying the pegmatitic field have their limitation regarding the delineation of exploration targets, or even, in constraining processes involved in the emplacement of LCT-type pegmatite field. This is where the spatial analysis, in this particular case for rare-elements pegmatites, can be used as a great analytical tool to produce a mapping of mineral potential, or unveil the regional zonation patterns for this type of mineralization. This type of approach has been first proposed and applied for others types of mineral deposits for, among others applicability, mining exploration (*e.g.* Knox-Robinson and Groves, 1997; Thiart and De Wit, 2000; Feltrin, 2008;

Carranza, 2009a; Porwal and Kreuzer, 2010; Zhao *et al.*, 2011), hydrogeology (*e.g.* Corsini *et al.,* 2009), geothermal fields (Carranza *et al.*, 2008) or biological sciences (*e.g.* Knudby *et al.*, 2010). All the case proposed above developed their statistical analysis using geocomputational techniques, especially the geographic information systems (GIS) technology (Bonham-Carter and Agterberg, 1990).

Taking into account the case of mining exploration, the main objective in using the spatial analysis is to delineate mineral exploration targets in a multistage mapping activity from regional to local scale. In every of these scales, the target delineation involves the collection, analysis and integration of various thematic geoscience data set to extract spatial geo-information. However, geocomputational modeling of exploration targets must pertain to just one type of mineral deposit (Carranza, 2011). The modeling of exploration targets follows specific steps (Fig. 14) starting with the definition of a conceptual model of exploration targets for the mineral deposit-type sought (Fig. 14) and requires the knowledge of various geological processes relevant to the formation of the mineral deposit. After this step, to create a predictor map, it is necessary to assign weight to evidential features through either knowledge-driven analysis or data-driven geocomputation of their spatial association (Bonham-Carter, 1994).

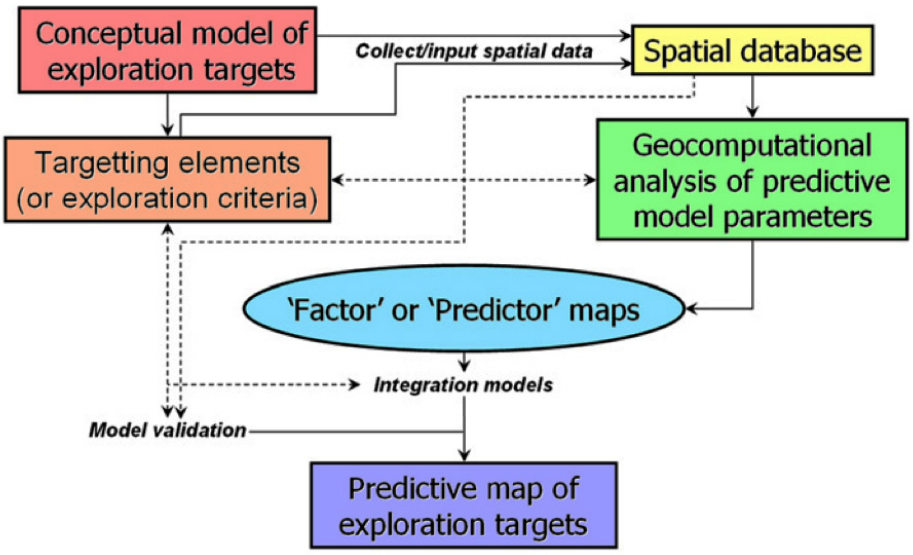

Fig. 14 Elements of predictive modeling of mineral exploration targets. (From Carranza, 2011).

Knowledge-driven geocomputation is appropriate for 'greenfields' (*i.e.* in frontier or less explored geologically permissive areas) where no or few mineral deposits of the type sought are known to occur. Data-driven analysis is appropriate in 'brownfield' (*i.e.* moderately to well sampled mineralized landscapes) to delineate new targets of undiscovered deposits for further

exploration. To achieve the predictive maps, the most usual applied methods include the Boolean methods, weight-of-evidence scores estimation and fuzzy logic approach (Bonham-Carter, 1994), or algebraic *processus* (*e.g.* SIRIS*,* Vaillant *et al.,* 1995). Modeling of exploration targets using hybrid methods (fuzzy weight-of-evidence, data-driven fuzzy and neuro-fuzzy modeling) have been proposed to optimize the utilization of both knowledge-driven and data-driven conceptual methods (Carranza, 2011; Cassard *et al.*, 2008).

Relatively to spatial analysis concerning pegmatites, the paper of Deveaud *et al.* (2013) sets a good example of geocomputational methodologies used to study pegmatites within Variscan rare-elements granites. In their study, the GIS-based spatial statistical analysis is applied in the LCT-pegmatitic field of Monts d'Ambazac emplaced within the Saint Sylvestre Granitic Complex, belonging to the Variscan French Massif Central. The main objective of this study was not to create a model of exploring targets *per se* like the cases cited above, but instead, the principal purpose was to highlight any potential spatial link between pegmatites and the surrounding structures, especially the ductile shear zones, fault families and granitic units.

The spatial distribution of the pegmatitic bodies relatively to their scattering and aligning tendencies was also taken into account. In order to achieve the characterization and spatial distribution of the pegmatitic bodies trough the study area, the Distance to Nearest Neighbor (DNN) (Berman, 1977 and 1986) has been used has an alternative to the Fry analysis (*e.g.* Fry, 1979; Vearncombe and Vearncombe, 1999), that permits to assess distribution patterns and potential geological controlling structure, and fractal analysis (*e.g.* Carranza, 2009b), useful to determine the scales at which certain mineralization controls operates. Other geocomputational methods for numeric variable as Ripley's L'-function, Euclidean distance, spatial density distribution and cluster analysis were also implemented to bring any spatial distribution abnormality between the pegmatites and the cartographic structures. This method presents real advantages relatively to the classical methods of studying the pegmatite field emplacement (*i.e.* petrography, geochemistry and isotopic analyses), in part because the geocomputational methods are less time and money consuming. Another advantage is that this method can be easily applied to other pegmatitic field, especially for the exploration of LCT pegmatites field with poorly exposed domains. The aim of this study is to apply the GIS spatial method described above to the Barroso-Alvão pegmatitic field. Successful results obtained during the spatial statistical tests are then exploited to constrain mechanism used by pegmatitic melts during their emplacement.

3. 2. METHODOLOGY OF DATA ACQUISITION

The implementation of a statistical spatial analysis using a geocomputational GIS method requires different types of data to be compiled. This data, in intention to be used in GIS software, needs to include geographical information if expected to be projected and manipulated by the GIS software. The geographical information in the vectorial and raster format is essential, and because of that, for the vectorial format, the most common sources of analogic information are from the various types of cartographical maps and all type of georeferenced information. For the analogical information in map format, the information is digitalized as point, line or polygons layers, and all the important characteristics analogically represented as symbology or text is represented in the layer as a database. The georeferenced information is commonly acquired with a GPS unit and afterward introduced as GPS coordinates in the GIS software. For the raster type of data, the information is represented as a matrix, where the variable value is stored in each rectangular space, or pixel. The most common type of raster data are scanned maps, aerial photos, satellite imagery, Digital Elevation Models (DEM), and all sort of distance and density maps produced within the GIS software. This data is acquired by sensors or scanners and generated by calculation.

The Barroso-Alvão was chosen as object of this study, in part, because of factors already described in the previous chapters (*e.g.* large population of pegmatites, presence of Li mineral, similar age and tectonic setting than Monts d'Ambazac pegmatite field in Massif Central, France; Deveaud *et al,* 2013), but also because of the large GIS-applicable data available and published for this region (*e.g.* mineralogy, geochemistry, Li-content, orientation and localization of pegmatite dykes). This amalgam of data was published over the years in form of maps, papers and thesis by several authors (*e.g.* Noronha and Ribeiro, 1983; Noronha, 1987; Charoy *et al.*, 1992; Lima, 2000; Lima *et al.*, 2003a,b,c; Martins, 2009; Martins *et al.*, 2011, 2012). Other aspect that is relevant for the choice of Barroso-Alvão field is the past artisanal and actual modern industrial exploitation in pegmatites focused in this region. The fact that national and international companies (*i.e.* Imerys, Felmica, José Aldeia Lagoa & Filhos) as chosen this area for their exploration in Portugal, attests the importance in mineralized pegmatites for this region. To compute the different spatial statistical analyses, layers of information containing the localization and characteristics of the Barroso-Alvão region geological structures were compiled. All the layers and their content where georeferenced using the Lisbon Hayford-Gauss IGeoE datum for precise results. These layers are: i) Point layer (Pegmatites); ii) Line layer (Faults and thrust faults; Metasediment foliation), and iii) Polygon layer (Lithology). Each of them is individually described below.

3. 2. 1. PEGMATITE LAYER

The content of the pegmatite layer (Fig. 15) was compiled using the next informational sources: i) Geological maps of Portugal from the nº6 1:50.000 series [6A- Montalegre (Martins and Noronha, 1982), 6B- Chaves (Teixeira and Medeiros, 1969), 6C- Cabeceiras de Basto (Noronha, 1992), and 6D- Vila Pouca de Aguiar (Noronha *et al.,* 1998)]; ii) Maps included in publications (Granitic pegmatites: the state of the art – field trip guidebook, 2007; Prospeg project – pegmatite remote sensing and mapping. Final report, 2013); iii) Satellite imagery (World Imagery MapServer from Esri ArcGIS); iv) Personal pegmatite database provided by Alexandre Lima; and v) Personal data acquired *in situ* at Barroso-Alvão aplitopegmatitic field.

For the geological maps 1:50.000, the data was compiled digitalizing all the pegmatites visible in the maps. The pegmatites in the four maps are represented as lines, allowing extracting the orientation of the structure, or as pegmatites masses, representing pegmatites with sub-horizontal dipping. The difficulty was to digitalize, as lines, these pegmatites masses to obtain their orientations. Later, the segments digitalized were transformed into points based on the centroid of each segment. The same process was used for the maps extracted from the publications cited above. The only different aspect in the digitalization was on the map from Granitic pegmatites: the state of the art – field trip guidebook (2007), where some pegmatites were only represented, in the map, as points. In this case, the method applied was to digitalize the localization of these pegmatites directly as a layer point, without the extraction of orientation.

The satellite imagery was used to complete a specific area of the Barroso-Alvão pegmatitic field. This area, near, at west, to Vila Pouca de Aguiar pluton, is poorly represented with pegmatites in the maps described anteriorly. This fact is due to the step topology and dense vegetation, which makes nearly impossible to execute a proper mapping campaign. Although these difficulties, Professor Alexandre Lima (Porto University) as known this area as containing mineralized pegmatites, reason why the aforementioned area was targeted using satellite imagery for pegmatites digitalization. The digitalization process was the same as anteriorly described. The only difference was that the old artisanal exploitation was also targeted for digitalization.

Concerning the personal databases, the database from Professor Alexandre Lima was a compilation of fieldwork from Alexandre Lima himself in Barroso-Alvão region and in 6B-Chaves geological map region for the upgrade of this map, and from Tânia Martins (Porto University) during her doctoral program. The points from my personal database were acquired *in situ,* using a GPS unit, during a field trip with Alexandre Lima and BRGM (French

Geological Survey) geologists Eric Gloaguen, Sarah Deveaud and Arnaud Villaros

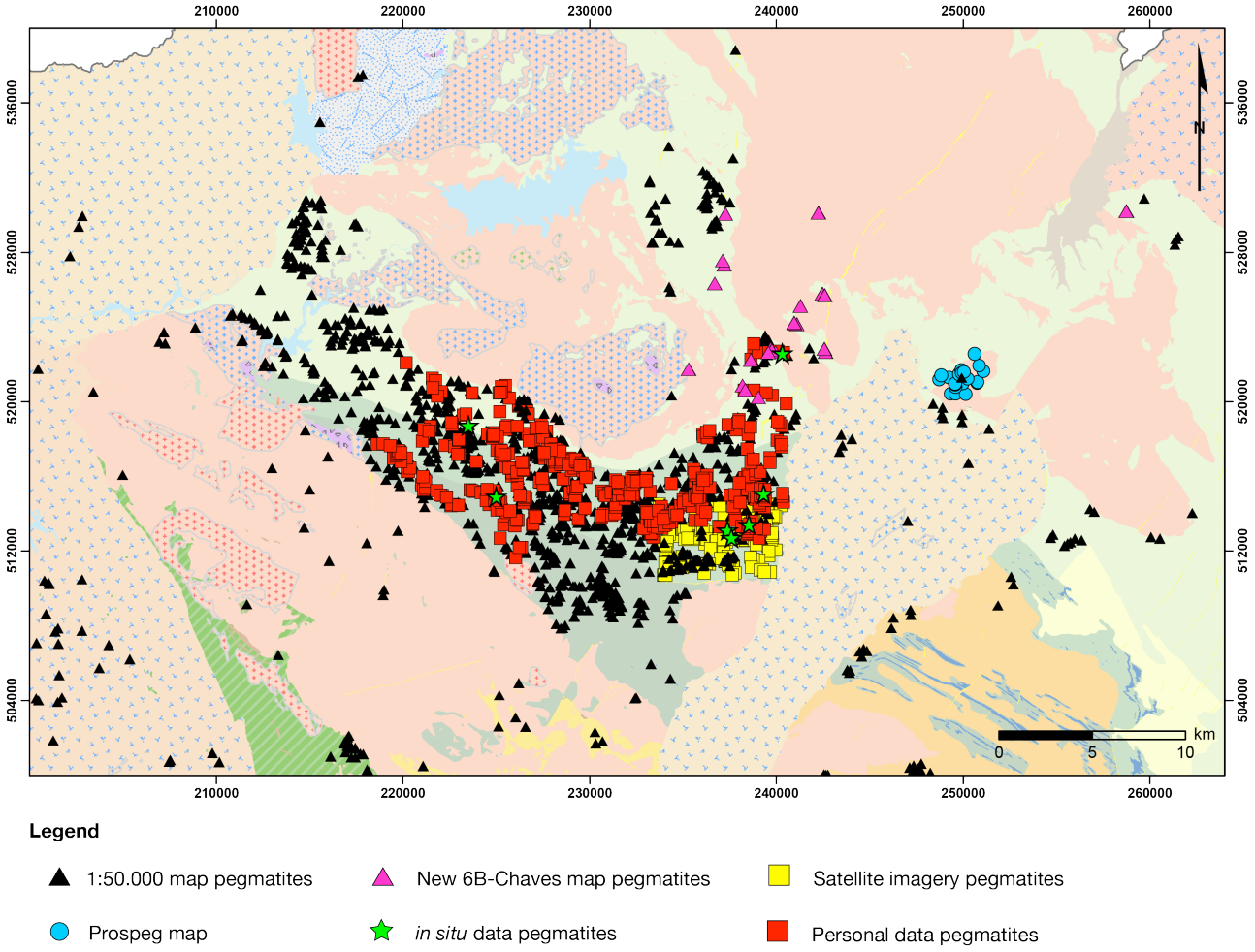

Fig.15 Point layer representing the complete set of pegmatite data, classified by compilation source.

3. 2. 2. FAULTS AND THRUST FAULTS LAYER

The content of the faults and thrust faults layer (Fig. 16) was compiled using the next informational sources: i) Geological maps of Portugal from the nº6 1:50.000 series [6A-Montalegre (Martins and Noronha, 1982), 6B- Chaves (Teixeira and Medeiros, 1969), 6C-Cabeceiras de Basto (Noronha, 1992), and 6D- Vila Pouca de Aguiar (Noronha *et al.,* 1998)]; ii) Geological map of Portugal 1:200.000, sheet nº2 (Pereira *et al.,* 2001); iii) Map included in publication Prospeg project – pegmatite remote sensing and mapping. Final report, 2013); iv) Satellite imagery [World Imagery MapServer from Esri ArcGIS; Landsat 7 ETM+ cover;

Shuttle Radar Topography Mission (SRTM), 2000].

Respecting the geological maps at 1:50.000 scale, the data was compiled digitalizing as lines all the faults and thrust faults (*i.e.* known, probable and concealed) observed in the maps. The dipping characteristic of individual faults was impossible to obtain, because this information is not provided in the maps. The only characteristic that was possible to extract was the orientation of each faults and thrust faults, using the GIS software for this calculation. This method to obtain the orientation was used in all the faults digitalized from the others informational sources. The method of digitalization described above was also used in the geological map of Portugal 1:200.000, sheet nº2 (Pereira *et al.,* 2001), and in the map included in the publication Prospeg project – pegmatite remote sensing and mapping. Final report (2013).

For the satellite imagery data, three different sources were used. The fault digitalization using these informational sources was used in purpose to fill the lack of fault in the 1:50.000 geological map 6B- Chaves (Teixeira and Medeiros, 1969). This lack of faults is due to the creation period of this map, 1969, when the structural aspects of the terrain were not as relevant to represent in the geological maps as today. The only faults represented in the map are almost entirely from the regional fault Régua-Verin. The other entire fault spectrum is not represented, reason why the focus for the satellite imagery digitalization is the area of the 6B- Chaves geological map. Examining the three different sources, the World Imagery MapServer from Esri ArcGIS was used for fault digitalization using the geomorphological information from is photographical terrain captures. For the Landsat 7 ETM + source, the digitalization was done using a 3-band (1, 2, 4) composite imagery with a resolution of 30 meters, permitting a good contrast between geological structures. Finally, the SRTM data with 90 meters resolution was used to create two Digital Elevation Models with two different angular solar expositions (45º and 135º), to better differentiate the geomorphological structures and improve the fault recognition. These three sources were used with the objective to acquire the most representative set of faults for the chosen area and to validate the choice for the interpreted fault digitalization.

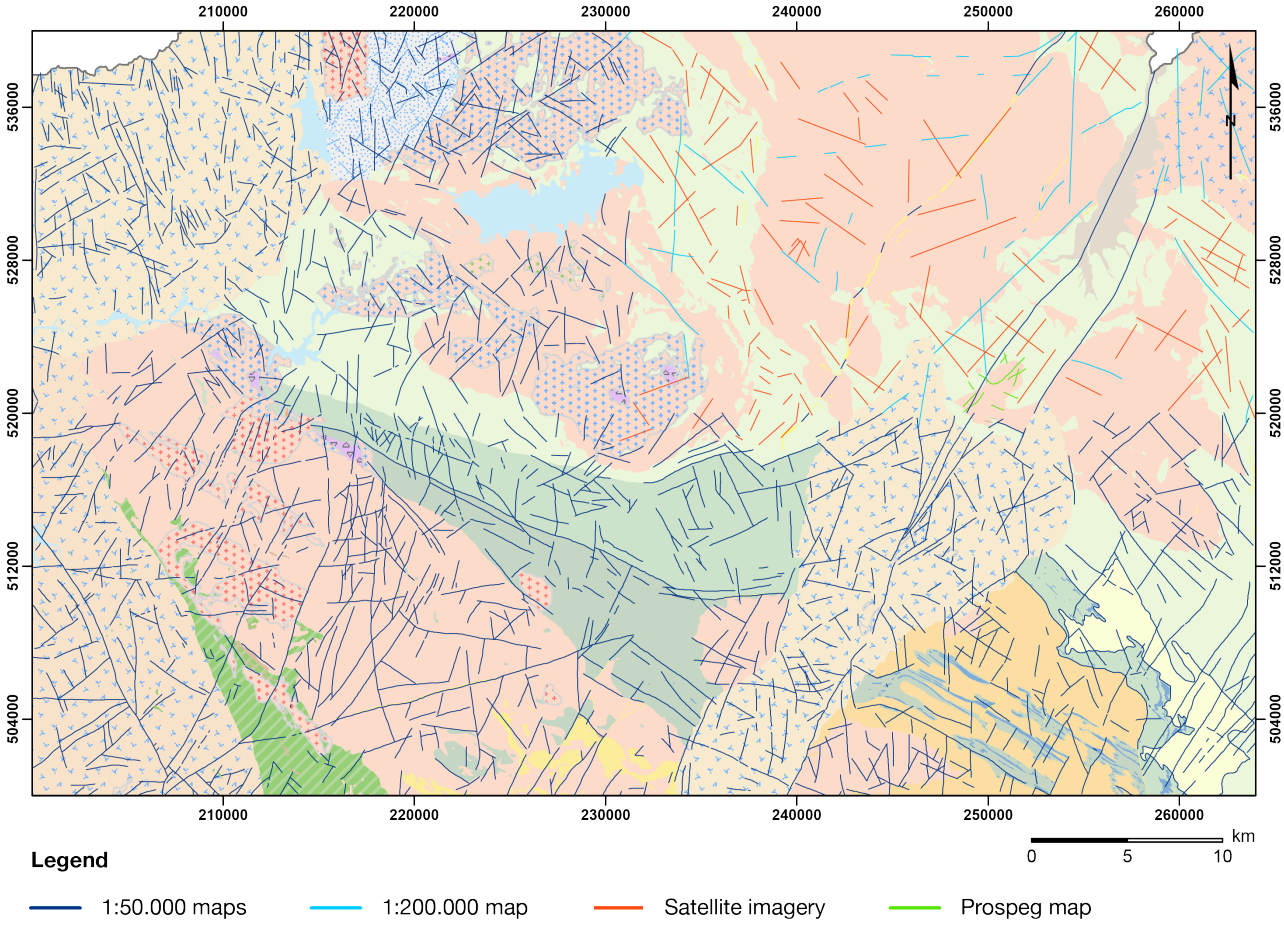

Fig. 16 Line layer representing the complete set of faults and thrust faults data, classified by compilation source.

3. 2. 3. METASEDIMENTS FOLIATION LAYER

For the metasediments foliation line layer (Fig. 17), the content was acquired with only two informational sources: i) Geological maps of Portugal from the nº6 1:50.000 series [6A- Montalegre (Martins and Noronha, 1982), 6B- Chaves (Teixeira and Medeiros, 1969), 6C- Cabeceiras de Basto (Noronha, 1992), and 6D- Vila Pouca de Aguiar (Noronha *et al.,* 1998)]; and ii) Map included in Ramos (2012).

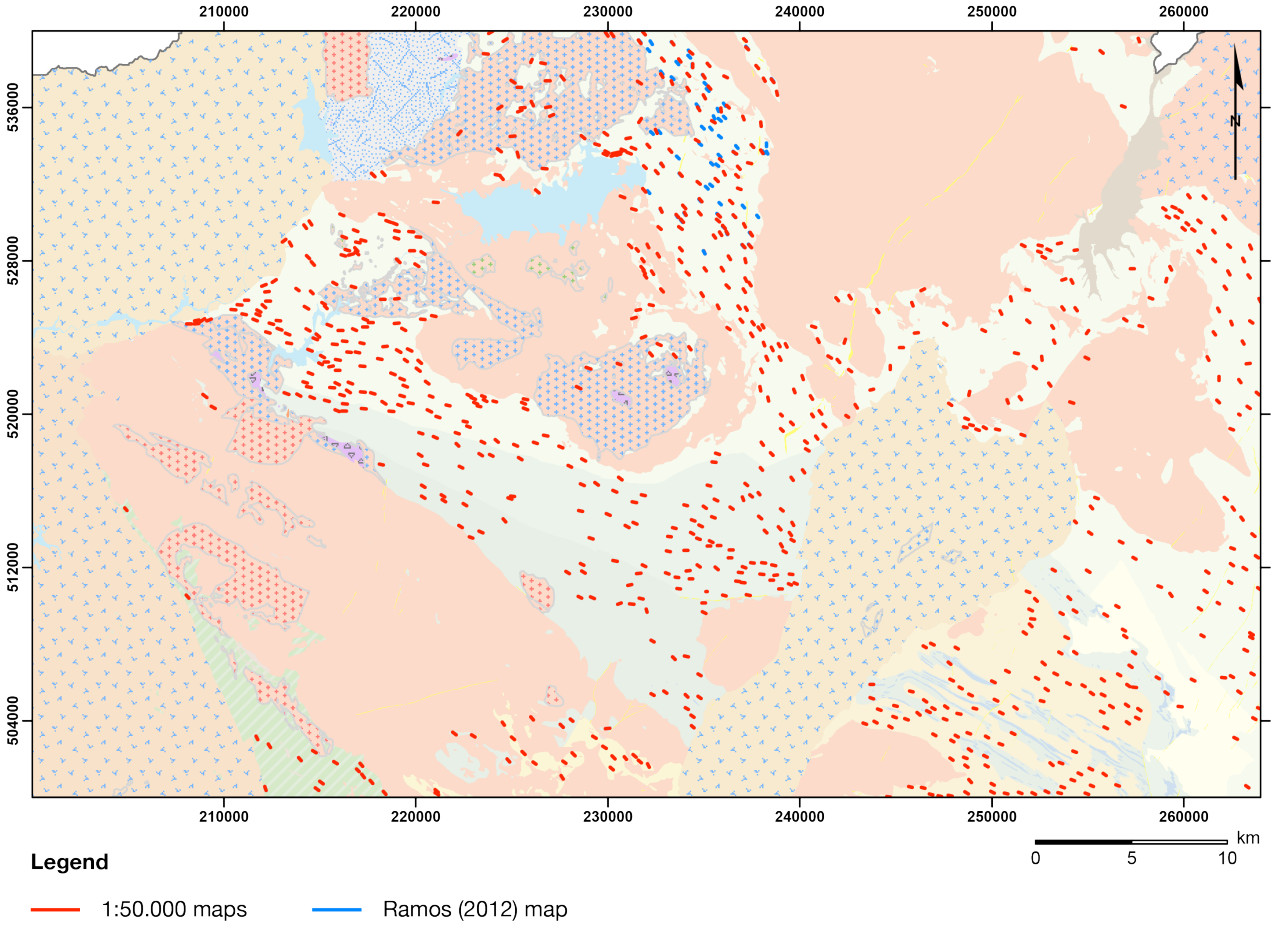

Fig. 17 Line layer representing the complete set of foliation data, classified by compilation source.

The digitalization process was similar to the previous pegmatites and faults digitalization. Each foliation observed in the maps was digitalized as a line, and is dip and dip direction characteristics compiled into the database layer. The orientation was later extracted using the extension EasyCalculate for ArcGIS software. Not all the foliations were digitalized, only the S3 foliation, because the S1 and S2 dip are frequently lower than 45º and the S3 foliation are always sub-vertical. This choice was made because of the chronological order of the regional cleavage, in which S3 is the last foliation created within Barroso-Alvão region, and the dense and highly visible presence of these foliations in the hinge zone of regional folds. A difficulty appeared when the foliation digitalization process reached the 1:50.000 geological maps 6A- Montalegre (Martins and Noronha, 1982), and 6B- Chaves (Teixeira and Medeiros, 1969). The problem lies in the fact that, in these maps, the foliation are not correlated and classified into the three regional deformation phases. We assume that the foliation represented in these maps are S3 foliations, because the S3 foliation is the most penetrative and represented in this region. The use of the map from Ramos (2012) for foliation

digitalization helped to validate our assumption about the S3 foliation from 6- A and 6- B maps.

3. 2. 4. LITHOLOGY LAYER

The content of the lithology polygon layer (Fig. 7 in Chapter 2) was compiled using the next informational sources: i) Geological maps of Portugal from the nº6 1:50.000 series [6A- Montalegre (Martins and Noronha, 1982), 6B- Chaves (Teixeira and Medeiros, 1969), 6C- Cabeceiras de Basto (Noronha, 1992), and 6D- Vila Pouca de Aguiar (Noronha *et al.,* 1998)]; ii) Geological map of Portugal 1:200.000, sheet nº2 (Pereira *et al.,* 2001).

For the Barros-Alvão aplitopegmatitic field, the polygon layer was created with the intention to unify the different geology, using their description and symbology, from the four geological maps at 1:50.000 scale. This task was not easily completed because of the almost forty years that separate the youngest and the oldest maps. To difficult this task even more, the 6B- Chaves map (oldest) and the 6D- Vila Pouca de Aguiar map (youngest) are edge-to-edge with each other. The criteria for rock classification changed over the forty years that separates these two geological maps. Some parts of the maps that were necessary unify, for example, the lithology in one of the maps is granitic and in the other is a metasediment. To resolve this problem, the geological map of Portugal at 1:200.000 scale was used to simplify this issue between sectors in the 6B and 6D map and also between 6B and 6A map.

The classification for the different lithologies was done using the classification proposed in the geological maps 6A, 6C and 6D. The granitic rocks were classified using a structural divisor (Sin-, Late or Post-D3; see section 2.3) combined with a mineralogical classification representing the mica content. The metasediments are classified following their structural level, composition and deformation. The continuity of the lithological classification over the years between the maps 6A, 6C and 6D is assured, because of the participation of Professor Fernando Noronha (Porto University) has the mapping manager for these three geological maps.

3. 3. STATISTICAL ANALYSIS OF THE COMBINED LAYERS

The Barroso-Alvão region shows a total of 1924 pegmatites occurrence, which 1828 (95%) of them are emplaced in the metasediment host lithology and 96 (5%) in the remainder lithologies. From these residual 96 pegmatites in other lithologies, 93 (4,8%) are situated in granitic lithology and 3 (0,2%) in migmatites. The ratio of pegmatites emplaced in granite versus metasediment is approximatively 1:20. Regarding the Li-mineralized pegmatites, in the 1924 total pegmatites, 78 (4%) of them are mineralized with Li minerals spodumene, petalite and lepidolite as the most representative phases. These mineral phases, regarding the major mineral phase present, were used to classify the pegmatites into three classes: i) **Spodumene pegmatites** (54 occurrences); ii) **Petalite pegmatites** (22 occurrences); and iii) **Lepidolite pegmatites** (2 occurrences). All the remainder pegmatites are unknown respecting their mineralization content.

The rectangle used to represent the study area as a dimension of 2560 km^2, in which the N-S extent is 40 km and the E-W extent is 64 km. Inside the rectangular study area, the granitoid lithology emerge as the dominant lithology with 1600,25 km^2 (62,5%), followed by the metasedimentary lithology with 854,35 km^2 (33,4%). Because of the disparity observed in Fig. 15 for the lithological localization of pegmatites, the spatial distribution analysis of pegmatites was carried using only the pegmatites within the metasediment host lithology (1828 occurrences). Moreover, a constriction was applied to the area of the pegmatites within metasediments lithologies (Fig 18). This reduction in the study area was necessary to obtain more precise results in the pegmatites distribution, particularly because of a visually obvious large concentration of pegmatite [1627 occurrences (89%)] in this specific sector of Barroso-Alvão pegmatitic field. The fact that all the 78 Li-mineralized pegmatites are emplaced in this sector also strengthened the choice made.

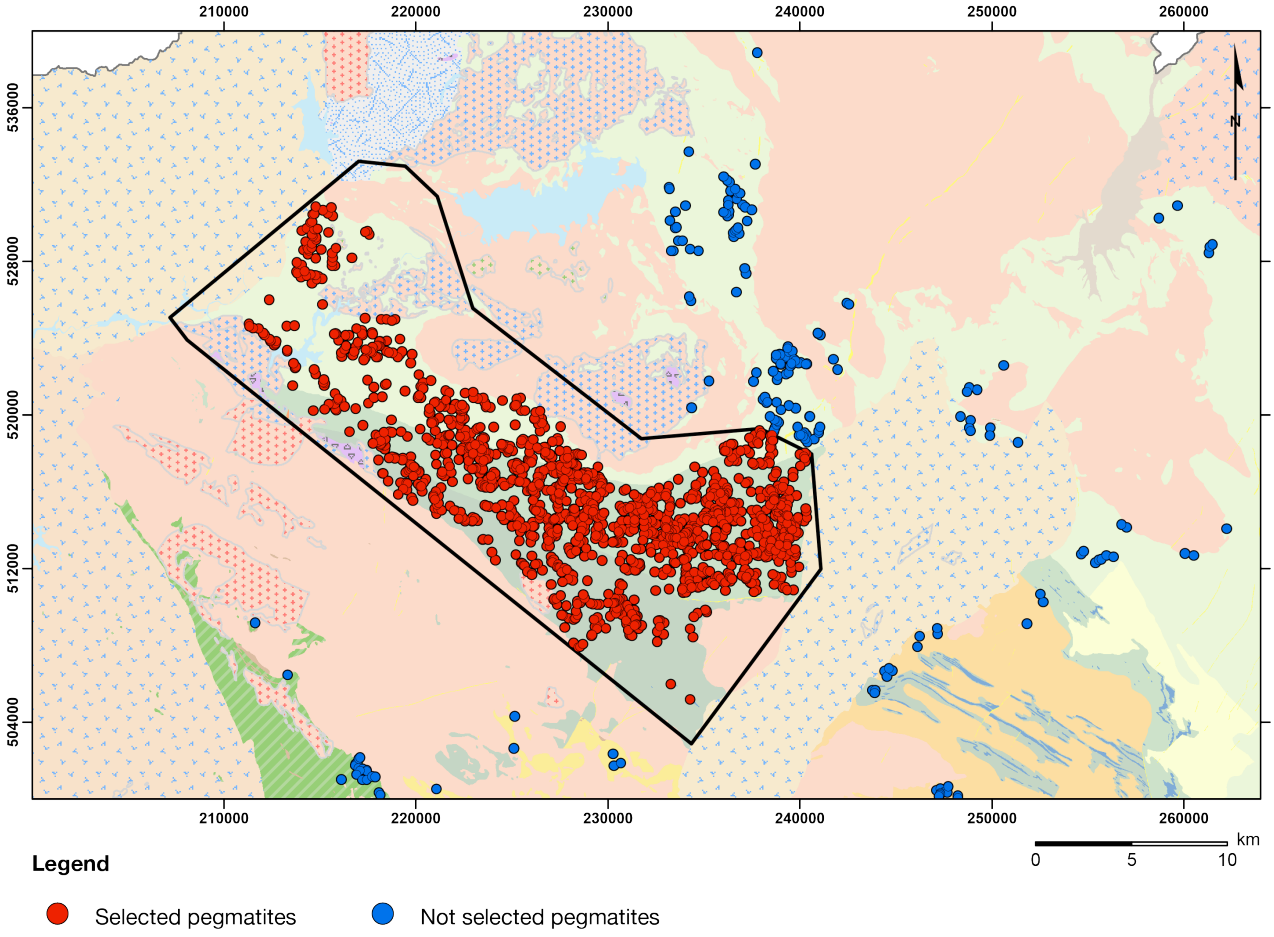

Fig. 18 Map of the selected pegmatites for the following spatial statistical analysis used in this study.

All the subsequent chosen analyses for this study followed the objective of describing the spatial association between the pegmatites emplaced in the Barroso-Alvão aplitopegmatitic field surrounding lithologies and structures presented in the anteriorly described layers. Some spatial relationships are easily observed in a map if the relations between the structures displayed are visually obvious. Unfortunately, these visually obvious relations are not common, and when observable, they lack in analytical information. It is precisely because of these difficulties that spatial statistical analysis are used in this study, to obtain analytical information that supports a regional model of pegmatites emplacement, and the relation with these pegmatites and the surrounding geological structures.

CHAPTER 4

RESULTS

CHAPTER 4 - RESULTS

4. 1. SPATIAL DISTRIBUTION ANALYSIS OF PEGMATITES

4. 1. 1. DISTANCE TO NEAREST NEIGHBOR (DNN)

4. 1. 1. 1. METHODOLOGY

The analysis of spatial point pattern can be achieved using different methodologies as Fry analysis (*e.g.* Fry, 1979) or fractal analysis (*e.g.* Carranza, 2009b). For this study, to characterize and quantify the overall spatial distribution of the Barroso-Alvão pegmatite, the alternative method Distance to Nearest Neighbor (DNN) was applied. This statistical method was developed by Clark and Evans (1954) to obtain a measure of the spacing of individuals in a population of known density, and the spatial relationship in this population. To achieve the pretended results, this statistical method calculates the nearest neighbor index, in 2D map view, based on the average distance from each feature to its nearest neighboring feature. Complementary to the nearest neighboring distance measure, in the DNN calculation a R ratio is given, representing a measure of the degree to which the distribution pattern of the observed population deviates from random expectation. R ratio as a range from 0 for the maximum aggregation, where individuals occupy the same locus, to 2.1491 for the maximum spacing between individuals distributed in an even, hexagonal pattern.

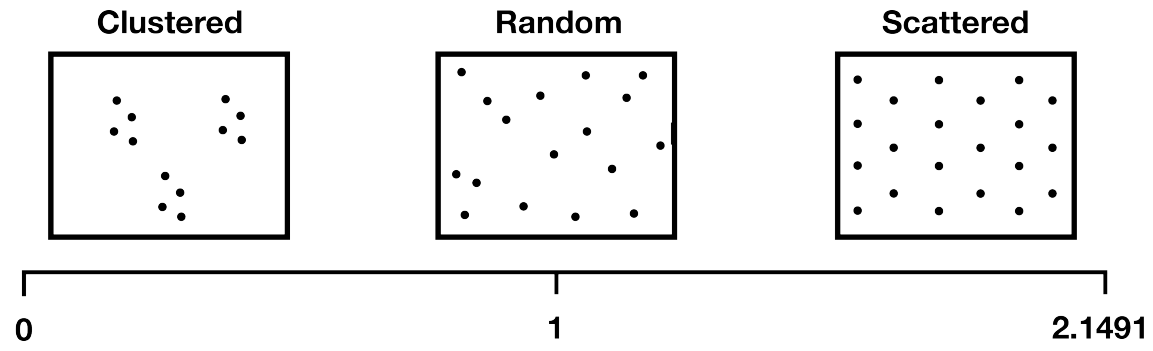

Fig. 19 Basic types of point patterns and R ratio range (Adapted from Carranza, 2009b).

The R ratio value is given with the formula:

$$R = \frac{\bar{r}_A}{\bar{r}_E} \quad (1)$$

where $\bar{r}_A$ is the observed average DNN value and $\bar{r}_E$ the average DNN distance for a perfectly random spatial distribution [see Clark and Evans (1954) for more details about the calculation].

This statistical method is widely applied in geosciences, among others, in mining exploration studies (*e.g.* Carranza, 2009b), volcanology (*e.g.* Bleacher *et al.*, 2009) or geomorphology (*e.g.* Wilkins and Ford, 2007), as well as in other branches of science.

4. 1. 1. 2. RESULTS

Analysis of the frequency distribution of the computed DNN for the 1627 pegmatites occurrences, shows an average neighbor distance of 143 m, a minimum distance of 5,6 m and a maximum distance of 1613 m. To obtain the calculation area necessary to complete the DNN methodology, a buffer was created using all the 1627 pegmatites (Fig. 20a, b and c). This buffer was calculated using the same maximum distance (1613 m), obtained in the frequency distribution of all pegmatites described above, to limit the buffer maximum distance calculation. The same exercise was also carried for all the Li-enriched pegmatites (Fig. 20a and d). In these pegmatites, the average neighbor distance obtained was 287 m, with a minimum distance of 44 m and a maximum distance of 2891 m

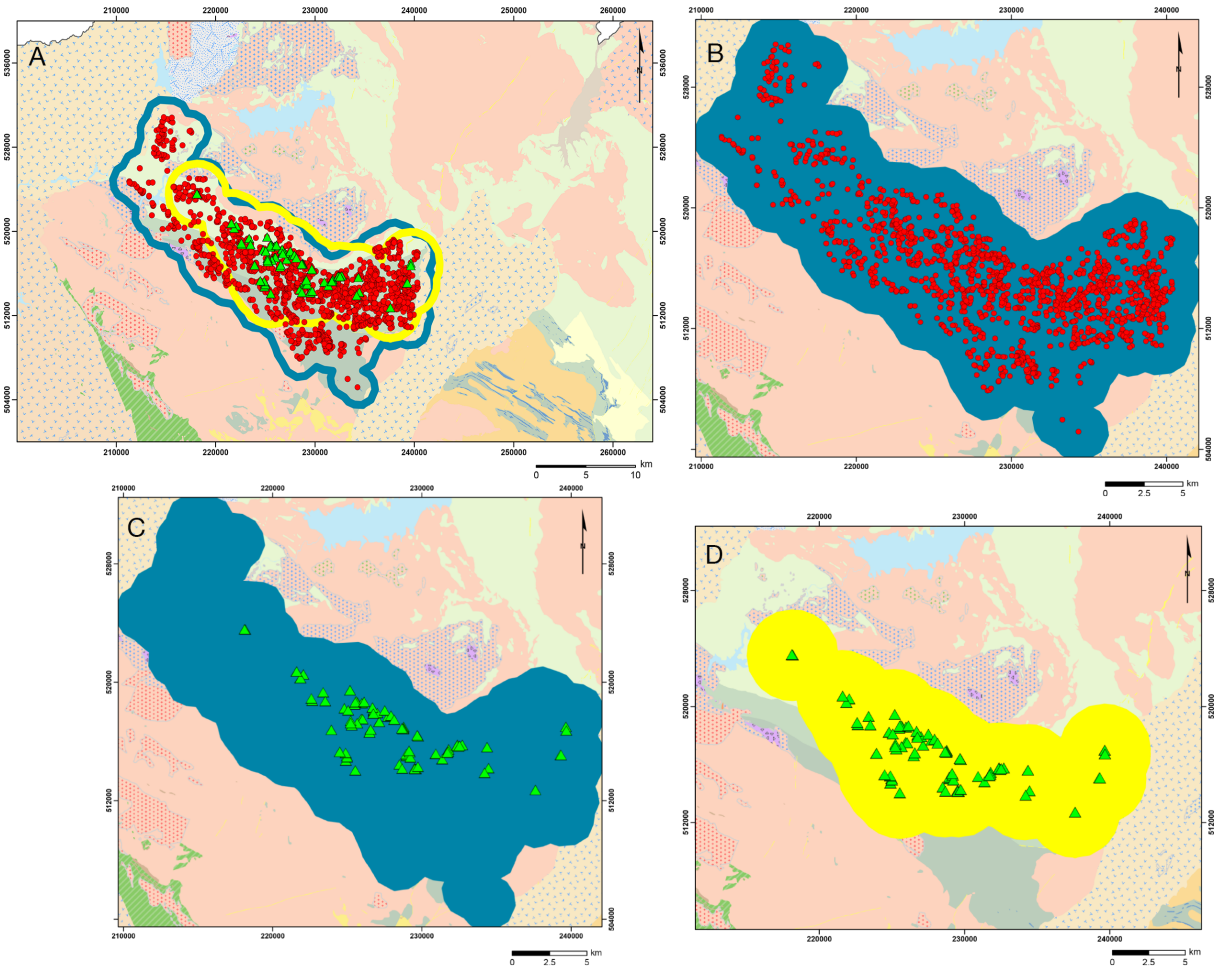

Fig. 20 Maps of the two buffers used for the DNN R ratio and Ripley's *K*-function calculation; (A) Localization of the buffers and groups of pegmatites in the study area; (B) All pegmatites group and respective buffer created from it; (C) Spatial pattern of Li-enriched pegmatites inside the buffer created from all pegmatites group; (D) Li -enriched pegmatites group and is respective buffer. Blue buffer - All pegmatites group; Yellow buffer - Li-enriched pegmatites group.

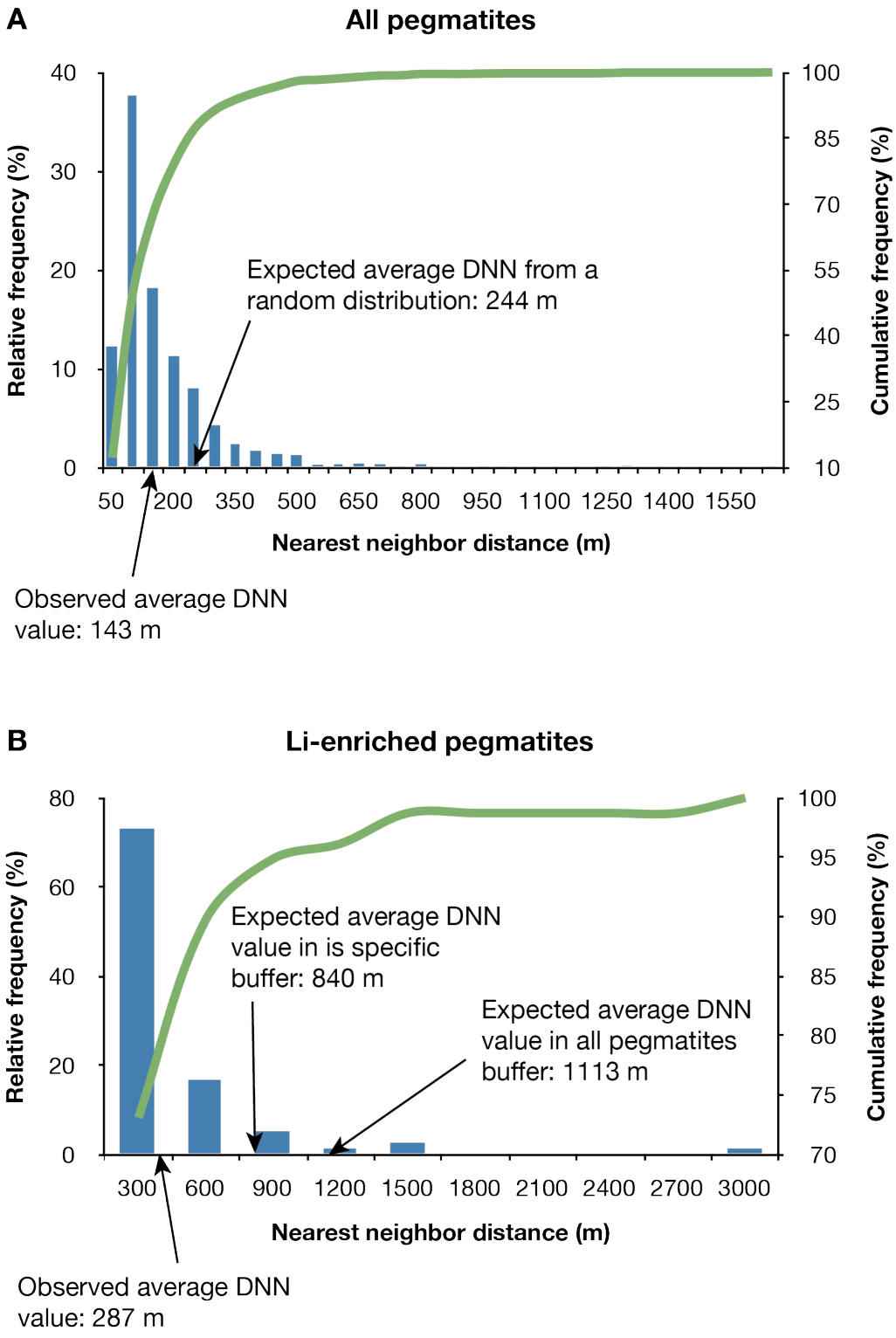

Fig. 21 Relative and cumulative frequency distribution of the DNN for the pegmatites considered in the Barroso-Alvão aplitopegmatitic field; (A) All pegmatites group DNN calculation histogram; (B) Li-enriched group DNN calculation histogram.

In Fig. 21a and b, it is possible to observe the close distal relationship existing between pegmatites. In these histograms, the large majority of pegmatites are located in the left side of the graphs, where the class distances of pegmatites nearest neighbor are smaller (143 m and 287 m for all pegmatites and Li-enriched pegmatites respectively). In the two groups of pegmatites analyzed, all pegmatites and Li-enriched pegmatites, the calculated DNN median values, 100 m and 168 m respectively, were smaller than the average DNN values for each group. This results show that more than 50% of the pegmatites occurrences, in his respective group, are at smaller distance to is neighbor than the average DNN calculated.

The calculated R ratio obtained for the total 1627 pegmatites in the high-density sector, using the respective buffer of 386,35 Km^2 (see Fig. 20c) as calculation area, is 0,59. Using the same area as previously, an identical calculation was performed for the Li-enriched pegmatites occurrences. This methodology was applied to determine if the Li-enriched pegmatites followed the same, or a different path of distribution, as the total 1627 pegmatites. The obtained R ratio of 0,26 for the Li-enriched pegmatites demonstrates a probable separated path of clustering relatively to the total pegmatite for the same area of calculation. A second R ratio calculation was applied to the Li-enriched pegmatites to strengthen the evidence of higher degree of clustering for these pegmatites. In this calculation, the difference to the previous R ratio calculation was in the buffer used as area of calculation (220,31 Km^2; in Fig. 20d). The buffer was created directly from the Li-enriched pegmatites using the maximum distance of 2891 m between these pegmatites, to limit the buffer maximum distance calculation. The R ratio of 0,34 obtained, even evidencing a smaller degree of clustering than the previous 0,26 R ratio, permits to confirm the segregated and higher degree of clustering previously evidenced for Li-enriched pegmatites relatively to the total pegmatites in the high pegmatite density sector.

4. 1. 2. RIPLEY'S *K-FUNCTION*

4. 1. 2. 1. METHODOLOGY

To complement the DNN first-order statistical analysis displayed above, another method for the spatial distribution analysis of pegmatites was applied. This method is the second-order statistic Ripley's *K*-function (Ripley, 1977). As the DNN, the Ripley's *K*-function, and its derivatives, are suited for analyzing completely mapped spatial point process data and highlights deviations from spatial random distribution of objects. Apart the similarities with

DNN point analysis, the Ripley's *K*-function is used as a test, where the null hypothesis for the point process under consideration is a homogeneous Poisson process and the alternative is that the point process exhibits clustering or scattering behavior at different scales (Veen and Schoenberg, 2006). The DNN analysis does not have this property of point process at many distance scales. This method has been extensively used in ecological sciences (*e.g.* Duncan, 1993; Haase, 1995; Stoyan and Penttinen, 2000; Rozas *et al.*, 2009) in point process data. It is possible that point pattern show a combination of effects (*e.g.* clustering at small scale and scattering at large scale). The combination can be seen as characteristic pattern in a plot of the *K*-function (Dixon, 2002).

Ripley's *K*-function express the average number of neighboring points lying at a maximum distance r from data points divided by the overall point density, as follows:

(2) $$K(r) = \frac{1}{n} \sum_{i=1}^{n} N_i(r) / \rho$$

with n the total number of points, $N_i(r)$ the number of points within a neighboring distance r of the point i from the data set and p is the overall point density value. As proposed by Besag (1977), the *K*-function can be normalized so that expected value is r (linear):

(3) $$L(r) = \sqrt{(K(r) / \pi)}$$

This first derivation can be further normalized [L'(r)] so that the expected value is 0, as a reference for the random distribution:

(4) $$L`(r) = L(r) - r$$

This second derivative of the Ripley's *K*-function [L'(r)] permits to better visualize the point distribution at various spatial scales. The constant values of L'(r) corresponds to a constant random distribution, positive values to a clustering and negative values indicates a dispersion (Kiskowski *et al.*, 2009). The slope in the graphical representation of L'(r) function is proportional to the rate of clustering/scattering for a given scale (Fig. 22).

In this study, the Ripley's *K*-function was applied only for the pegmatites within the high-density zone (see Fig. 20), following the same conclusion for the choice made previously described in the DNN calculation. The *K*-function statistic is very sensitive to the size of the study area. Identical arrangements of points can exhibit clustering or scattering depending on the size of the study area enclosing them. Therefore, to avoid this distribution discrepancies, the buffers created for all the pegmatites and for the Li-enriched pegmatites anteriorly used to calculate the DNN R ratio, were also used here in the *K*-function (Fig. 20b and d).

4. 1. 2. 2. RESULTS

Two different L'-function were computed, one in each buffer for their respective pegmatite. Regarding the L'-function computed for all pegmatites (Fig. 22), the L'(r) value increases (*i.e.* clustering) with distance and scatters immediately after r = 3600 m and becomes random at 7200 m. During the increase of L'(r), two distinctive clustering rates are observed: i) a moderate clustering rate up to 2000 m, ii) a low clustering rate from 2000 m up to 3600 m.

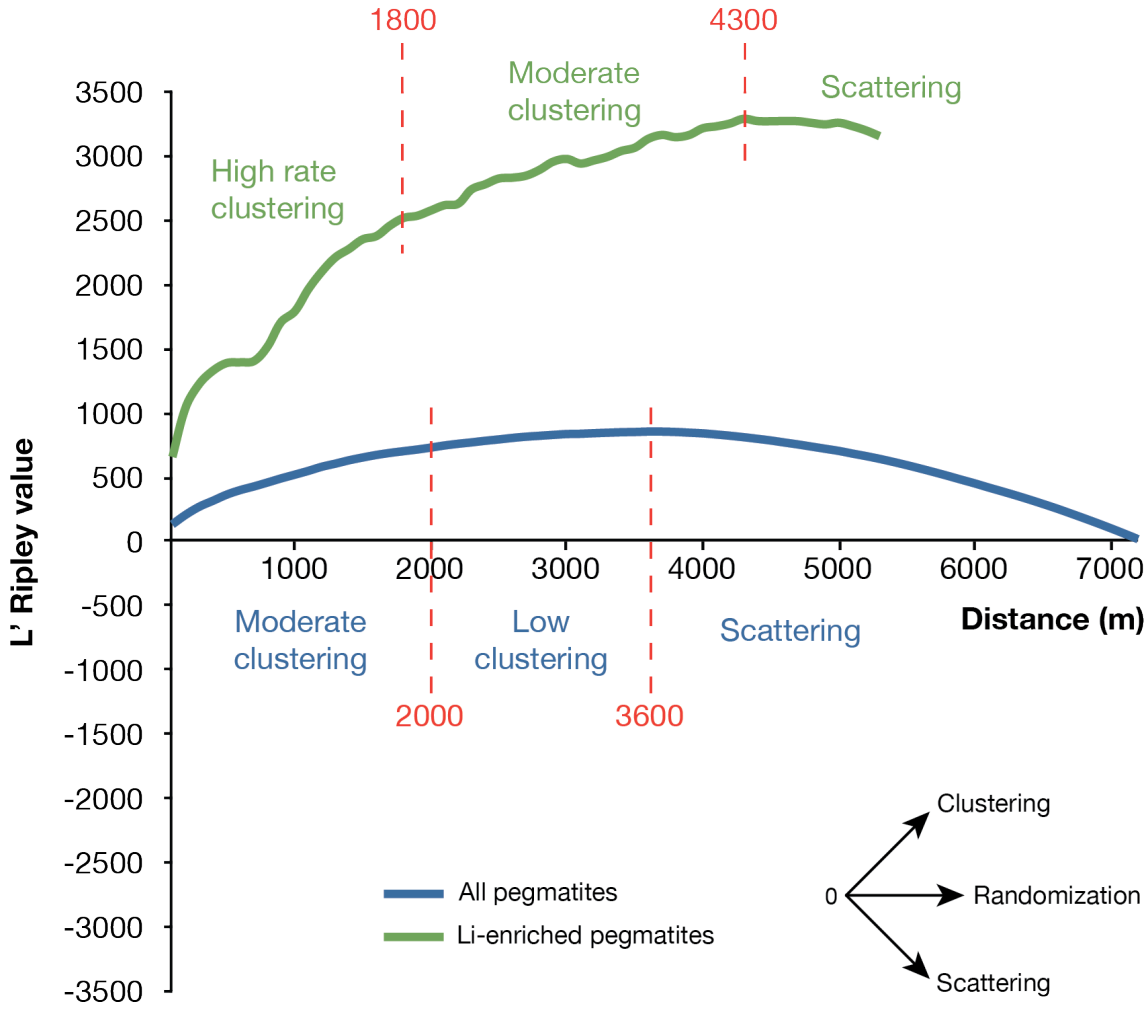

Fig. 22 Ripley's L'-function *(4)* computed to detect spatial deviation from a homogeneous Poisson distribution. All pegmatites present a Ripley L' function value = 730 for the moderate clustering rate at a distance of 2000 m and a L' function value = 854 for the low clustering rate at a distance of 3600 m. Li mineralized pegmatites present a Ripley L' function value = 2516 for the high clustering rate at a distance of 1800 m and a L' function value = 3288 for the moderate clustering rate at a distance of 3600 m.

The L'-function computed for the Li-enriched pegmatites presents different paths and clustering rates, compared with the computed values for all pegmatites. The first difference is in the maximum extent of spatial point pattern calculation. For the Li-enriched pegmatites, the maximum extent is 5300 m compared with the higher 7200 m for all pegmatites. This smaller extent for Li-enriched pegmatites show a smaller dispersion in the terrain for these pegmatites in comparison with all pegmatites. The second difference is the almost total clustering path observed and the rates of clustering presented by the Li-enriched pegmatites. The L'(r) value increases up to 4300 m, scattering from there until 5200 m (*i.e.* the maximum calculation distance extent for these pegmatites). During the increase of L'(r), two distinctive rate of clustering are observed: i) high rate of clustering up to 1800 m, ii) moderate clustering rate from 1800 m up to 4300 m. The results obtained from Ripley's *K*-function permitted to

validate the results from DNN calculation, showing that the Li-enriched presents a distinctive path and rate of clustering compared to the remainder pegmatites in the same zone.

4. 1. 3. SPATIAL DISTRIBUTION DENSITY OF PEGMATITES

4. 1. 3. 1. METHODOLOGY

The spatial distribution of pegmatites density inside the Barroso-Alvão aplitopegmatitic field was performed with the intention to highlight a possible relationship between the two groups of pegmatites considered in this study, the all pegmatites group and the Li-enrichedLi-enriched pegmatite group (Fig. 23). To achieve our goals, the density of the all pegmatites group was performed in ArcGIS 10 using the function kernel density calculation. This function calculate the magnitude per unit area, in our case km^2, from the all pegmatites points using a kernel function to fit a smoothly tapered surface to each pegmatites. Later, the spatial localization of the Li-enriched group was compared with the all pegmatites density calculation anteriorly described. Because of the major different Li minerals present in the pegmatites from the Li-enriched pegmatites group (*i.e.* spodumene, petalite and lepidolite pegmatites sub-groups), the analysis of the spatial correlation between the Li-enriched pegmatites group and the all pegmatites density was also performed individually for these three sub-groups of pegmatites different Li mineral content.

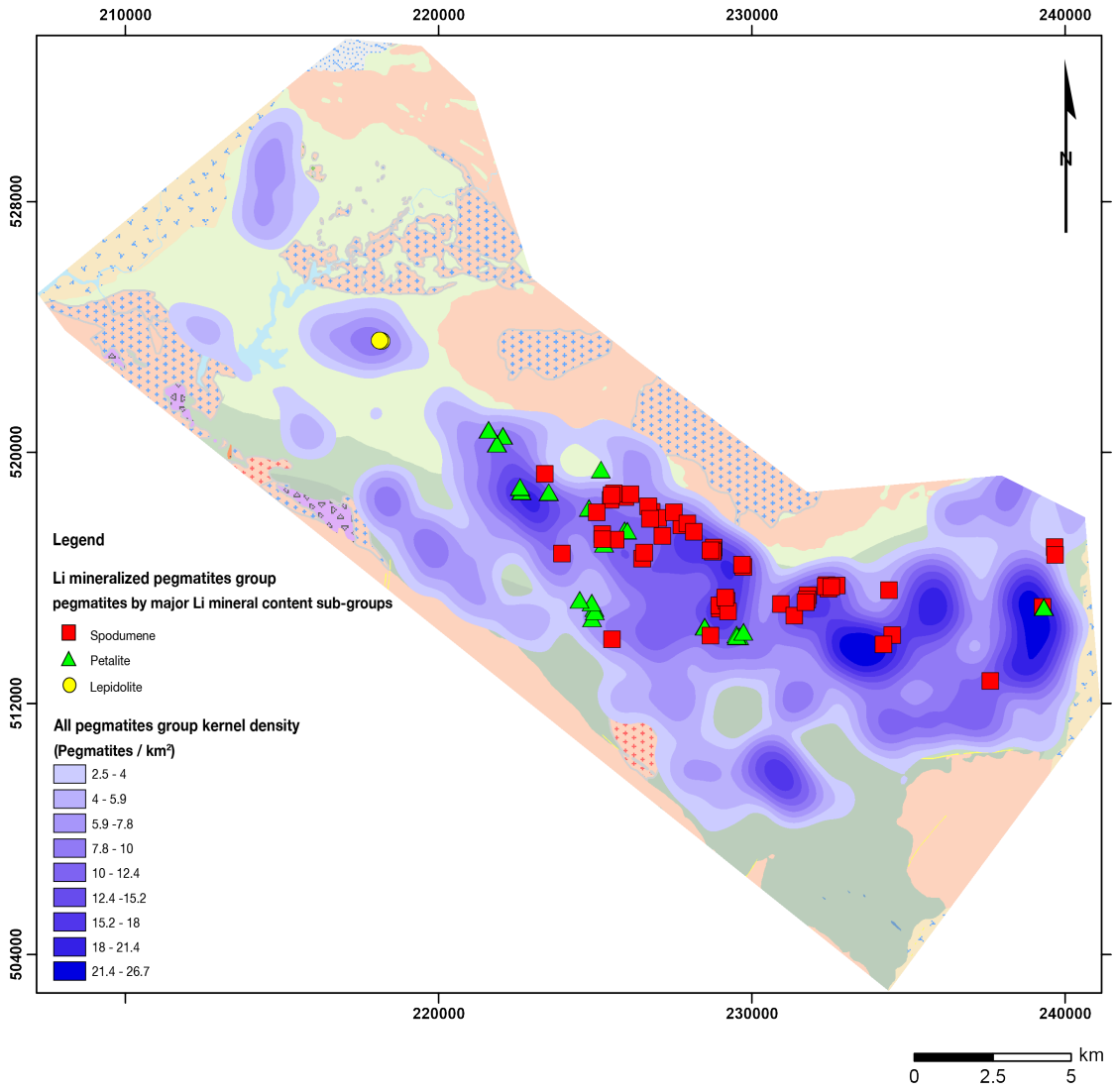

Fig. 23 Map of the kernel density (km^2) for the all pegmatites group, and spatial distribution of the Li-enriched pegmatites group and respective major Li mineral content (spodumene, petalite and lepidolite) pegmatites sub-groups.

In this study, to highlight the spatial relationship between the pegmatites emplaced in the Barroso-Alvão aplitopegmatitic field, the frequency distribution of pegmatites is always compared to a set of points evenly distributed within the same area as the corresponding pegmatites, following the method applied by Deveaud *et al.* (2013). These evenly distributed points are called reference points and are calculated relatively to the same geological neighboring unit used for the pegmatites. The comparison between pegmatite frequency distribution and the reference frequency distribution permits to categorize the pegmatites distribution into three categories, depending on the pegmatite/reference points ratio (Fig. 24). If the pegmatite/reference points frequency distribution ratio is < 1.2, the pegmatite distribution is called a Normal Distribution (*ND*); a ratio value within the range [1.2; 1.5[is a Low Abnormal Distribution (*LAD*), and for a ratio value > 1.5 the pegmatite distribution is called a High Abnormal Distribution (*HAD*).

4. 1. 3. 2. RESULTS

The analysis of the histogram representing the total Li-enriched pegmatites group distribution comparatively to the all pegmatites group kernel density (Fig. 24a) shows that the Li-enriched pegmatites frequency distribution extends from the all pegmatites density per km^2 value 2 to 24, whereas the reference distribution extends from 0 to 26. The first class in the histogram, representing the lowest pegmatites density, does not contain any Li-enriched pegmatite, but for the reference distribution it is in this class where the highest frequency value is observed (>30%). The first two classes where Li-enriched pegmatites are present, [2-4[and [4-6[, shows that the reference distribution values are much higher than the values for the pegmatites distribution, classifying therefore these two classes for pegmatite distribution as *ND*. In contrast, beyond all pegmatites density of 6, the Li-enriched pegmatites distribution is always sufficiently higher to be classified as *LAD* for the classes [6-8[and [8-10[, and as *HAD* for the classes from [10-12[to [22-24[. The only exception is the last class [24-26[where no Li-enriched pegmatites are present. These results highlights that the Li-enriched pegmatite group are apparently spatially linked to higher pegmatites density values, and especially with density values within the range 10 to 24. However, none of the Li-enriched pegmatite is emplaced within the maximum class density [24-26[.

The histogram for the spodumene-enriched pegmatites (Fig. 24b) present in the Li-enriched pegmatite group, shows the same frequency distribution extent as the total Li-enriched pegmatites, from pegmatite density 2 to 24. However, the spodumene pegmatites are absent in the class [4-6[and [20-22[from this range. The first density class where spodumene pegmatites are present shows a frequency distribution strongly inferior compared to the reference frequency distribution, classifying this class as *ND*. Identically to the total Li-enriched pegmatites, it is beyond the pegmatite density value of 6 that the spodumene pegmatites distributions become statistically abnormal, exception to the class [8-10[. Within the range density 6 to 24, the density class [6-8[is the only classified as *LAD*. All the other classes from this range presenting abnormal distributions show spodumene pegmatites with a *HAD* type.

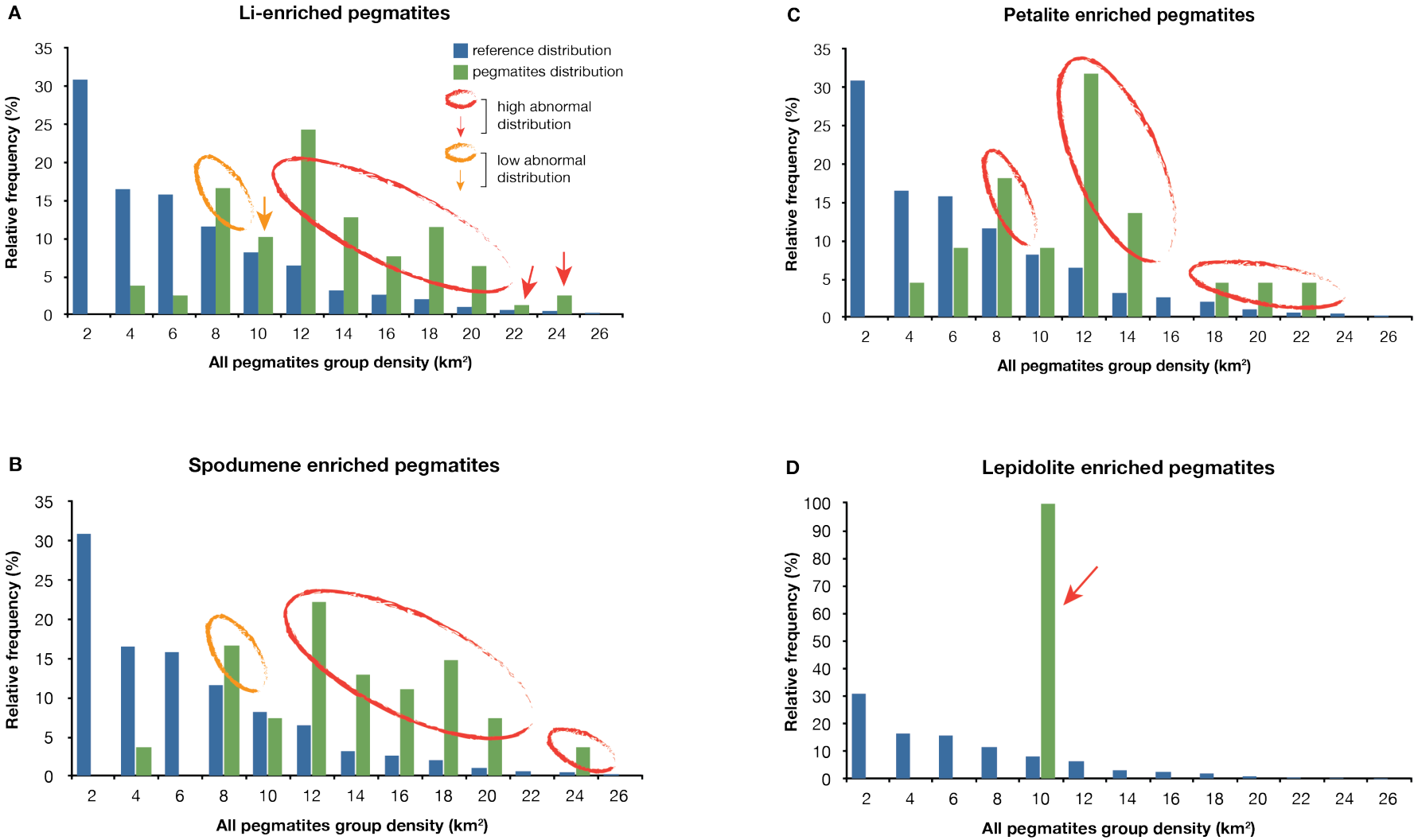

Fig. 24 Histograms representing the Li-enriched pegmatites group and respective sub-groups distribution comparatively to the all pegmatites group kernel density.

The petalite-enriched pegmatites histogram (Fig. 24c) shows a distribution extent slightly shorter than the previous total Li-enriched and spodumene pegmatites, from 2 to 22. Other differences observed comparatively to the Li-enriched pegmatite distribution are the absence of petalite pegmatites in the density class [14-16[, and in absence of *LAD* pegmatites type for this sub-group. It is beyond the pegmatite density of 6, as seen for the total Li-enriched and spodumene pegmatites, that the abnormal pegmatites distributions are observed. Different to the previous histograms, the petalite-enriched pegmatites presents a *HAD* for all the abnormal distribution beyond the pegmatite density of 6, exception for the class [8-10[with an *ND* type and the aforementioned absence of petalite pegmatites in the class [14-16[. The spodumene and petalite-enriched pegmatites present approximately a similar spatial distribution as observed in the total Li-enriched. Comparing the spodumene and petalite-enriched pegmatites, the petalite pegmatites, as a whole, are apparently emplaced in lower pegmatites density relatively to the spodumene pegmatites.

The lepidolite pegmatites sub-group presents only two occurrences in all the study area, with almost the same spatial emplacement. Because of that reduced number of occurrences and almost the same localization for the two occurences, the lepidolite pegmatites frequency distribution histogram (Fig. 24d) presents lepidolite pegmatites only in the [8-10[class of pegmatite density. However, even presenting a reduced number of pegmatites, these pegmatites show apparently the same spatial correlation with the higher pegmatite value density observed in the previous pegmatites group and sub-groups.

4. 1. 4. SPATIAL EMPLACEMENT OF PEGMATITES ORIENTATION FAMILIES

4. 1. 4. 1. METHODOLOGY

As described by several authors (*e.g.* Charoy *et al.*, 1992; Lima, 2000; Martins, 2009) and also described in the numerical description of the Barroso-Alvão pegmatites in the beginning of this chapter, the Barroso-Alvão aplitopegmatitic field presents a large set of almost two thousand pegmatites occurrences. Observing the emplacement of the pegmatites in the study area from the digitalized pegmatite layer and using field measurements from the authors described before as examples, we observed that this large set of pegmatites does not present the same orientation of pegmatite emplacement in the entire Barroso-Alvão

aplitopegmatitic field. To better understand the pegmatites emplacement from the Barroso-Alvão region, it is essential to classify these pegmatites into orientation families, to extract paths or regions of preferential pegmatites emplacement. The classification into orientation families permits to visualize: i) a range of pegmatites orientation without the background noise from the other families, ii) better understand if the different families of pegmatites follow the same emplacement mechanism, and iii) the interaction between the different families of pegmatites.

The pegmatites grouping into orientation families were achieved using the 1616 pegmatites orientation from the all pegmatites group database. In the database, the number of pegmatites orientation is slightly inferior from the total number of pegmatites in the all pegmatites group because of 11 pegmatites, essentially Li-enriched pegmatites, do not present accessible orientation data. These pegmatites were represented in maps and extracted as points without data about their orientation. All the 1616 values were transformed from 0º-360º to 0º-180º to facilitate the visualization of the histogram for the frequency distribution of pegmatites orientation (Fig. 25).

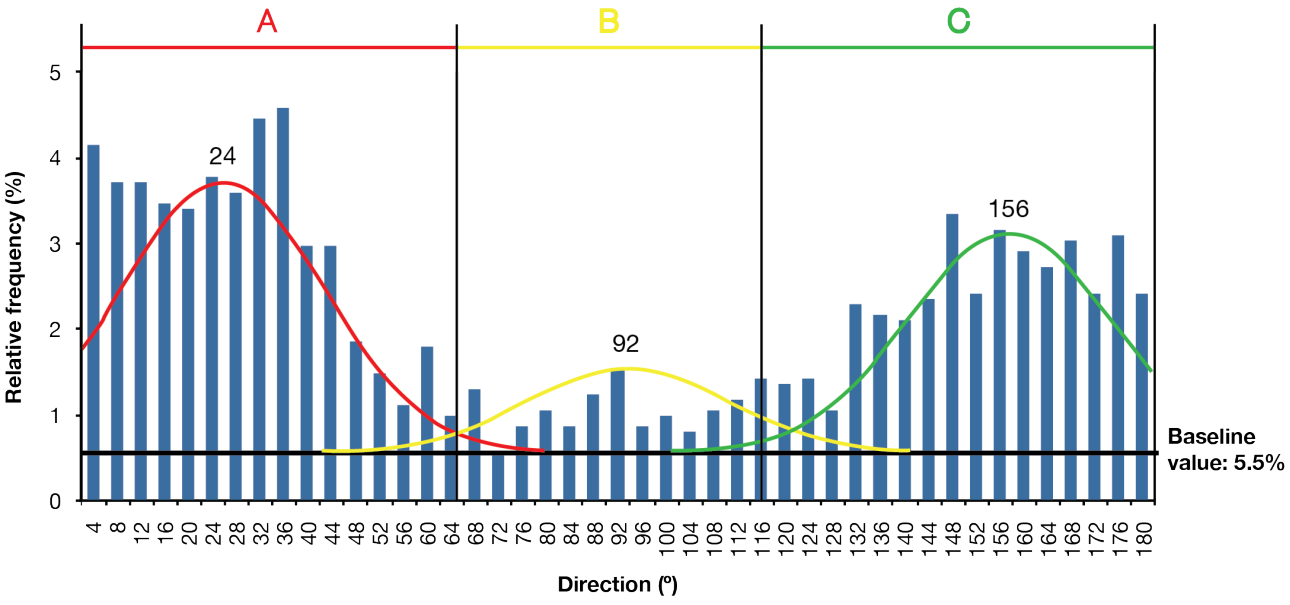

Fig. 25 Histogram representing the domainal distribution of the pegmatites orientation by families.

To obtain the best-fit decomposition calculation of the frequency distribution histogram (Fig. 25), the software PeakFit was used. This software computed the deconvolution of the values using a Gaussian type function and a rather low base level value of 0.6% (representing the noise in the pegmatites orientation data set). The distribution of the pegmatites orientation was entirely decomposed into three classes families: **i)** A class family (n = 775)

from N0º to N63º (including N180º as directional data are of circular type) with a maximum at N24º; **ii)** B class family (n = 216) from N64º to N113º with a maximum at N92º; **iii)** C class family (n = 625) from N114º to N179º with a maximum fixed at N156º.

4. 1. 4. 2. RESULTS

After the calculation of the three pegmatites orientation families, these three classes of orientation were applied to the pegmatites layer to create maps displaying only one family at a time (Fig. 26).

In the A class family pegmatites orientation map (Fig. 26a), we observe that the spatial distribution of this pegmatite family covers approximately all the study area, with higher density cluster of A family pegmatite localized in the eastern part of the study area. This sector is also where the highest densities of pegmatites are found in all Barroso-Alvão region. It is also observed that the A family pegmatites show a preference (88% of the pegmatites) for the emplacement in upper stratigraphic levels (Sb and Sc unit from the Carrazedo structural domain).

The B class family map (Fig. 26b) shows a pegmatite spatial distribution to be almost entirely concentrated in the central and eastern sector of the study area, with a preference for the upper stratigraphic levels of the Sb and Sc metasedimentary units (83% of the pegmatites).

Finally, in the C class family map (Fig. 26c) we observe that these pegmatites cover almost the entirety of study area. Different to the A class family, the higher density distribution for the C class family is observed in the central sector and not in the east sector. Another differences observed are in the respectively higher (22%) and smaller (16%) spatial emplacement within the Sa and Sc unit compared to the previous families (see Fig. 26 pie charts). It is also in this pegmatite family where the pegmatites appear to follow more clearly an alignment, especially in the central sector of the study area.

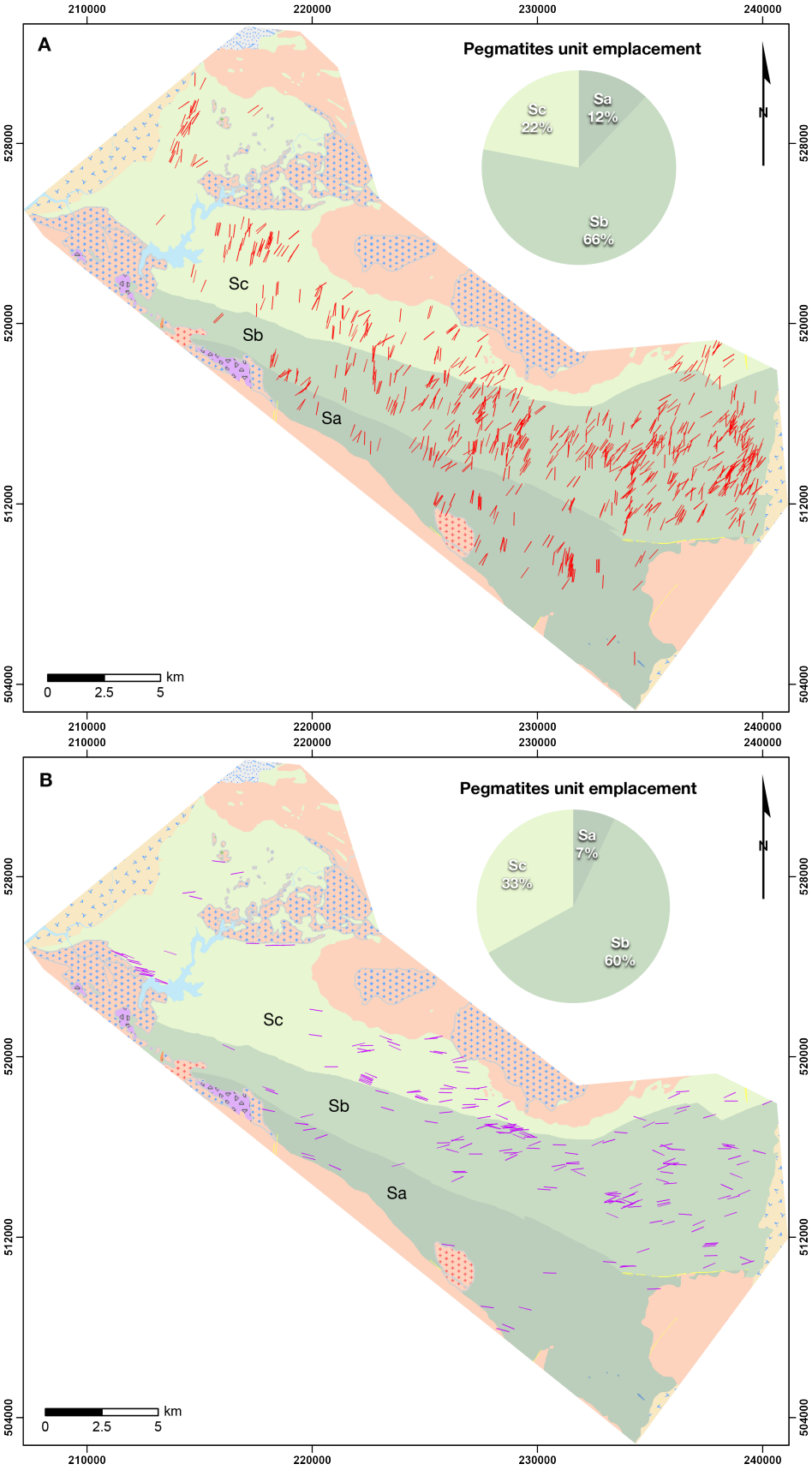

Fig. 26 Maps showing the spatial distribution and orientation of the all pegmatites group divided by family of pegmatites orientation: (A) Map of the A class family of pegmatites orientation. (B) Map of the B class family of pegmatites orientation. (C) Map of the C class family of pegmatites orientation. Pie charts illustrates the percentage distribution of pegmatites in the Sa, Sb and Sc metasedimentary units.

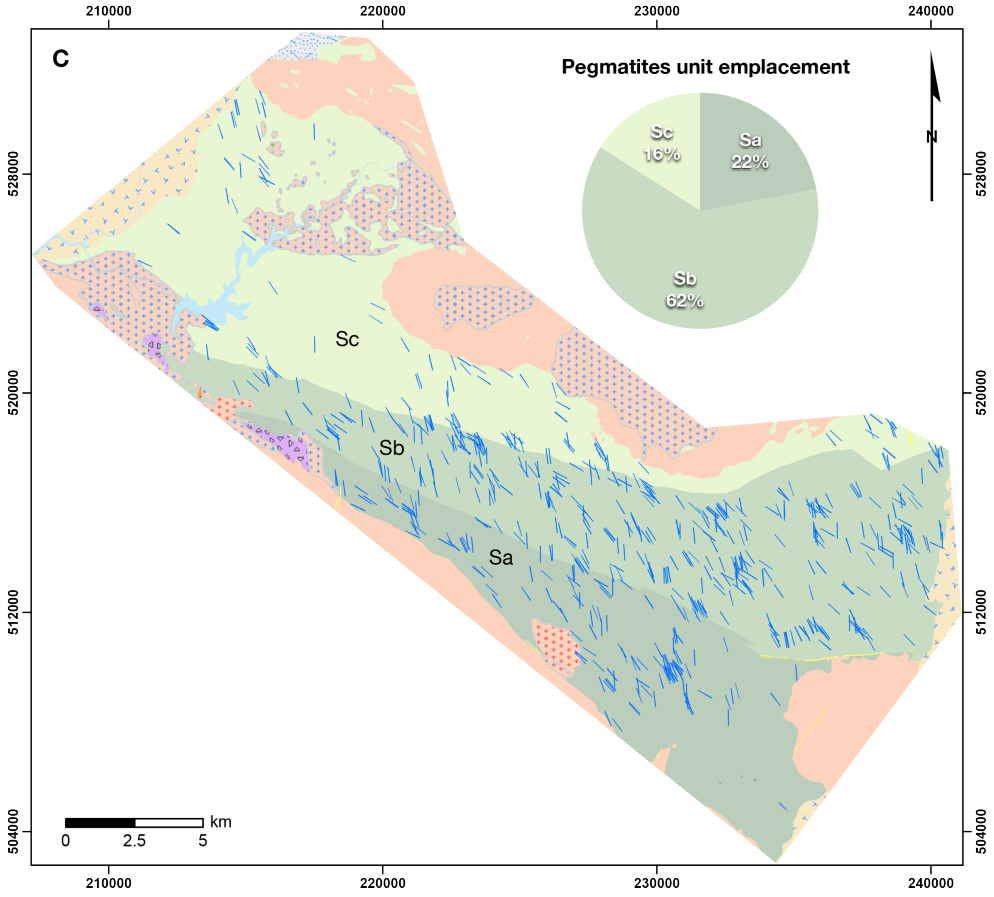

Fig. 26 (Contd.) Maps showing the spatial distribution and orientation of the all pegmatites group divided by family of pegmatites orientation: (A) Map of the A class family of pegmatites orientation. (B) Map of the B class family of pegmatites orientation. (C) Map of the C class family of pegmatites orientation. Pie charts illustrates the percentage distribution of pegmatites in the Sa, Sb and Sc metasedimentary units.

The three classes of pegmatites orientation were later applied to the Li-enriched pegmatite group, creating, as previously described for the all pegmatites group, maps displaying individually the pegmatites orientation families A, B and C (Fig. 27).

The map of the A Li-enriched pegmatites class family orientation (Fig. 27a) shows a narrower spatial extent of emplacement, compared to the distribution from the all pegmatites A family pegmatites map. Here the clusters of higher densities are localized in the east sector of the study area, as for the A Li-enriched pegmatites they are preferentially localized in the central sector. The Li-enriched pegmatites concentration in the central sector of the study area is also observed in the B and C families of Li-enriched pegmatites (Fig. 27b and c), as well as the apparent preference for the upper metasedimentary units, with almost 100% of the Li-enriched pegmatites emplaced in the Sb and Sc units.

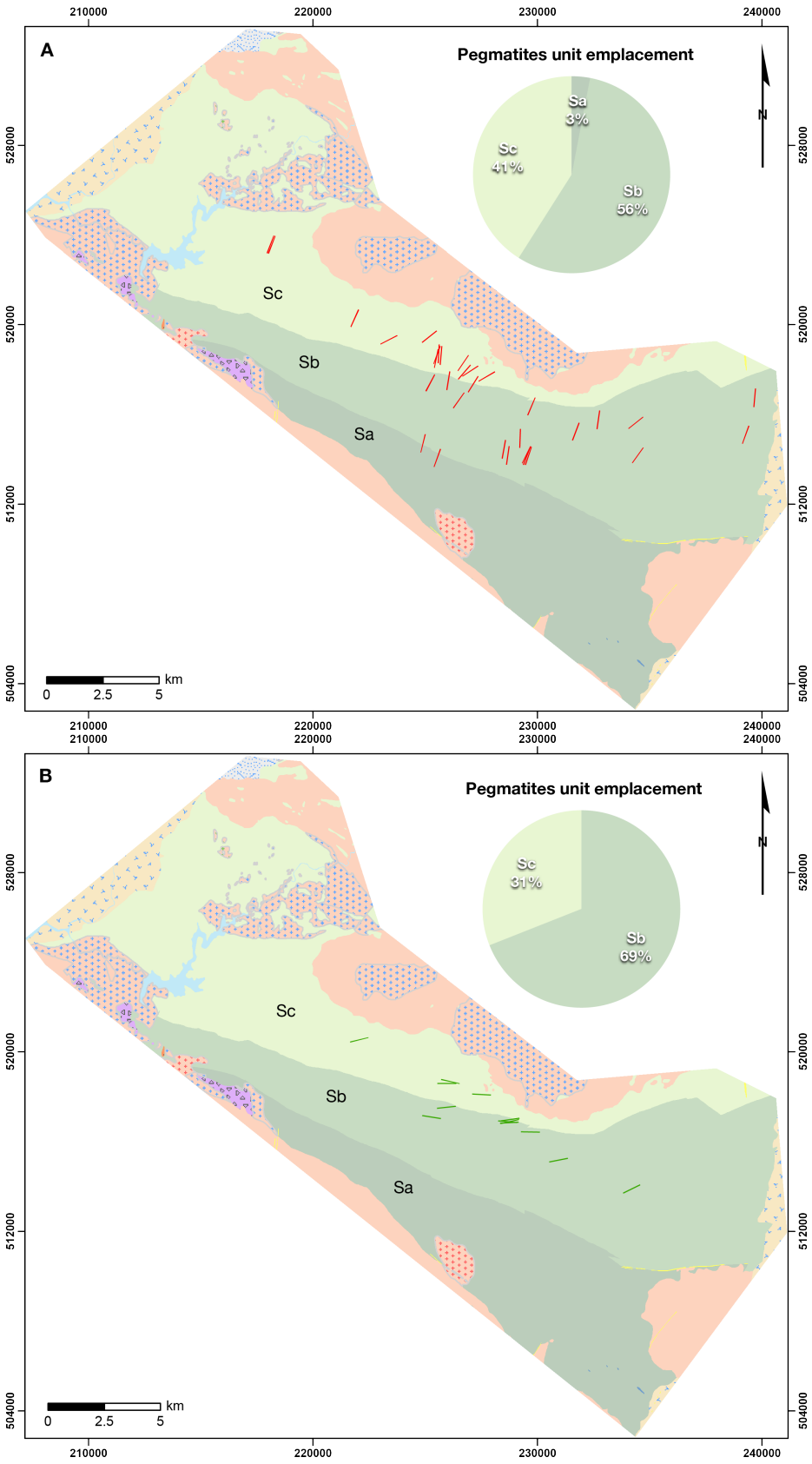

Fig. 27 Maps showing the spatial distribution and orientation of the Li-enriched pegmatites group divided by family of pegmatites orientation: (A) Map of the A class family of pegmatites orientation. (B) Map of the B class family of pegmatites orientation. (C) Map of the C class family of pegmatites orientation. Pie charts illustrates the percentage distribution of pegmatites in the Sa, Sb and Sc metasedimentary units.

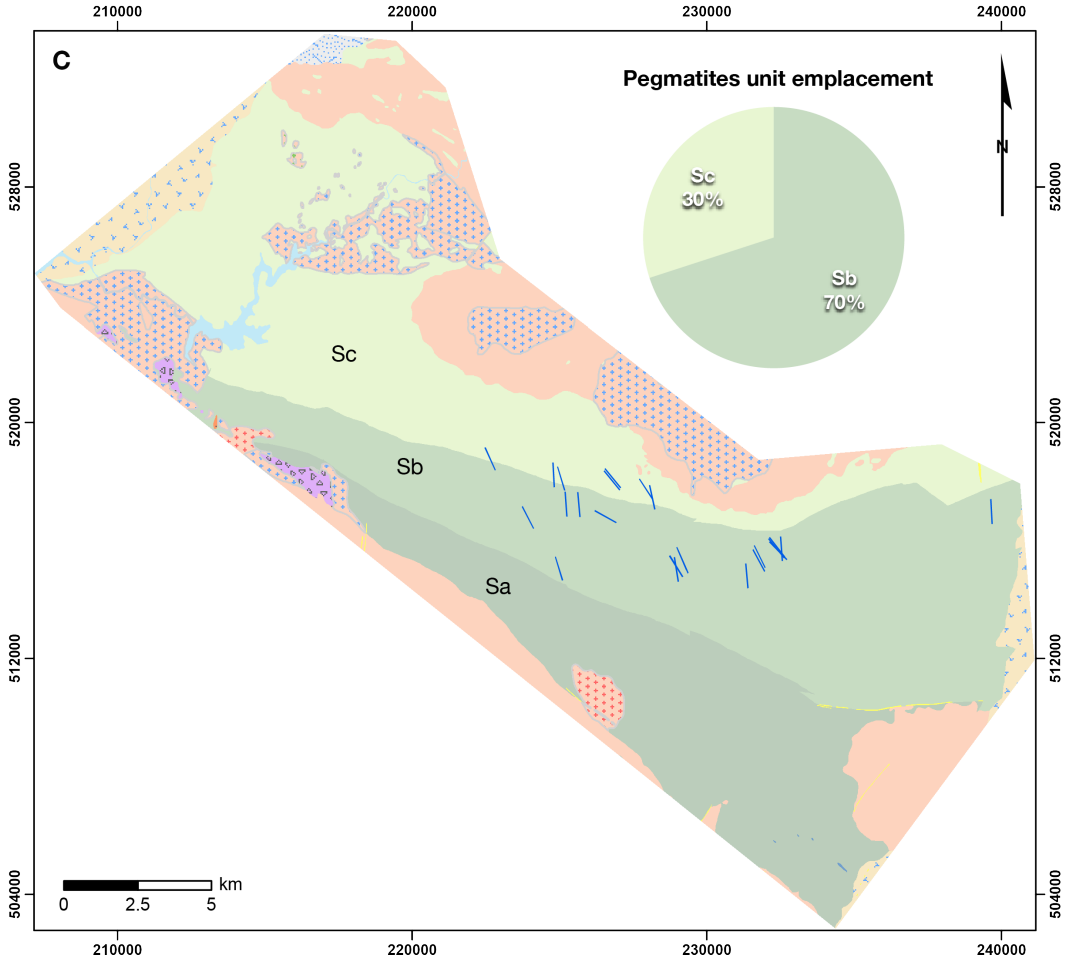

Fig. 27 (Contd.) Maps showing the spatial distribution and orientation of the Li-enriched pegmatites group divided by family of pegmatites orientation: (A) Map of the A class family of pegmatites orientation. (B) Map of the B class family of pegmatites orientation. (C) Map of the C class family of pegmatites orientation. Pie charts illustrates the percentage distribution of pegmatites in the Sa, Sb and Sc metasedimentary units.

4. 2. PEGMATITE RELATIONSHIP WITH SURROUNDING GRANITIC ROCKS

In this section, we compare the Euclidean distance spacing all pegmatites and Li-enriched pegmatite sub-groups from Barroso Pluton and Cabeceiras de Basto granite. The results from the frequency analysis of the all pegmatites group, and the Li-enriched pegmatites sub-groups regarding the shortest Euclidean distance to the surrounding granitic plutons of Barroso and Cabeceiras de Basto (Fig. 28) are displayed. The descriptive methodology using reference points to describe the distribution as *ND*, *LAD* or *HAD* previously used in this study is also followed here, to highlight any anomalous distributions.

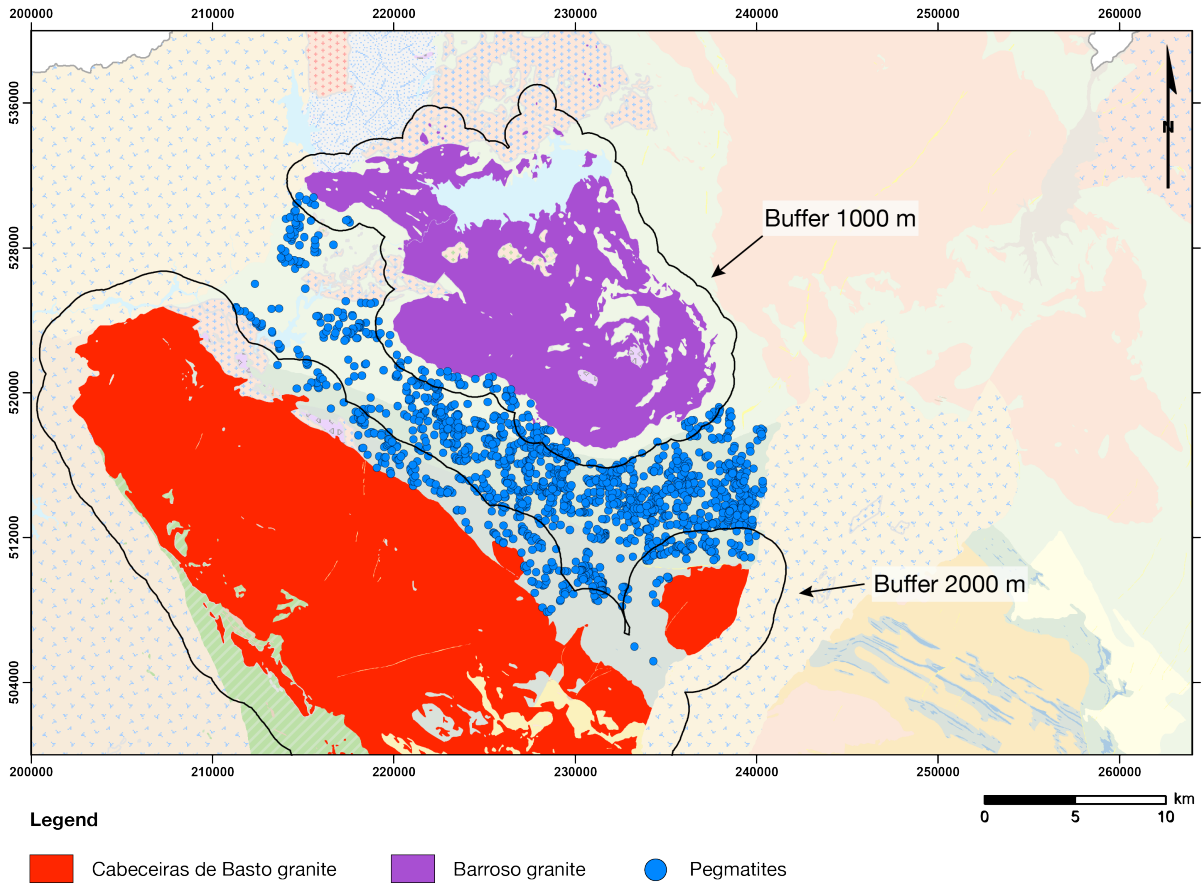

Fig. 28 Map highlighting the two granite from the study area used for the pegmatite distance relationship analysis. Buffers of 1000 and 2000 m are displayed to help the visualization of the pegmatite distance from the selected granites.

4. 2. 1. DISTANCE ANALYSIS BETWEEN PEGMATITES AND BARROSO GRANITIC PLUTON

The all pegmatites group spatial distribution extends from 0 to 12300 m, whereas the reference point distribution is slightly more extensive, from 0 to 14100 m (Fig. 29a). The total pegmatites present an average distance from the Barroso pluton of 3844 m. The first three classes of distance, from [0-300 m[to [600-900 m[, show that the frequency distribution for the reference point in this range of distance are always superior than the pegmatites distribution, representing 6% of the total pegmatites. For this range, the frequency distribution between pegmatites and reference points show also an almost perfect anti-correlation. The range of distance from [900-1200 m[to [4500-4800 m[is where the majority of pegmatites are emplaced (62%) and it is also in this range where the pegmatites are observed to display the only *LAD* and *HAD* type in all the study area. The pegmatites presenting *LAD* type are present in the classes of [900-1200 m[, [1800 to 2400 m[, [2700 to 3300 m[and in the [4500-4800 m[,

representing 28% of the total pegmatites. The *HAD* type are only present in three class of distance, [2400-2700 m[and [3300 to 3900 m[, representing 18% of the total pegmatites.

The spodumene-enriched pegmatites has a spatial extension up to 6000 m, which is more than 50% smaller than the extension of the all pegmatites group (Fig. 29b). The average distance from the Barroso pluton is 1937 m. From [600 m[to [2400-2700[all the classes present *HAD*. Further than 2700 m, all the pegmatites present frequency values smaller than the reference points, exception to the *LAD* class [3300-3600 m[. The spodumene-enriched pegmatites of pegmatites shows a closer relationship to the Barroso granitic pluton than the all pegmatites group.

The petalite-enriched pegmatites presents an extension from 900 to 4800 m with an average distance from the Barroso pluton of 2807 m (Fig. 29c). Similar to the spodumene-enriched pegmatites, the petalite-enriched pegmatites follows clearly a *HAD* type starting from the class [900-1200 m[, but contrary to this sub-group, this *HAD* path is observed in the complete range [900-4800 m] of extension. Only in one class where the pegmatites are present, [3900-4200 m[, the *HAD* is not observed. In 46% of is extent, 50% of the total petalite pegmatites sub-group overlaps the spodumene-enriched pegmatites *HAD* range distance.

The lepidolite sub-group pegmatites are observed only in the [1800-2100 m[distance class, locating this sub-group within the range distance where the two previous pegmatites sub-groups shows their preferential *HAD* paths (Fig. 29d).

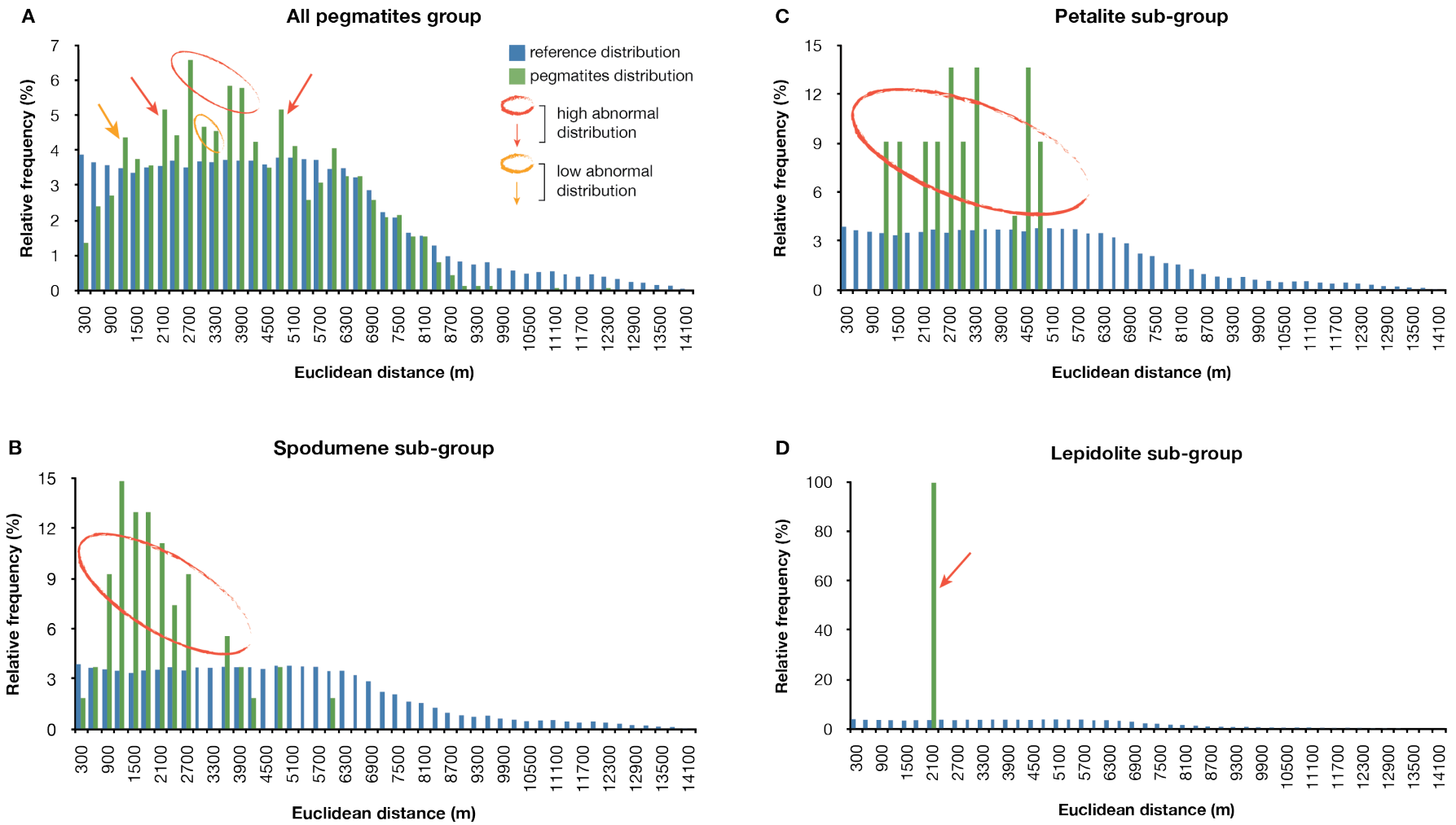

Fig. 29 Histograms representing the all pegmatites group and Li-enriched pegmatites sub-groups distance analysis from the Barroso granitic pluton.

4. 2. 2. DISTANCE ANALYSIS BETWEEN PEGMATITES AND CABECEIRAS DE BASTO GRANITIC PLUTON

The all pegmatites group spatial distribution extends from 0 to 10000 m, whereas the reference point distribution is more extensive in almost 4000 m, from 0 to 13750 m (Fig. 30a). The total pegmatites present an average distance from the Cabeceiras de Basto pluton of 3963 m. From the class of distance [2000-2250 m[to [6000-6250 m[all the pegmatite frequency values are higher than the reference points, with the exception of the class [3250-3500 m[presenting a ratio of 0.93. 70% of the pegmatites are emplaced in the range of distance from the Cabeceiras de Basto granitic pluton described above. It is also in this range where all the pegmatites with *LAD* and *HAD* type are observed. 58% of the total pegmatite present an anomalous distribution path in the study area. The pegmatites presenting *LAD* type have a more extensive class of spatial extension, [2250 to 6250 m[, compared to the pegmatites presenting *HAD*, [4000 to 5750 m[. From [6250 m[, almost no class presents pegmatites with frequency values higher than the reference points.

The spodumene-enriched pegmatites presents an extension from 2250 to 6750 m with an average distance from the Cabeceiras de Basto pluton of 5421 m (Fig. 30b). 9% of the total spodumene-enriched pegmatites are observed in the range starting from initial class [0-250 m[to [4000-4250 m[, despite this range representing more than 60% of the total spodumene-enriched pegmatites extent. In this range, it is also observed that the reference points values are always higher than the pegmatite frequency values, exception to the class [2250-2500 m[. The remainder 91% of the spodumene-enriched pegmatites is emplaced in the range distance from class [4250-4500 m[to the maximum extent 6750 m following clearly a *HAD* path, exception to the classes [5000-5250 m[and [5250-5500 m[presenting pegmatites frequency values under the reference points. The spodumene-enriched pegmatites shows an overall distribution more distant from the Cabeceiras de Basto pluton than the all pegmatites group.

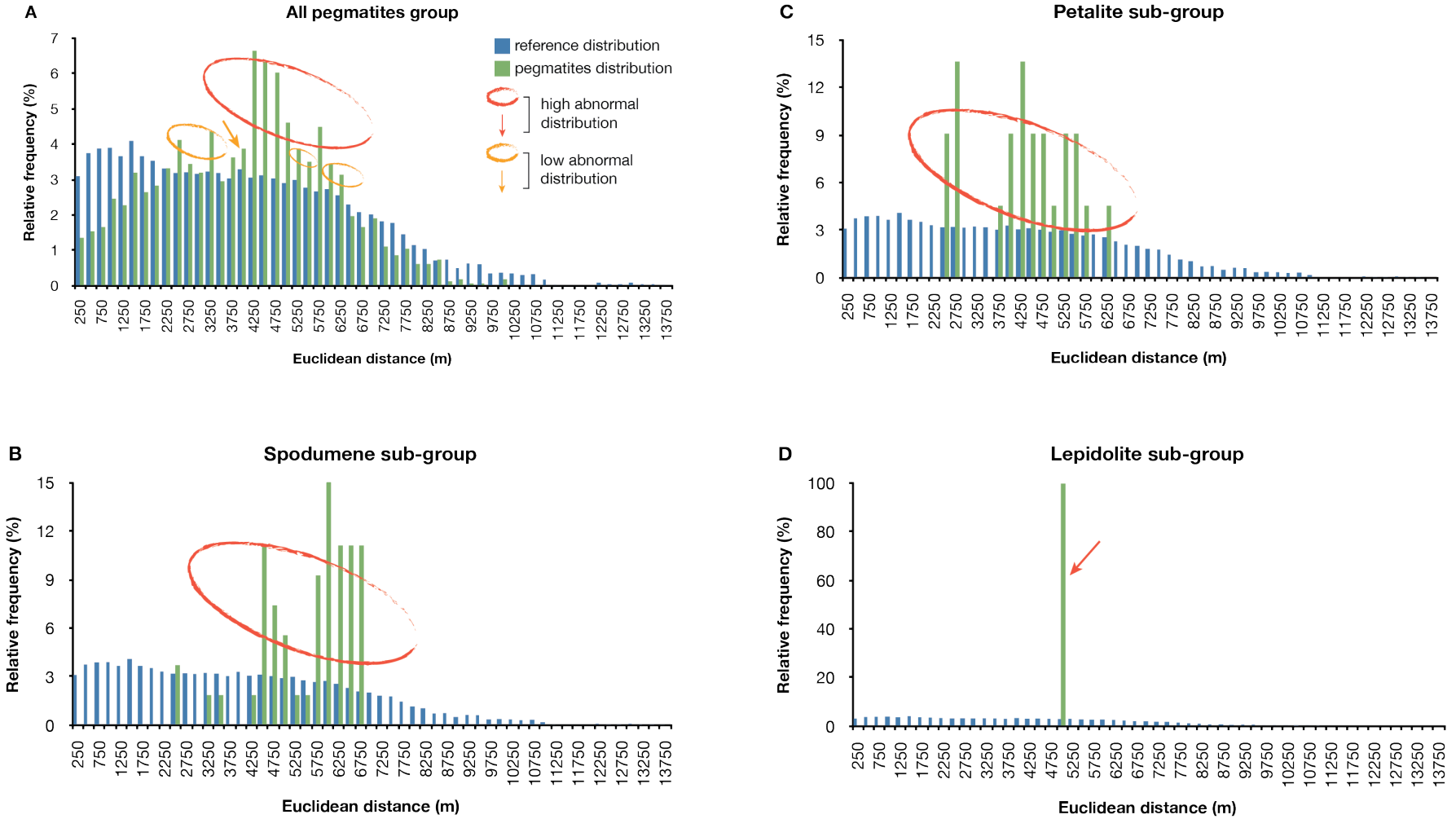

Fig. 30 Histograms representing the all pegmatites group and Li-enriched pegmatites sub-groups distance analysis from the Cabeceiras de Basto granitic pluton.

The petalite-enriched pegmatites has a spatial extension up to 6250 m and an average distance from the Cabeceiras de Basto pluton of 4176 m (Fig. 30c). As the spodumene-enriched pegmatites, the first pegmatite appearance occurs in the class [2250-2500 m[. This first observed emplacement of petalite-enriched pegmatites pegmatites marks the first range, from 2250 to 2750 m, where is observed petalite pegmatites following an *HAD* path. The second *HAD* path is localized up from 3500 m to the maximum extent of 6250 m, with the exception of the class [5750-6000 m[where no petalite pegmatite is present. 25 % of the total *HAD* observed in the petalite-enriched pegmatites pegmatites are emplaced closer to the pluton than the *HAD* range presented by the spodumene-enriched pegmatites.

The lepidolite sub-group pegmatites are observed only in the [4750-5000 m[class of distance, locating this sub-group within the range distance where the two previous pegmatites sub-groups shows preferential *HAD* paths (Fig. 30d).

4. 3. SPATIAL RELATIONSHIPS BETWEEN PEGMATITES AND FAULT-STRIKE FAMILIES

In the same manner as the anterior spatial statistical analysis described above, the all pegmatites group and the Li-enriched pegmatites group were used to perform the pegmatite relationships with the fault-strike families. Two analyses were performed: i) pegmatites distance to faults, and ii) pegmatite emplacement regarding the faults density. The same methodology applied anteriorly to obtain the Euclidean distance and the kernel density distance, was here applied for the faults in the study area.

The first step consists to obtain the fault families (Fig. 31). To obtain these families, the same methodology used anteriorly for the deconvolution of the frequency distribution of pegmatites orientation was here performed. However this time, it was applied for the selected faults in the corresponding layer, using the same area that delimited the all pegmatite group. The distribution of the fault-strikes was entirely decomposed into two families using a low base level value of 1.8%: i) Alpha family (n = 141) from N0º to N91º (including N180º as directional data are of circular type) and a maximum at N30º; Beta family (n = 193) from N91º to N179º and a maximum at N150º. These two families of faults orientation were applied to the fault layer in the GIS software to create a map displaying their spatial distribution in the study area (Fig. 32).

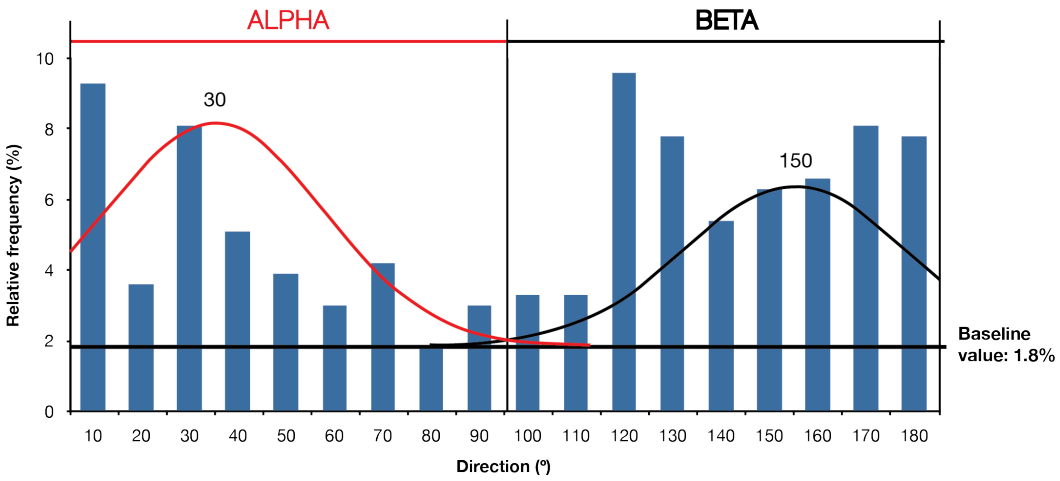

Fig. 31 Histogram representing the domainal distribution of the fault-strikes orientation by families.

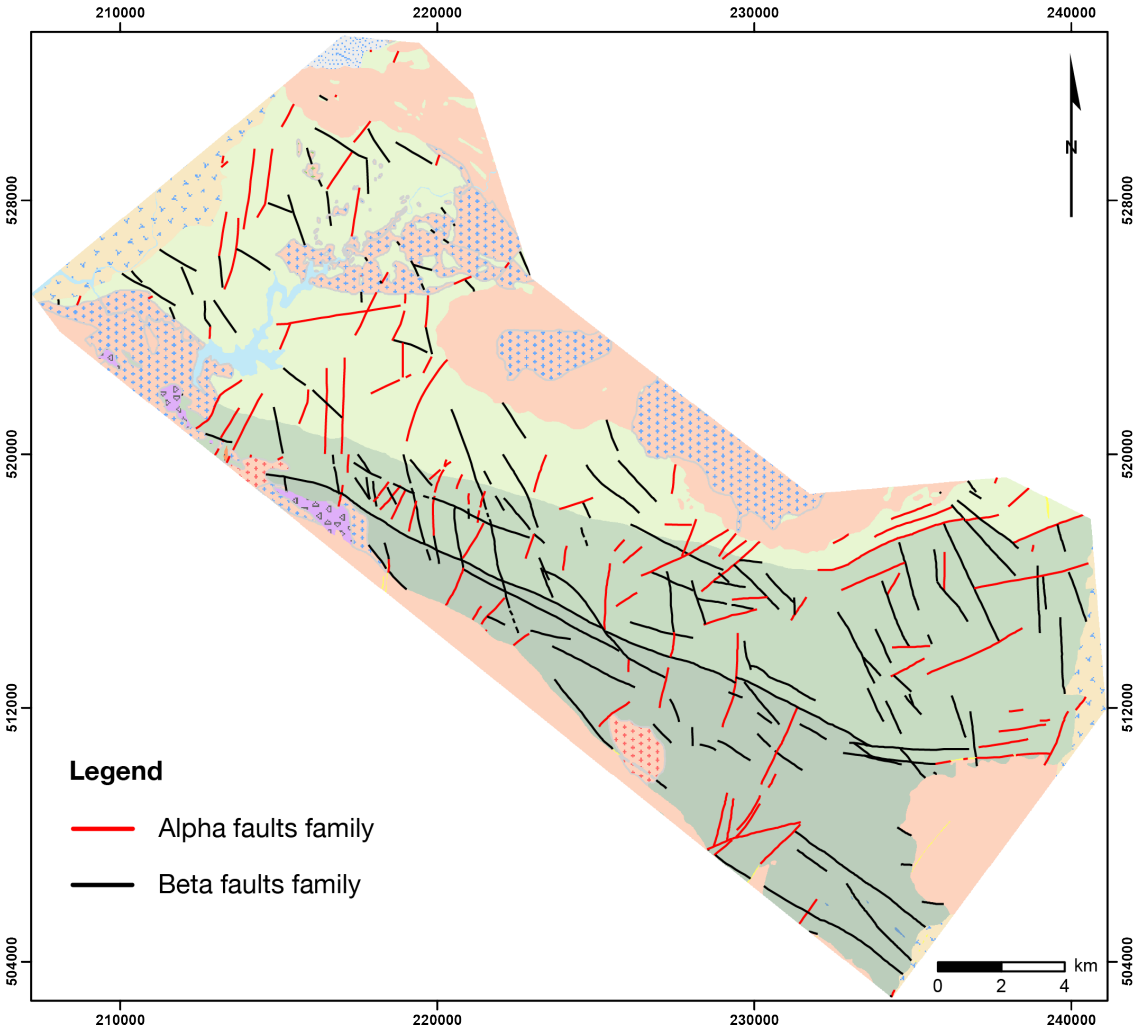

Fig. 32 Spatial distribution of the obtained alpha and beta fault-strikes families.

4. 3. 1. DISTANCE SPACING PEGMATITES FROM FAULT-STRIKE FAMILIES

4. 3. 1. 1. DISTANCE FROM ALL FAULTS

The all pegmatites group spatial distribution extends from 0 to 1440 m, whereas the reference points spatial extend slightly more, up to 1560 m (Fig. 33a). The total pegmatites and reference points present an average distance to the faults of 269 m and 278 m respectively. Three of the closest class of distance displayed in the histogram, [40 to 160 m[, show a frequency value of the pegmatites (34% of the total pegmatites) higher than the reference value. In one of this class, the pegmatites present a frequency value following a *LAD* with a ratio of 1.34. Others *LAD*'s are observed in the classes [600-640 m[, [1040-1080[and [1400-1440 m[, although for the last two, with very low frequency values of representativity (below 1%). The same path occurs for the class showing *HAD*, where the class [520-560 m[is the only one showing a representativity above 1%, in this case with a frequency value of 3%. Based on these results, the pegmatites show a slightly closer relationship below 100 m and close to 500 m to all the faults compared to the reference frequency value.

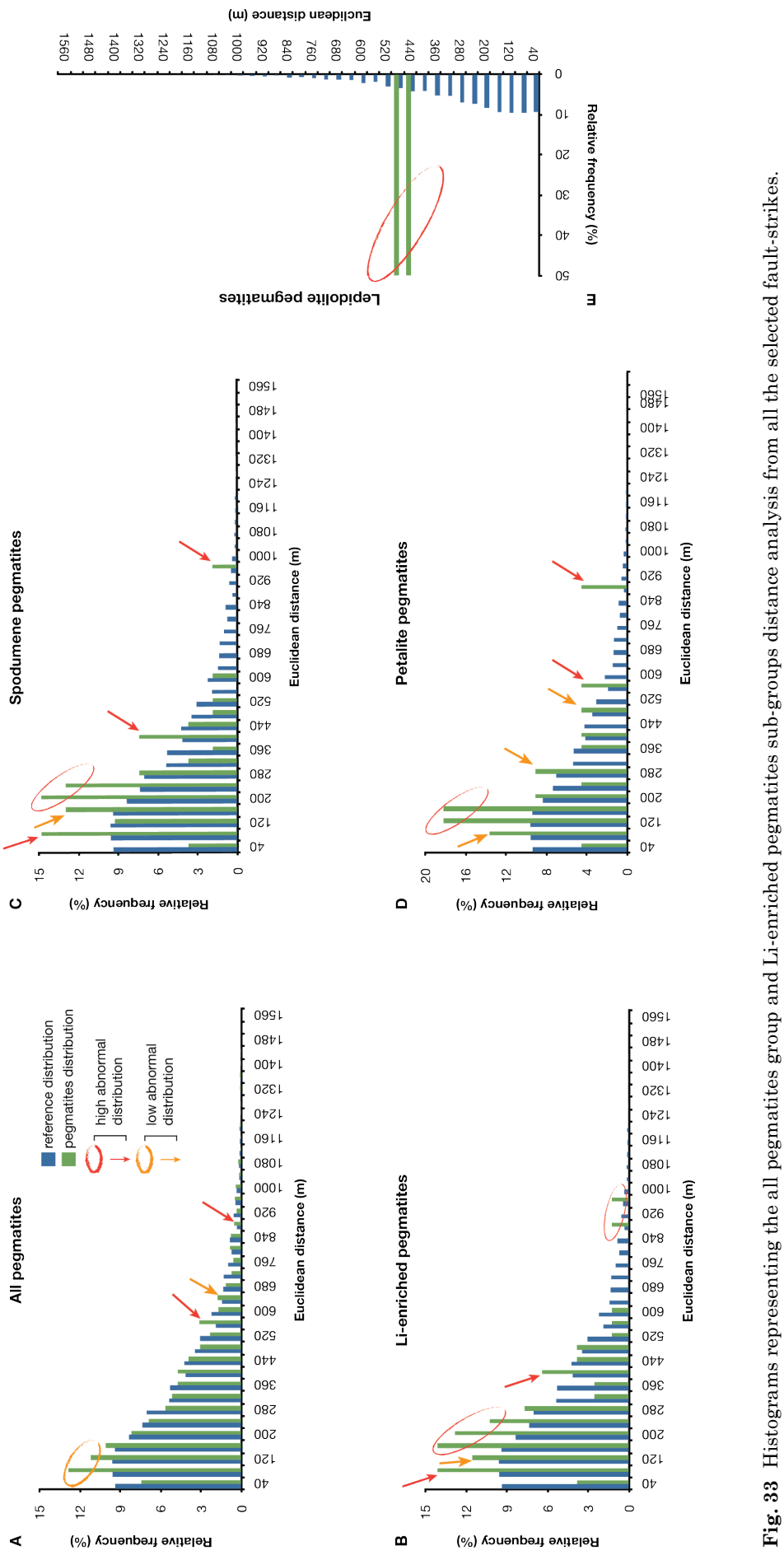

Fig. 33 Histograms representing the all pegmatites group and Li-enriched pegmatites sub-groups distance analysis from all the selected fault-strikes.

Li-enriched pegmatite presents a shorter extent than the all pegmatite group, with a maximum distance fixed at 960 m (Fig. 33b). The average frequency value of distance of 225 m for the Li-enriched group is also inferior to the average reference distance. Li-enriched pegmatites present an abnormal distribution from 40 to 240 m. Another *HAD* classes are present in the histogram, one close to the strong path *LAD* and *HAD* in the distance [360-400 m[, and two others close to the maximum extent in the classes [840-880 m[and [920-960 m[, although these last two class under 1% of frequency values. Li-enriched pegmatites present a stronger proximity relationship to the faults compared to the all pegmatites group.

In the Li-enriched sub-groups, the spodumene (Fig. 33c) and petalite (Fig. 33d) present almost the same extent and spatial distribution, overlapping in the majority of the classes where they are present. The two sub-groups show also the same percentage of the total pegmatites (76% for the spodumene and 77% for the petalite-enriched pegmatites) and almost the same average *LAD* ratio for the distance to faults range [0-280 m[. The lepidolite sub-group shows the most distant relationship to the faults, with a very limited range from 400 to 480 m, and an average distance of 446 m (Fig. 33e).

4. 3. 1. 2. DISTANCE FROM ALPHA FAULTS-STRIKES FAMILY

The all pegmatite group shows an extent of spatial distribution from 0 to 2250 m and an average distance of 553 m (Fig. 34a). The first three classes of distance, [0-75 m[, [75-150 m[and [150-225 m[present frequency values above the reference ones for the study area, where simultaneously the last of them is a *LAD*. After one class from this range, the second *LAD* class appear in the distance [300-375 m[. More distant from the alpha faults-strikes family, the classes [900-975 m[and [1050-1125 m[also show *LAD*. The overall distribution for the all pegmatite group shows that, in average, on almost all is extent, the frequency values are similar or superior to the values presented by the reference points.

In the Li-enriched pegmatites group, it is observed a major *HAD* and *LAD* path starting from the class [75-150 m[to [450-525 m[(Fig. 34b). This path represents 77% of the total Li-enriched pegmatites. Another *LAD* and *HAD* is observed in the range 1425 to 1575 m, but in this case with a frequency representativity of only 4%. The Li-enriched pegmatites are characterized by a strong spatial relationship with the alpha faults-strikes family up to 525 m, showing also a much higher proximity to the faults than the all pegmatite group.

Relatively to the Li-enriched sub-groups spodumene (Fig. 34c) and petalite (Fig. 34d), it is observed in these two sub-groups *LAD* and *HAD* ranges within the smaller distance classes, from 75 to 525 m. Comparing the spodumene-enriched pegmatites to the petalite-enriched

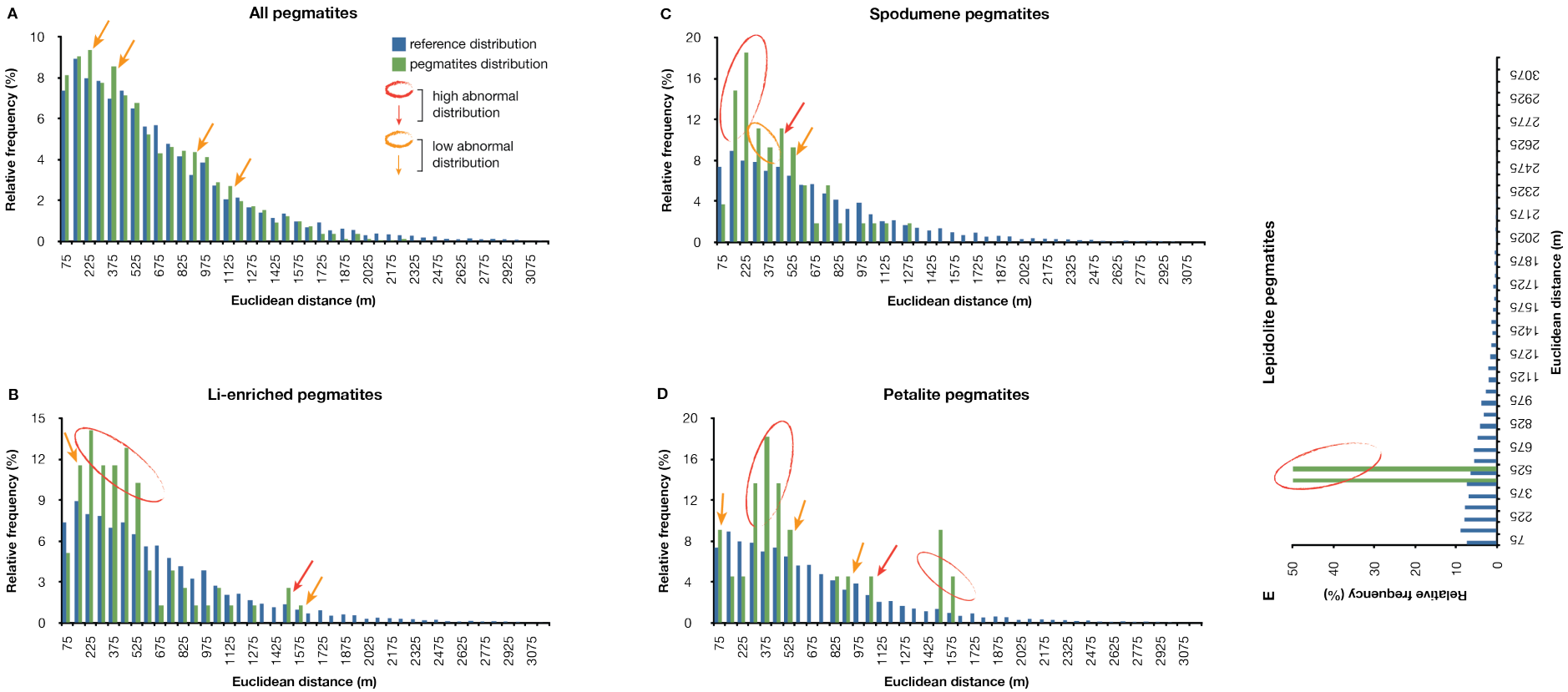

Fig. 34 Histograms representing the all pegmatites group and Li-enriched pegmatites sub-groups distance analysis from the alpha faults-strikes family.

pegmatites, it is observed for the spodumene a closer proximity with the alpha faults. This relationship is observed for the spodumene pegmatites in the *HAD* classes [75-150 m[and [150-225 m[, contrary to the petalite pegmatites that show frequency values way below the reference values for the same classes. The petalite pegmatites also show a range from 1425 to 1575 m with *HAD* that exceed the maximum extent of the spodumene pegmatites. The lepidolite pegmatites sub-group (Fig. 34e) shows the smaller distance extent within the three sub-groups present in the Li-enriched pegmatites with a maximum distance of 525 m. This sub-group shows also an overlapping with the higher abnormal distribution presented by the spodumene and petalite pegmatites.

4. 3. 1. 3. DISTANCE FROM BETA FAULTS-STRIKES FAMILY

The all pegmatite group shows a spatial distribution extent from 0 to 1800 m and an average distance to the beta faults of 417 m (Fig. 35a). This pegmatite group shows for the four first classes of distance (47 % of the total all pegmatites), frequency values higher than the reference points frequency. Within this range, the second lowest class of distance, [75-150 m[, shows a *LAD*. A second *LAD* is observed in the class [1350-1425 m[, but with a frequency value below 1%. An overall overview of the spatial distribution shows that the all pegmatites group frequencies rarely present values below the reference distribution, and the representative *LAD* in the histogram is observed in the second smaller class of distance.

The Li-enriched pegmatites present a spatial distribution extent inferior compared to the extent displayed by the all pegmatites group, with a maximum distance at 1200 m (Fig. 35b). However, similar to the all pegmatites group, it is in the second smallest class of distance that the most representative *LAD* for the Li-enriched pegmatites is observed. The remainder classes presenting *LAD* and *HAD* are concentrated in the range [525-825 m[. These results highlight the spatial relationship existing between Li- enriched pegmatites and the beta fault-strike family.

The spodumene-enriched pegmatites presents an average distance to the faults of 393 m (Fig. 35c), while the petalite-enriched pegmatites shows an average 255 m (Fig. 35d). Relatively to their range of maximum *LAD* and *HAD* class concentration, the spodumene show a more extended and distal range, [225-825 m[, while the petalite-enriched pegmatites show a range from 75 to 225 m. The comparison of the spodumene and petalite-enriched pegmatitess spatial distribution shows that the petalite pegmatites present a smaller extent and a closer overall proximity to the beta faults-strikes family. The lepidolite pegmatites sub-group shows,

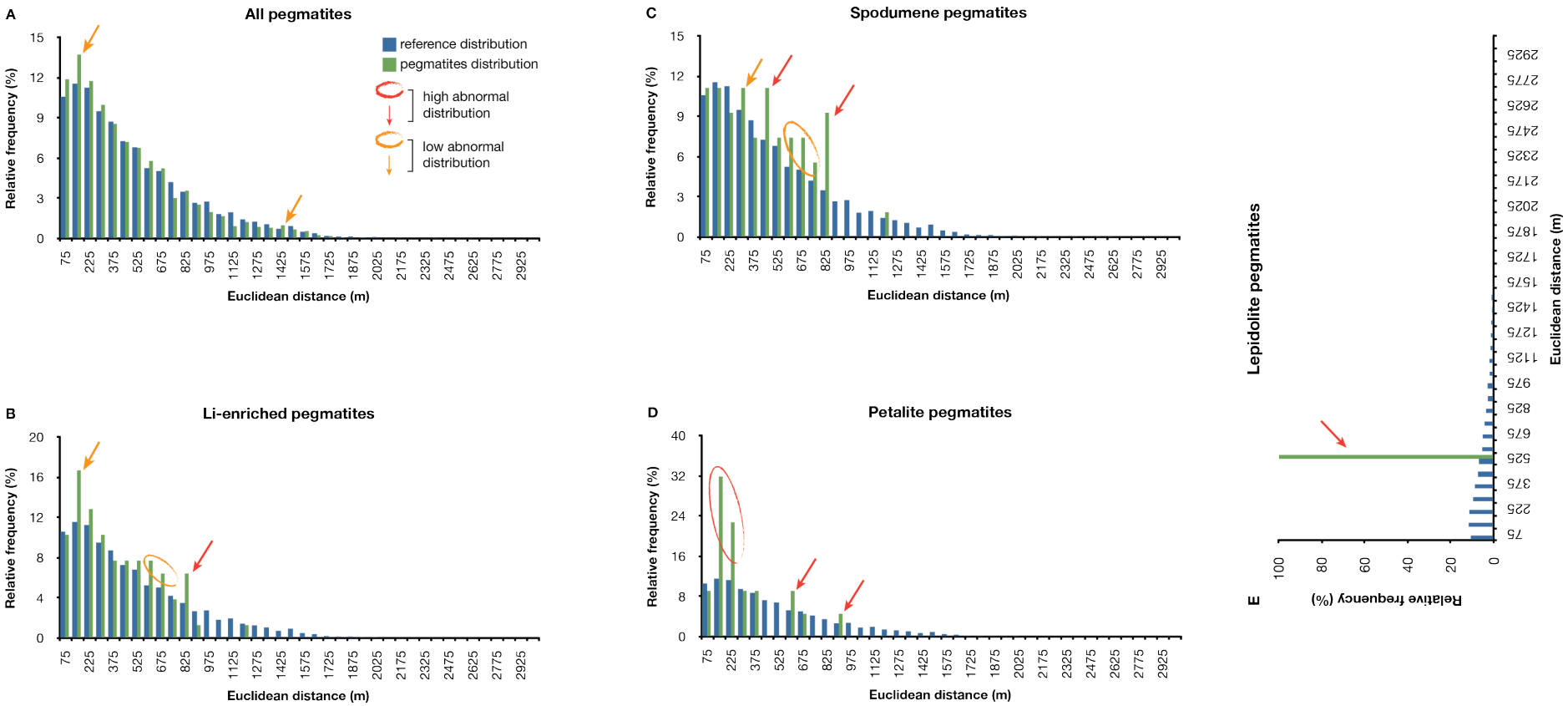

Fig. 35 Histograms representing the all pegmatites group and Li-enriched pegmatites sub-groups distance analysis from the beta faults-strikes family.

similar to the results observed for the alpha faults-strikes family, the smaller distance extent within the three Li-enriched sub-groups (Fig. 35e). However, in this case, the lepidolite sub-group is in average the more distant from the beta faults .

4. 3. 2. SPATIAL RELATIONSHIP BETWEEN PEGMATITES AND DENSITY OF FAULT-STRIKE FAMILIES

4. 3. 2. 1. DISTRIBUTION FROM ALL FAULTS

The all pegmatites frequency distribution extends from the all faults density per km^2 value of 0.2 to 3.2, the same range value also displayed by the reference distribution (Fig. 36a). Up to the faults density of 0.8, the first four classes show all pegmatites frequency values inferior to the reference ones. From values of density higher than 0.8, the ratio of distribution in this histogram becomes to be equal or higher than 1. Four classes of density presents *LAD*, two of them side-by-side in the range [1.4-1.8[and the other two in higher density classes [2.2-2.4[and [2.8-3[, but this last with a frequency value extremely low. A range containing two *HAD* classes is visible in the 2.4 to 2.8 density range. These results seems to highlight a slightly preference for the pegmatites to be emplaced in areas of higher fault densities.

The Li-enriched pegmatites, with a maximum extent of 2.8, show a lower spatial frequency distribution extent than the all pegmatites group (Fig. 36b). The distribution is also more fragmented and presenting more oscillations in the frequency values. The lower frequencies of pegmatites are observed in two ranges of density. The first is observed in the three initial classes from 0 to 0.6, including the class [0.2-0.4[with no pegmatites, and the second range following the same decreasing path of reference frequency values in the class range [1.4-2[. Relatively to the higher frequency values of pegmatites, in the five classes presenting abnormal distribution, only one of them is *LAD*. This show a *HAD* path for the abnormal distribution in the Li-enriched pegmatites group. The higher oscillation of frequency values in the Li-enriched pegmatites can potentially be explained by the higher rate of clustering than the clustering rate of all pegmatites group.

The spodumene-enriched pegmatites (Fig. 36c) show a very similar fragmented path and oscillating frequency distribution than the Li-enriched pegmatites distribution. The major differences are in the presence of a *LAD* in the class [0.6-0.8[, and in the higher frequency (15%) of spodumene pegmatites in the highest classes [2.4-2.6[and [2.6-2.8[. The petalite-enriched pegmatites (Fig. 36d) presents an even higher oscillating and fragmented distribution than the spodumene pegmatites, but similar in the localization of the abnormal

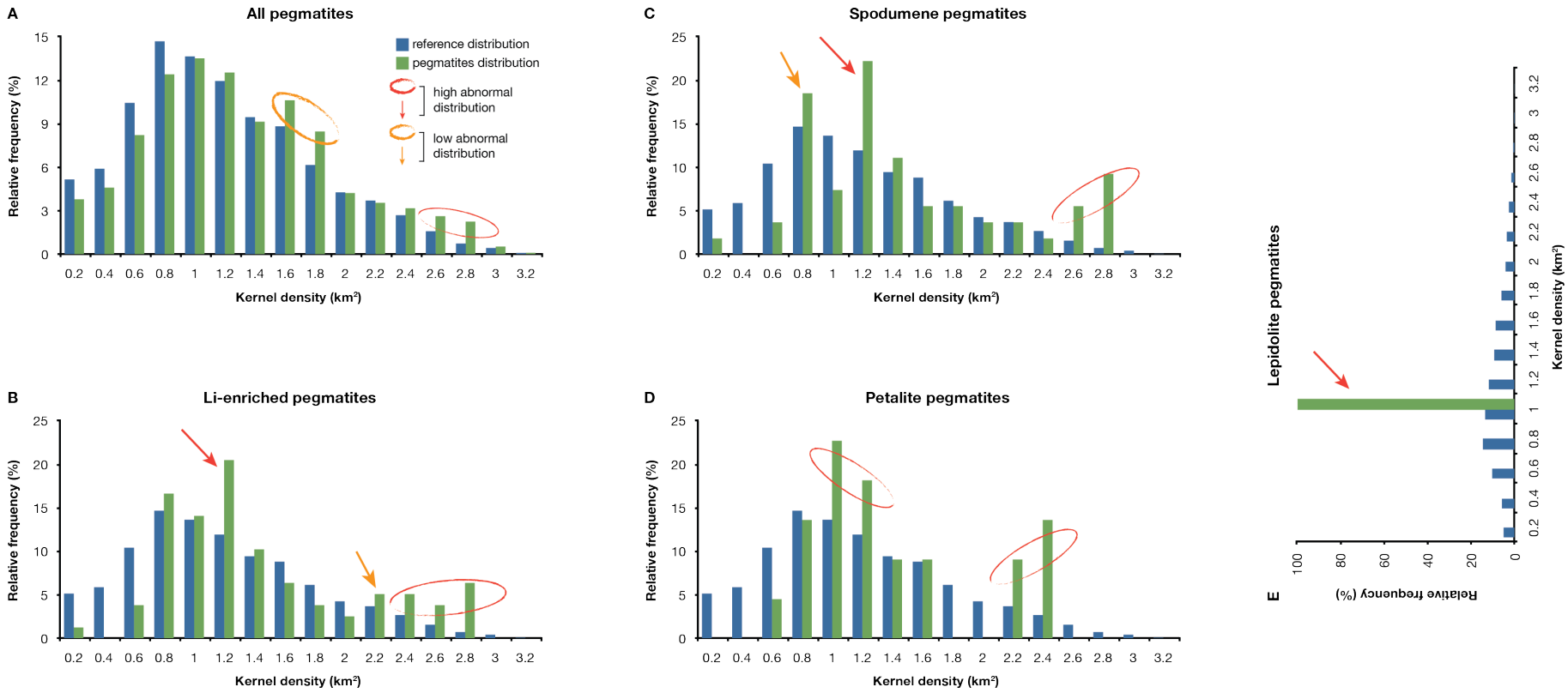

Fig. 36 Histograms representing the all pegmatites group and Li-enriched pegmatites sub-groups distribution analysis from all the faults-strikes density.

distribution. The extent is also different, with the petalite pegmatites presenting a narrower extent from 0.6 to 2.4. No petalite-enriched pegmatite is observed in areas lacking faults. If we compare spodumene- and petalite-enriched pegmatites, petalite-enriched pegmatites present a stronger spatial relationship with the highest fault density areas. The lepidolite sub-group is localized in only one class of density, showing a total presence in the density [0.8-1[(Fig. 36e).

4. 3. 2. 2. DISTRIBUTION FROM ALPHA FAULTS-STRIKES FAMILY

The spatial analysis of the all pegmatite group shows an extent of spatial distribution from 0 to 2.4 (Fig. 37a). Observing the overall distribution of this group of pegmatites, no apparent spatial relationship with the alpha faults is presented. The pegmatite frequency distribution follows, in all is extent, the decreasing path observed in the reference frequency values. Not in one case, the classes in the pegmatites frequency distribution show a higher value that is anterior class. The abnormal distributions observed are present in the class [0.2-0-4[, the second lowest, and above the class density of [0.6-0.8[in low frequency value representativity.

The Li-enriched shows a different spatial distribution compared to the all pegmatites group (Fig. 37b). It is observed for this group an apparent spatial relationship with the alpha fault-strikes family, above the [0.6-0.8[class. 42% of the total Li-enriched pegmatites are present in this portion of the histogram, showing in the extremes of this range *HAD* classes, and in between *LAD* classes. No Li-enriched pegmatites are present in the range class [1.4-1.8[.

The spodumene-enriched pegmatites follows almost identically the spatial distribution path observed in the Li-enriched pegmatites group (Fig. 37c). The major difference observed is that the spodumene follows an overall path of *HAD* when the abnormal distribution is present in classes of density. The petalite pegmatite sub-group shows a more limited extent, from 0 to 1, than all the previous pegmatites extent for the alpha faults density (Fig. 37d). The abnormal distribution range [0.2-0.8[represent 73% of the total petalite pegmatites sub-group, showing an *HAD* in the central position of this range. The apparent spatial relationship for these pegmatites is contrary to the previous pegmatites related to the lower density of alpha faults. The lepidolite pegmatites sub-group is the narrowest sub-group. This time however, it is dispersed into two classes, from 0.6 to 1 (Fig. 37e).

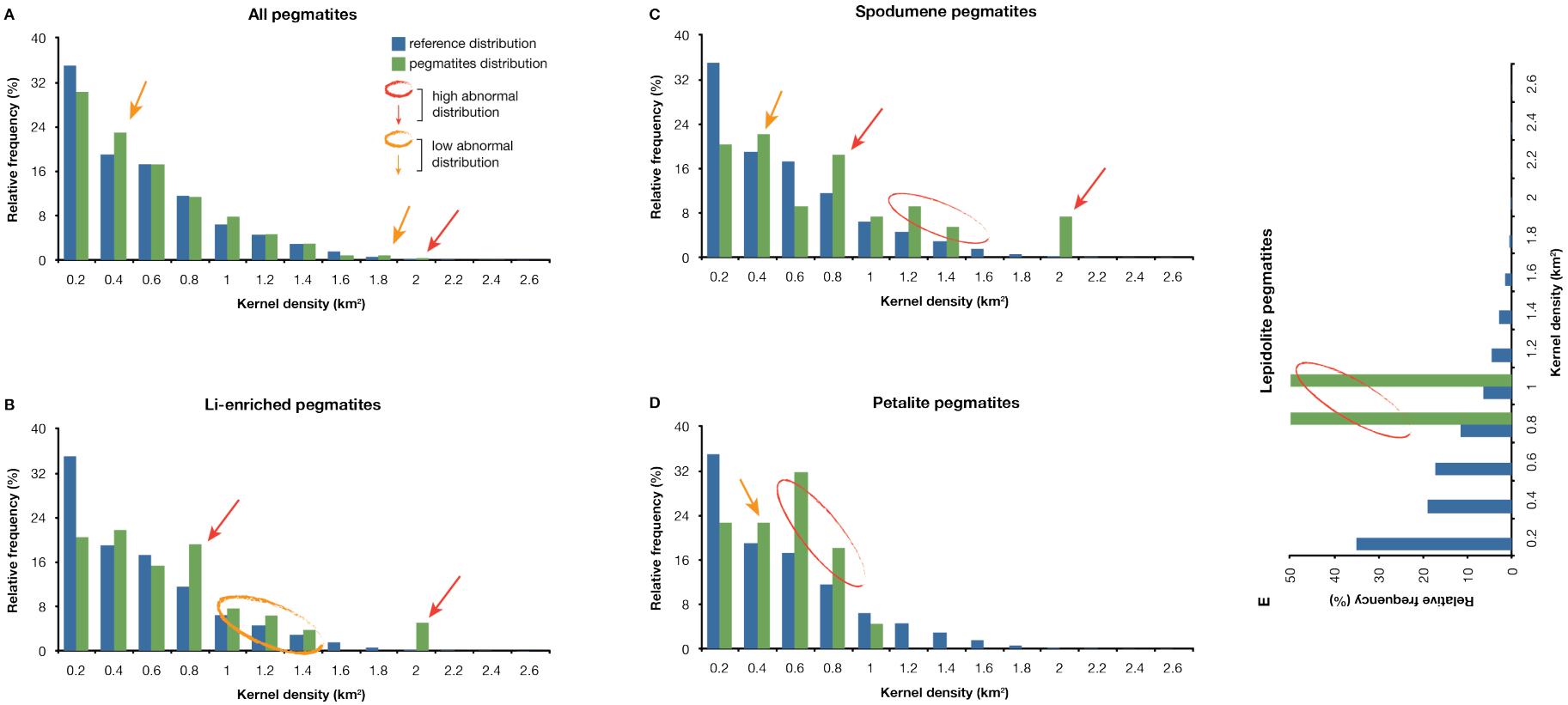

Fig. 37 Histograms representing the all pegmatites group and Li-enriched pegmatites sub-groups distribution analysis from the alpha faults-strikes density.

4. 3. 2. 3. DISTRIBUTION FROM BETA FAULTS-STRIKES FAMILY

The all pegmatites group present a spatial distribution extent from 0 to 2.6 (Fig. 38a). Above the class [0.4-0.6[up to the class [1.8-2[, these pegmatites follow a path where the pegmatite frequency distribution is higher than the reference distribution values. Within this range that represents 54% of the total pegmatites, three class of density present abnormal distribution, two with *LAD* in the class [0.8-1[and [1-1.2[, while the other in the class [1.2-1.4[presents *HAD* with a ratio of 2.0. In the right extremity of the histogram, the higher class of density also presents *HAD*, but with a frequency below 1%.

The Li-enriched pegmatites group shows a narrower extent, up to faults density of 2 (Fig. 38b). In this extent, 50% of the pegmatites are emplaced within the range of density [0.6-1.4[, presenting all of them *LAD* and *HAD*. An isolated *HAD* is also observed in the class [1.6-1.8[, one of the highest classes in the histogram, but not with the same representativity as the other abnormal distributions. Comparing the two previous groups of pegmatites, it is observed that the distribution of the all pegmatites presents a much higher frequency in the lower class of density. However, for the abnormal distribution, their emplacement is highly similar.

In the sub-groups of Li-enriched pegmatites, the spodumene pegmatites (Fig. 38c) show a similar overall pattern of distribution with the Li-enriched group, presenting also a high percentage (60%) of pegmatites in the range of density [0.6-1.4[. Presenting a *HAD* ratio of 2.3, the class [0.8-1[is the more representative in all the histogram. The petalite pegmatites (Fig. 38d) present a more fragmented distribution than the previous histograms, with three preferential abnormal range of density for their emplacement from 0.4 to 2. The most representative is, with 40% of the total pegmatites, the class range [0.4-0.8[. Between the abnormal density ranges, the classes [0.8-1[and [1.2-1.4[presents no petalite pegmatites. The lepidolite sub-group is emplaced exclusively in the lower class of density, representing this sub-group as the less spatially related to areas of high beta faults density (Fig. 38e).

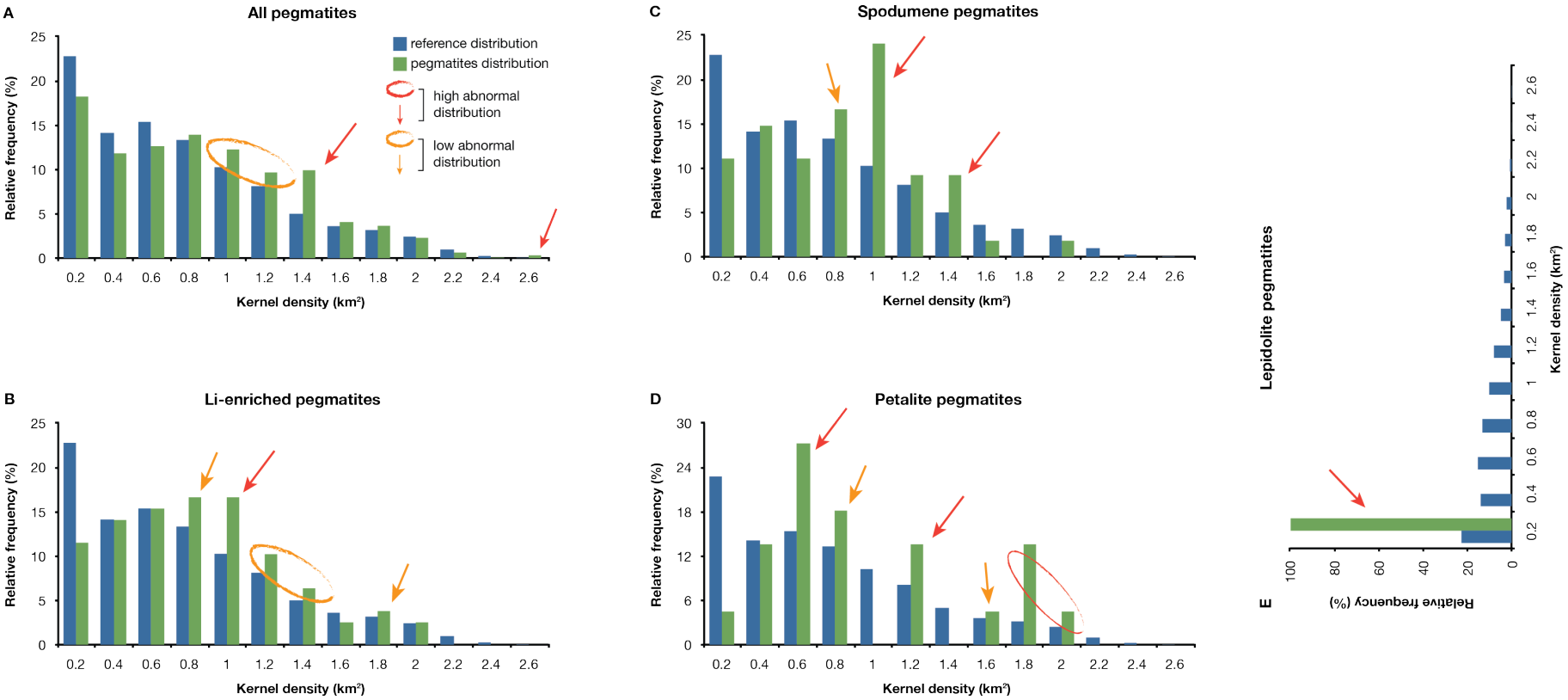

Fig. 38 Histograms representing the all pegmatites group and Li-enriched pegmatites sub-groups distribution analysis from the beta faults-strikes density.

4. 4. SPATIAL RELATIONSHIP BETWEEN PEGMATITES LOCATION AND INTERPOLATED METASEDIMENTARY SCHISTOSISTY

The measured metasediment foliations are an important part of the data analyzed in this study. Using this type of punctual data, it is possible to detect the principal orientation of regional deformation in geological structures, taking account that the orientation of a set of foliation in a given area is regarded as a representation of the continuous regionalized deformation for this same area. In this study, the methodology developed by Gumiaux *et al.* (2003) that automatically interpolate a set of orientation is applied. In this method, the interpolation of a set of foliation is represented as schistosity trajectories. The map of schistosity trajectories obtained for a specific region permits to highlight the regional deformation that occurred within this sector, more specifically ductile structures associated with shear zone (*e.g.* sigmoid or rotation of the formed foliation).

4. 4. 1. METHODOLOGY

Following the geostatistical data interpolation developed by Matheron (1962), the automatic interpolation methodology developed by Gumiaux *et al.* (2003) applies a treatment of orientation data to analyze their spatial variations within a selected domain or sector. This methodology uses the *Kriging* method developed by Matheron (1962). The *Kriging* method permits to interpolate spatially distributed data point, following the principle that spatially close points tend to exhibit more similar values than distant points. A first problem arises when the interpolation is applied for circular data. Due to their variation from 0^{o} to 360^{o}, classic statistical calculation used in non-circular algebraic data, like the *Kriging* method, is impossible to apply (Annex 1). To bypass this problem, instead of using algebraic difference between the orientation points, Gumiaux *et al.* (2003) obtain the *Kriging* interpolation using direction cosines, where each orientation of the data points is represented by its two direction cosines (Annex 2). This direction cosine method is used in the first part of the *Kriging* interpolation that consists in quantify the spatial variation of the data set by the calculation of experimental variograms.

Before using the data available for the Barroso-Alvão region, it was necessary to constrain the set of foliation orientation present in the foliation layer (793 orientations). A spatial constriction was applied in the data set using the area already used anteriorly in this study for the delimitation of the all pegmatites group. This permitted to focus the foliation interpolation for the sector of higher pegmatite density and only known presence of Li-enriched pegmatites in all Barroso-Alvão region. After the spatial delimitation of the foliation orientation data to 269 measurements, a minimum inclination of 45º for the structures was applied. This restriction was applied because the interpolation is, in this study, calculated in two dimensions, requiring high inclination of the structure to execute the calculation. From the 269 measurements, only 14 (5%) of them are bellow 45º. These 14 foliations orientation are evenly distributed in all the study area, not interfering to the calculation of the foliation interpolation.

Another requisite to perform the foliation interpolation is to analyze the direction variation of the total foliation measurements. This step is essential because the *Kriging* only can be applied to a data set of homogeneous values. For the foliation within the study area, the orientation distribution follows a bell shaped Gaussian curve. This mainly omni-directional distribution permits to follow to the calculation of the orientation variogram of the study area.

The experimental variogram (Fig. 39) was calculated using 269 orientation data points, presenting a maximum distance calculation of 12 km, which corresponds approximately at half diagonal distance of the study area, and a distance interval calculation of 250 m. The spatial correlation between data pairs (range value) is observed up to approx. 5500 m, the "sill" (constant values with increasing distance) at approx. 300 degree and the "nugget effect" (background noise data or effect at scales inferior than the study area) at 60 degree, representing 20% of the total contribution. The experimental trend of the variogram follows an exponential theoretical function. Using the range value from the experimental variogram as the search radius for the *Kriging* (Annex 3), the interpolation of orientation data was latter performed using GIS software. The *Kriging* interpolation raster created was used to produce a map of regional foliation orientation trajectories and to calculate the angular difference between the interpolated schistosity and the pegmatites orientation.

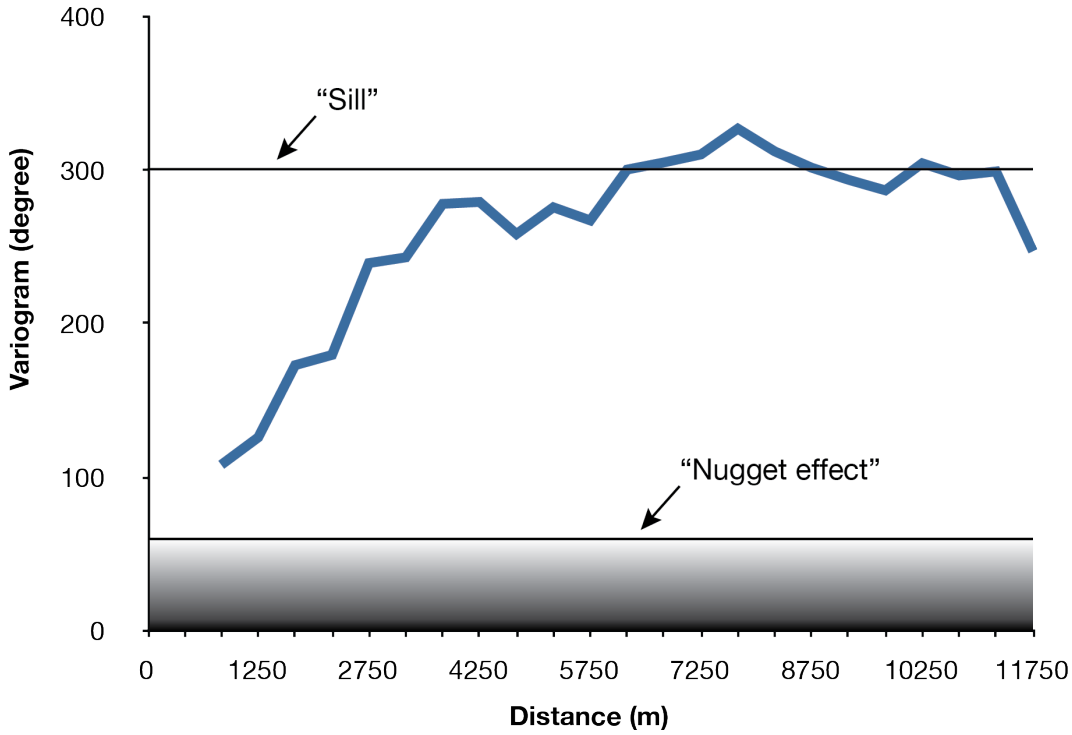

Fig. 39 Experimental variogram calculated using the Barroso-Alvão metasediment foliations orientation.

4. 4. 2. RESULTS

One of the principal objectives of the foliation orientation interpolation was to create an schistosity trajectory map (Fig. 40) that allows the visualization and better understanding of the regional deformation occurred in the study area. We observed that the trajectories follow an approximately constant direction in all the study area. This observation is strengthened by the histogram of the directional foliation data (in Fig. 40), showing an almost omni-directional path with a maximum N109º direction. However, the direction of the trajectories in the extremities of the study area, close to the post-tectonic granites pluton of Gerês and VPA, changes relatively to the regional overall schistosity. Although following an approximately overall homogeneous direction, the schistosity trajectories presents small changes in their directions creating an apparent undulation or sigmoidal path in all the study area.

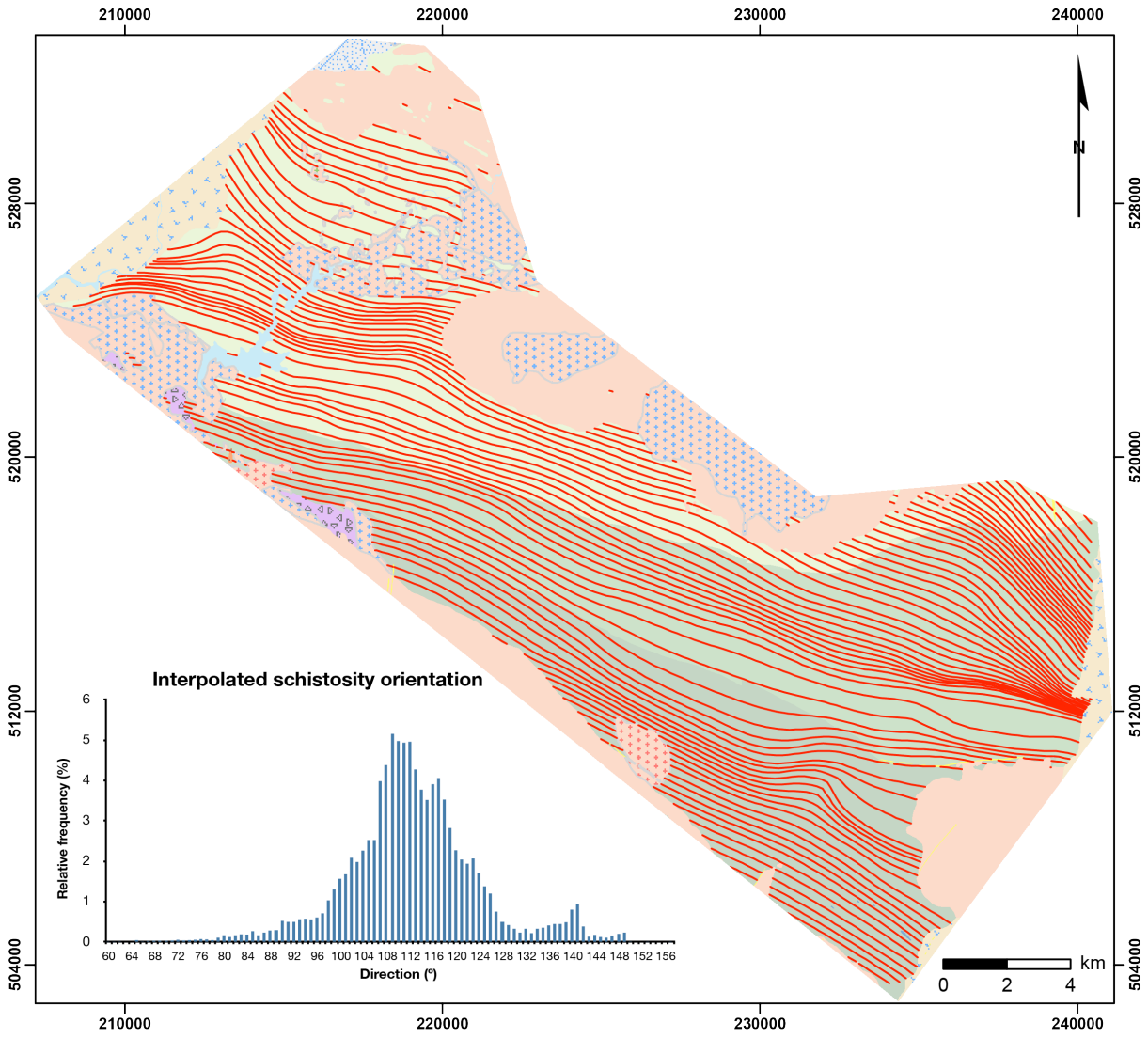

Fig. 40 Map showing the interpolated S3 schistosity trajectories within the study area. To complement the information about the interpolated schistosities, the histogram of the interpolated schistosity orientation is also displayed.

Using the interpolated raster of schistosity for the Barroso-Alvão aplitopegmatitic field, it was possible to create a histogram showing the relationship between the pegmatites orientation and the calculated schistosity for the whole study area (Fig. 41). This histogram shows frequency of the absolute angular difference between the pegmatite orientation and the interpolated schistosity orientation extracted at the same spatial emplacement of the pegmatite occurrence.

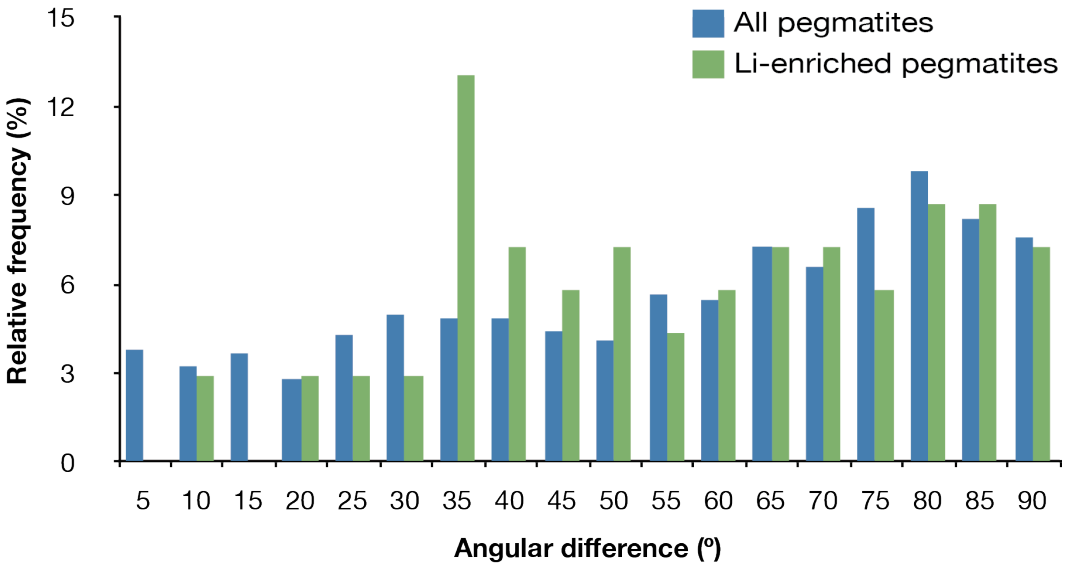

Fig. 41 Histogram representing the frequency of the absolute angular difference between the pegmatite orientation and the interpolated schistosity orientation.

The absolute angular difference was applied for the all pegmatites and the Li-enriched pegmatites group. In the all pegmatites group, 48% of the total all pegmatites are emplaced in a range of angular differences with the interpolated foliation orientation from 60º up to the maximum 90º. Admitting a maximum angular difference of 15º, only 11% of the pegmatites are considered as following the metasediment schistosity. The Li-enriched pegmatite group shows a similar frequency distribution for the angular range [60º-90º], with 45% of them to be within this range. Although this resemblance of frequency for this range, below the angular difference of 60º, the Li-enriched pegmatites group presents a distribution more focalized in the range [35º-50º[(33% of the Li-enriched pegmatites) and only 3% below 15º, whereas the all pegmatites group presents a distribution more evenly distributed for the angular differences bellow 60º.

CHAPTER 5

SYNTHESIS AND INTERPRETATION

CHAPTER 5 - SYNTHESIS AND INTERPRETATION

In this chapter, the results obtained from the pegmatites spatial statistical analyses relatively to their i) spatial distribution, ii) Euclidean distance relationship from the syn-tectonic plutons of Barroso and Cabeceiras de Basto, iii) relationship with fault-strike families and iv) relationship with interpolated foliation orientation, are here interpreted. The main goal is to understand the most probable mechanism of pegmatite emplacement for the Barroso-Alvão aplitopegmatitic field.

Two major groups of pegmatites where considered in this study. A first group containing all the pegmatites for the study area, and a group containing only the pegmatites known to be mineralized with the lithium minerals spodumene, petalite or lepidolite, subdivided in sub-groups within the Li-enriched group according to this criterion. The large majority of the pegmatites are emplaced within the metasediments lithology, despite the predominance of granitic lithology for the Barroso-Alvão region.

The statistical analyses concerning the spatial distribution of the pegmatites occurrences, for now considering only the Distance to Neighbor Distance (DNN) and the Ripley's *K*-function computation, showed that the pegmatites in the study area are emplaced following a clustered distribution. Although this pegmatite clustering, the rate and ratio of clustering for the all pegmatites group and the Li-enriched group is not equal. The two R ratios of 0.26 and 0.34 for the Li-enriched pegmatite group, compared to the 0.56 R ratio from the all pegmatites group, shows that a segregated and higher degree of clustering is present in the Li-enriched pegmatites group. The Ripley's *K*-function reinforced the previous DNN result showing that separated rate of clustering is present for the two groups of pegmatites. It is observed up to 1800 m an especially high rate of clustering for the Li-enriched group, while the all pegmatites group presents a much lower rate of clustering up to 3500 m followed by scattered distribution. The Li-enriched group also differs in this last characteristic of distribution from the all pegmatites group, showing clustering in all the 4300 m range distribution.

Within the analysis of the spatial distribution of pegmatites, the spatial density distribution of the all pegmatites was performed with the intention to understand the spatial relationship between this mentioned density and the emplacement of the Li-enriched pegmatite group. In this analysis, the Li-enriched pegmatites, as a group, show a spatial relationship with the higher densities of pegmatites. Individually, the sub-groups of Li-enriched pegmatites demonstrate the same spatial relationship with the higher pegmatites

density. These results show an apparent contradiction to the models of fractionated crystallization of pegmatites from parental granite. In this models, the more fractionated pegmatites are generally more distant from the barren pegmatites, and not, as observed for the more evolved pegmatites in Barroso-Alvão, in the higher densities of pegmatites.

The last results obtained for the analysis of the spatial distribution of pegmatites were the families of pegmatites preferential orientation for the two groups of pegmatites. Three families were obtained, family A (N0º to N63º), B (N64º to N113º) and C (N114º to N179º). All the families, either in the all pegmatites group or Li-enriched group, show a preferential emplacement in the upper stratigraphic sub-units Sb and Sc of the Carrazedo structural domain, as well as a preference to be emplaced in the central and eastern sector of the study area. From all the families, the family C is the family that shows the more evident alignments of the pegmatites. Two preferential directions are observed, one ~NNW-SSE more evident in the western part of the central sector, and a second following a ~NW-SE direction in the central and eastern sector. These alignments suggest that corridors of preferential pegmatites emplacement following these two directions are possibly present in the study area. The maximum N24º and N156º orientation values for the orientation pegmatites family A and C respectively, corresponding to a minimum angular difference between them of 48º, as well as the visual observation of these two families in the western part of the central sector, suggest a possible integration of these pegmatites into the same model of emplacement.

In the Euclidean pegmatites distance relationship from the syn-tectonic plutons of Barroso and Cabeceiras de Basto, and taking into account the parental granitic models presented by Černý (1989) and London (2014) as comparison, the expected higher distribution around the pluton and farthest distance from the sub-types spodumene, petalite and lepidolite are not observed for the Barroso granitic pluton. It is apparently the opposite that occurs, with the all pegmatites group abnormal distributions classes to be more distant from the pluton, and the spodumene, petalite and lepidolite sub-groups at similar or closer distance of the pluton. The only aspect slightly concordant with the above granitic parental models is the average higher petalite sub-group distance from the pluton, relatively to the spodumene sub-group.

Similar to the distance analysis between the pegmatites and the Barroso granitic pluton, it is suggested that the emplacement of the pegmatites relatively to Cabeceiras de Basto pluton distance does not follows the parental granitic model as proposed by Černý (1989) and London (2014). Also similar to Barroso pluton, the pegmatites are preferentially emplaced at higher distance from the Cabeceiras de Basto granite. The Li-enriched pegmatites group suggest also an emplacement that contradicts the granite parental model, with: i) a pegmatite emplacement at similar or closer distance from the granite compared to the all

pegmatites group, ii) the inverted distance fractionation of the sub-groups and iii) an overlapped distribution, in some part of the extent, of the spodumene, petalite and lepidolite-enriched pegmatites.

The spatial statistical analyses aiming the pegmatites relationship with fault-strike families showed that, concerning the orientation of the faults in the study area, two large families appears in the study area: i) Alpha family (N0º to N91º) and the Beta family (N92º to N179º). The all pegmatites group present a moderate distance relationship with all the faults, showing in the closest classes of distance frequency values superior to the presented by the reference points distribution, although a slightest tendency to the all pegmatites to be closer to the beta family is observed. Relatively to the kernel density of all faults, the same all pegmatites group show a strong relationship with fault density. However, the correlation observed for all pegmatites to be emplaced in higher faults density is only observed for the beta family.

For the Li-enriched pegmatites, the distance and density relationship observed to all faults are clearly more correlated than for the all pegmatites group where 77% of the total Li-enriched pegmatites are spaced less than 525 m from alpha family fault-strikes, compared to the 53% of the reference distribution. Contrary to these results, the same Li-enriched pegmatites show for the faults density a preferential emplacement for the beta family. An inversion in the distance relationship is observed for the spodumene and petalite-enriched pegmatites relatively to the two alpha and beta family. The spodumene-enriched pegmatites show a closest relationship for the beta family, whereas the petalite pegmatites present the closest relationship for the alpha family.

To conclude, the results from the pegmatites relationship with fault-strike families suggest: i) a preferential association of all pegmatites group and higher beta family fault densities; ii) a stronger Li-enriched pegmatites spatial association to faults and correlation to fault density compared to the all pegmatites group; iii) Li-enriched pegmatites spatially associated to alpha family and simultaneously correlated to higher densities of beta family faults.

Finally, the interpolation of metasedimentary foliation orientation permitted the creation of a map of schistosity trajectory, and the statistical analysis of the angular difference between the pegmatites and the interpolated foliation direction. In the map of schistosity trajectory, it is observed an apparent undulation or sigmoidal path in the computed trajectories, suggesting a horizontal deformation with dextral movement that deformed the already formed schistosity within the Barroso-Alvão aplitopegmatitic field. The angular difference between the pegmatites orientation and the interpolated foliation histogram shows that the all pegmatites group demonstrate a preference to be emplaced within a range of 60º to

90º differences from the metasediment schistosity. Admitting a maximum angular difference of 15º, only 11% of the pegmatites are considered as following the metasediment schistosity. The Li-enriched pegmatites group shows a similar path, but also a high preference to be emplaced at 35º to 50º relatively to the schistosity. These results show that the pegmatites are preferentially emplaced discordant to the metasediment schistosity, suggesting that the majority of the pegmatites were emplaced in a late stage or after the D3 deformational phase.

Altogether, these results suggests that the pegmatites spatial emplacement in Barroso-Alvão aplitopegmatitic field followed dextral shear-zones presenting ~NW-SE and ~NNW-SSE orientations. Following this line of thought, we continued to try to find these proposed shear zones using ASTER imagery. The methodology consisted in the interpretation of terrain lineations in the satellite imagery using different image processing (*e.g.* solar exposition, aspect, slope). These lineations where lately included in a map from the study area containing the pegmatites by groups and faults by families, to observe the relationship between them (Fig. 42).

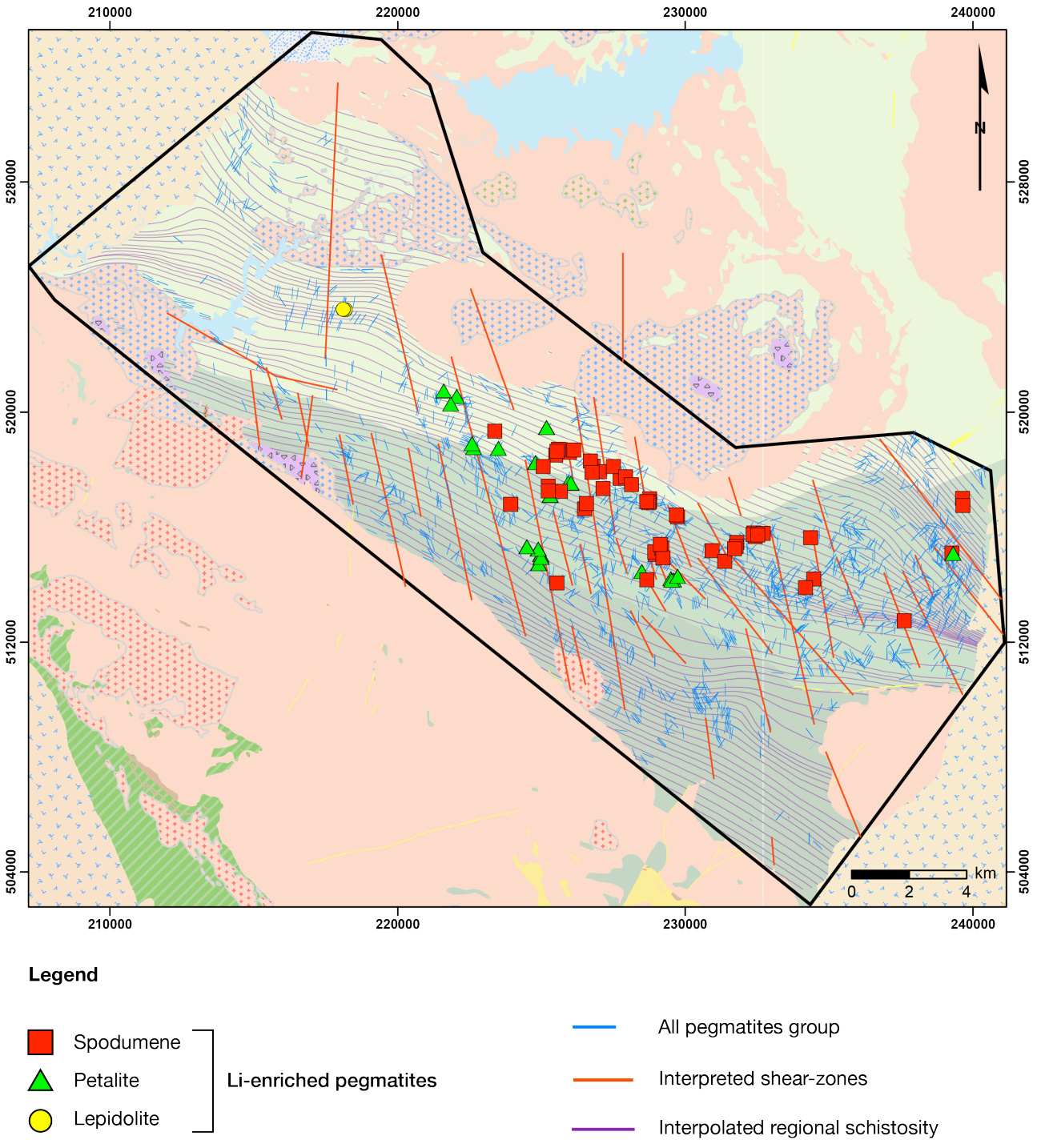

Fig. 42 Map showing the spatial emplacement of the all pegmatites and Li-enriched pegmatites relatively to the interpreted shear-zones and the interpolated regional schistosity.

The interpreted shear zones displayed in Fig. 42 shows in some occasion a superposed localization to beta family faults, following almost the same direction. This aspect of the interpreted shear zones is especially well observed in the western part of the central sector of the study area, presenting also in this sector a certain spatial emplacement rhythmicity concerning the distance between them. In this same western sector, it is observed a shear zone that presents a visually obvious spatial relationship with several Li-enriched pegmatites. This spatial relationship is also observed with the pegmatites from the C-family of orientation. The corridors of deformation between the interpreted shear zones present numerous pegmatites following the A-family of pegmatites orientation, suggesting that these pegmatites were preferentially emplaced within these corridors. These shear zones and associated corridors of deformation probably created channel-ways within the metasedimentary units that permitted the emplacement of the pegmatitic melts precursor of the pegmatites bodies. The B-family of pegmatite orientation does not present a particular relationship with the interpreted shear zones, following preferentially orientations similar to the interpolated trajectory of schistosity. Therefore, the emplacement of the B-family pegmatites orientation is probably correlated with the metasedimentary foliations, and possibly, at least, synchronous with the last phase of regional deformation. These visual interpretation showing an association between the pegmatites and the interpreted shear-zones are reinforced with the empirical results from the histogram representing the pegmatites distance from the interpreted shear-zones (Fig. 43). In this histogram, it is possible to observe that the pegmatites presents HAD and LAD in distance bellow 400 m for the all pegmatites group and 600 m for the Li-enriched pegmatites, showing a close relationship between pegmatites and the interpreted shear-zones.

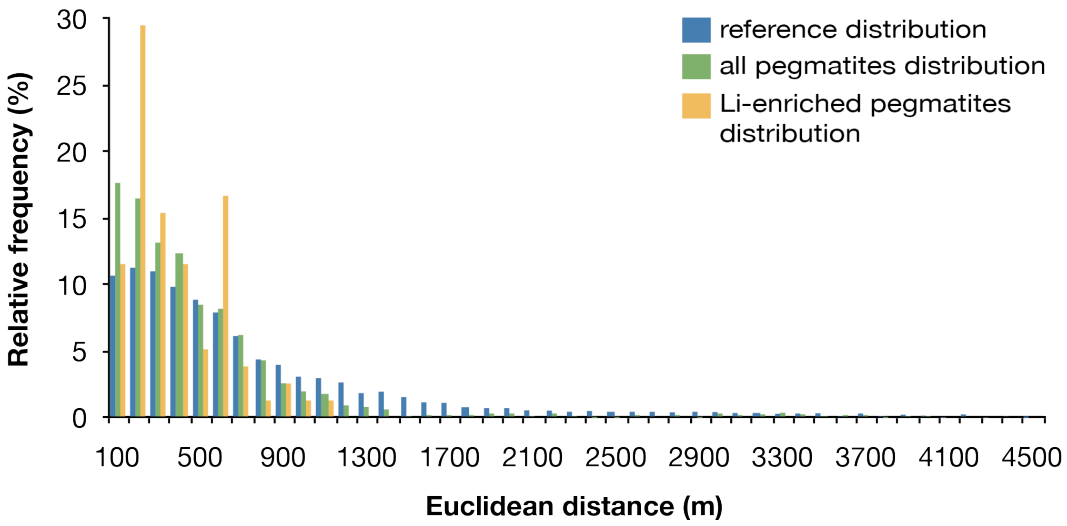

Fig. 43 Histogram showing the distance relationship of the Barroso-Alvão pegmatites from the interpreted shear-zones obtained using ASTER imagery.

CHAPTER 6

DISCUSSION

CHAPTER 6 – DISCUSSION

In this study, the spatial statistical analysis methodology permitted to follow an approach of studying the pegmatites emplacement that is not easily found in the literature, compared to the more "classical" methods like the petrography, geochemistry or geochronology of pegmatites. Different to these last methods, the spatial statistical analysis presents a special focus in determining the spatial emplacement relationship between pegmatites and the surrounding structures (*e.g.* granites, faults, schistosity), while the "classical" methods are more suited to link the pegmatites to the original source and the degree of chemical fractionation. Because of this difference, these methodologies are ideal to be used as a whole, complementing each other deficiencies.

The methodology applied in this study has brought new evidences concerning i) the difficulty to relate the Barroso-Alvão pegmatites with the Černý (1989) and London (2014) parental granite model, and ii) a model of pegmatites emplacement related with dextral shear-zones oriented from NW-SE to NNW-SSE.

In the first point, the pegmatites distance from the specialized in Li, Sn and W Cabeceiras de Basto granite, and from the Barroso granite showed an anti-correlation not compatible with the parental granite pegmatites model proposed by Černý and London. The fact that the Li-enriched pegmatites showed preferential emplacement within high density of pegmatites also contraries the London and Černý model, which predicts that the pegmatites more fractionated, and therefore more chemically evolved, are distant from the higher densities of pegmatites. Previously to our study, Martins *et al.* (2011, 2012) obtained similar conclusions to our results with their mineralogical chemical evolution for the Barroso-Alvão pegmatites, in which they not observe a strong pegmatite chemical evolution from the aforementioned granite.

The second point is related to the mechanism of pegmatite emplacement in Barroso-Alvão aplitopegmatitic field and present similarities with the model of pegmatites emplacement proposed by Demartis *et al.* (2011) for the Comechingones pegmatites field in Argentina. In their model of pegmatites emplacement, the pegmatites are emplaced in spaces developed in a shear-zone according to the Riedel model of fracturation. Our results show that the pegmatites in Barroso-Alvão appear to be emplaced in association with corridors of deformation presenting C-S planes of deformation. Extrapolating the Riedel fracturation for the Barroso-Alvão pegmatites emplacement, the C-family of pegmatite orientation are proposed to be emplaced and oriented following the dextral C-shear zones or principal plane of

deformation. Following the Riedel fracturation, the ~45º between the A and C-family of pegmatite orientation suggest that the A-family of pegmatite were emplaced in tensional fractures perpendicular to the maximum horizontal compression in Barroso-Alvão region, and highly discordant to the metasediment foliation. Due to their orientation, the pegmatites included in the B-family of pegmatite orientation are the only pegmatites that cannot be integrated in this Riedel fracturation model of emplacement. We contend that the emplacement of these pegmatites was controlled by the metasediment foliation. This mechanism of emplacement is not exclusive to the B-family of pegmatite orientation, since some pegmatites from the C-family of pegmatite orientation also present orientation similar to the metasediment direction in some parts of the study area. The highly diverse orientation of the metasediment foliation is a factor that difficult the interpretation of the mechanism of pegmatites emplacement, allowing possible mixture of process of pegmatites emplacement for the B and C-family of pegmatite orientation.

Concerning the Li-enriched pegmatites, it is observed that the average distance from the interpreted shear-zones (327 m) is inferior to the distance presented by the all pegmatites group (474 m). These results, integrated within a model of pegmatite emplacement associated with shear-zones corridors, appear to evidence that the Li-enriched pegmatites are younger in comparison to the all pegmatites group. The same results are observed relatively to the spodumene and petalite pegmatites. The spodumene pegmatites present a slightly higher distance (334 m) from the C-shear planes in comparison to the petalite pegmatites (290 m) and an emplacement in a more central position within the corridor of deformation, suggesting that the spodumene pegmatites were emplaced before the petalite pegmatites. These results, although not presenting a strong statistical evidence, are in concordance with the higher fractionation of the Li-enriched and petalite pegmatites, therefore younger, in comparison respectively to the all pegmatites and spodumene pegmatites proposed by Martins *et al.* (2011, 2012).

A careful interpretation of the results is proposed since all the computational methodologies applied in this study were purely executed in two dimensions, not taking into account the pegmatites emplacement in association with the topography of the Barroso-Alvão region.

Compiling all the observation and results obtained in this study, a graphical model of pegmatites emplacement for the Barroso-Alvão aplitopegmatitic field is here proposed (Fig.44)

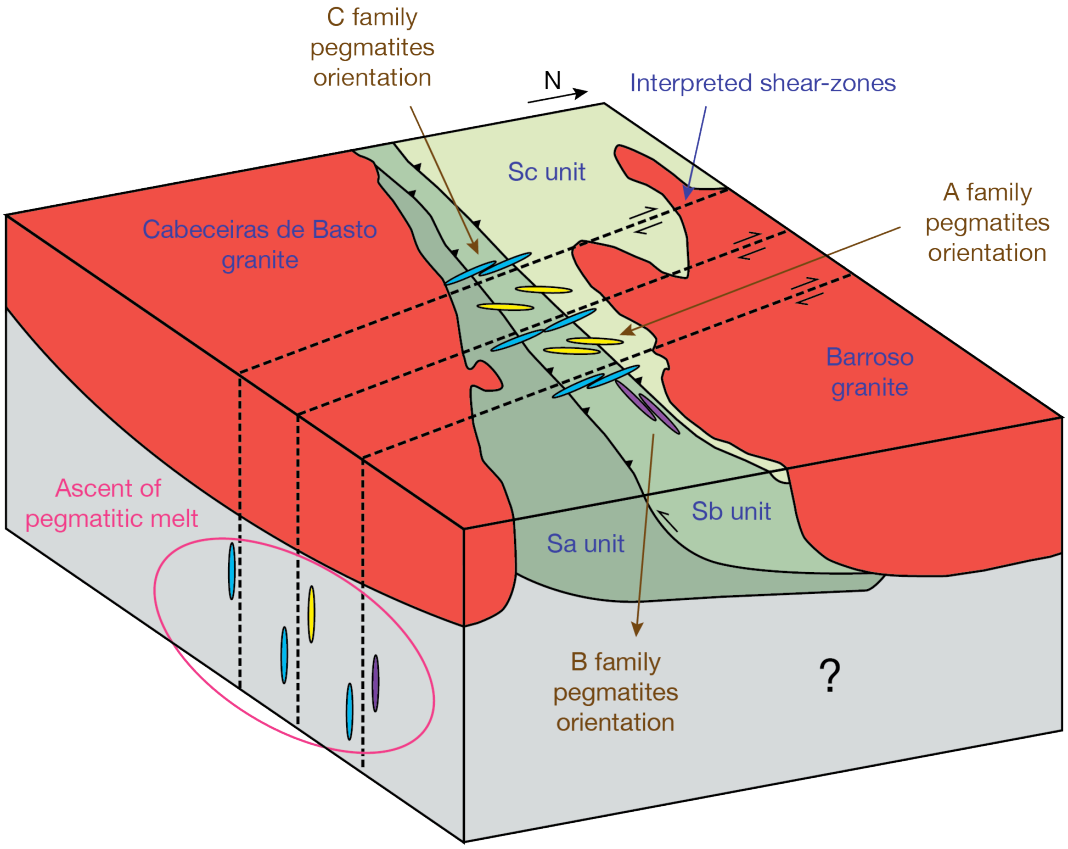

Fig. 44 Simple emplacement model for the pegmatites in the Barroso-Alvão aplitopegmatitic field.

Analyzed all the results, we contend that the mineralized pegmatites are emplaced preferentially within upper metasedimentar structural levels (Sb and Sc units), closer to the Barroso granite but at distance higher than 600 m from this granite, and spatially close to the interpreted shear-zones oriented from ~NW-SE to ~NNW-SSE acquired using satellite imagery. We propose that this results provides a practical and accurate prospection model for the mineralized pegmatite within the Barroso-Alvão pegmatite field.

Future studies focusing the Barroso-Alvão pegmatitic field are needed to better understand some properties of the pegmatites emplacement within the metasedimentary units. One of these possible studies involves the study of the structural emplacement of barren and Li-enriched pegmatites in the proposed shear-zones corridors. Geophysical methods can be applied to understand the continuity of the granites and the metasedimentary units in depth or evidence a possible parental granite that not outcrop. More detailed whole rock geochemistry and mineral geochemistry can also be applied to better define the spatial heterogeneity of the Li-enriched pegmatites within the Barroso-Alvão pegmatitic field.

BIBLIOGRAPHY

BIBLIOGRAPHY

ALMEIDA, A., 1994. Geoquímica, petrogénese e potencialidades metalogénicas dos granitos peraluminosos de duas micas do complexo de Cabeceiras de Basto. (Geochemistry, petrogenesis and metalogenetic potential of the two-mica peraluminous Cabeceiras de Basto granitic complex) Unpublished Ph.D. thesis, Universidade do Porto, 305 p.

ALMEIDA, A., LETERRIER, J., NORONHA, F., BERTRAND, J. M., 1998. U-Pb zircon and monazite geochronology of the Hercynian two-mica granite composite pluton of Cabeceiras de Basto (Northern Portugal). Comptes Rendus de l´Académie des Sciences 326, 779-785.

ARAÚJO, M.N.C., ALVES DA SILVA, F.C., JARDIM DE SÁ, E.F., 2001. Pegmatite emplacement in the Seridó belt, Northeastern Brazil: Late stage kinematics of the Brasiliano orogen. Gondwana Research 4, 75-85.

BAKER, D.R., 1998. The escape of pegmatite dikes from granitic plutons: constraints from new models of viscosity and dike propagation. Canadian Mineralogist 36, 255–263.

BERMAN, M., 1977. Distance distributions associated with Poisson processes of geometric figures. Journal of Applied Probability 14, 195–199.

BERMAN, M., 1986. Testing for spatial association between a point processes and another stochastic process. Applied Statistics 35, 54–62.

BESAG, J., 1977. Comments on Ripley's paper. Journal of the Royal Statistical Society, Series B 39, 193-195.

BLEACHER, J.E., GLAZE, L.S., GREELEY, R., HAUBER, E., BALOGA, S.M., SAKIMOTO, S.E.H., WILLIAMS, D.A., GLOTCH, T.D., 2009. Spatial and alignment analyses for a field of small volcanic vents south of Pavonis Mons and implication for the Tharsis Province, Mars. Journal of Volcanology and Geothermal Research 185, 96-102.

BONHAM-CARTER, G.F., 1994. Geographic Information Systems for Geoscientists: Modelling with GIS. Pergamon, Ontario. 398 p.

BONHAM-CARTER, G.F., AGTERBERG, F.P., 1990. Application of a microcomputer-based geographic information system to mineral potential mapping. In: Hanley, T., Merriam, D.F. (Eds), Microcomputer Application in Geology, vol. 2. Pergamon Press, Oxford, 49-74.

BRISBIN, W.C., 1986. Mechanics of pegmatite intrusion. American Mineralogist 71, 644-651.

BRITISH GEOLOGICAL SURVEY, 2011. Niobium-Tantalum. British Geological Survey, Commodity Profiles, April 2011.

BRONGNIART, A., 1813. Essai d'une classification minéralogique des roches mélangées. (Essay of a mineralogical classification for mixed rocks) Journal des Mines 34, 32

BUDDINGTON, A.F., 1959. Granite emplacement with special reference to North America. Geological Society of America bulletin 70, 671-747

CAMERON, E.N., JAHNS, R.H., MCNAIR, A.H., PAGE, L.R., 1949. Internal structure of granitic pegmatites. Economic Geology Monograph 2, 115.

CARRANZA, E.J.M., 2009a. Controls on mineral deposit occurrence inferred from analysis of their spatial pattern and spatial association with geological features. Ore Geology Reviews 35, 383-400.

CARRANZA, E.J.M., 2009b, Geochemical Anomaly and Mineral Prospectivity Mapping in GIS. Handbook of Exploration and Environmental Geochemistry, vol. 11. Elsevier, Amsterdam. 351p.

CARRANZA, E.J.M., 2011. Geocomputation of mineral exploration targets. Computer & Geoscience 37, 1907-1916.

CARRANZA, E.J.M., WIBOWO, H., BARRITT, S.D., SUMINTADIREJA, P., 2008. Spatial data analysis and integration for regional-scale geothermal potential mapping, West Java, Indonesia. Geothermics 33, 267-299.

CASSARD, D., BILLA. M., LAMBERT, A., PICOT, J.-C., HUSSON, Y., LASSERRE, J.-L., DELOR, C., 2008. Gold predictivity mapping in French Guiana using an expert-guided data-driven approach based on a regional-scale GIS. Ore Geology Reviews 34, 471-500.

ČERNÝ, P., 1989. Exploration strategy and methods for pegmatite deposits of tantalum. In: Lanthanides, Tantalum and Niobium (P. Moller, P Černý & F. Saupe, eds). Springer-Verlag, Berlin, 274-302.

ČERNÝ, P., 1991. Rare-element granitic pegmatites. Part 1: Anatomy and internal evolution of pegmatite deposits. Part 2: Regional to global environments and petrogenesis. Ore deposits models, Volume II (P.A. Sheahan & M.E. Cherry, eds.) Geoscience Canada, Reprint Series 6, 29-62.

ČERNÝ, P., BLEVIN, P.L., CUNEY, M., LONDON, D., 2005. Granite-related ore deposits. Economic Geology 100th Anniversary Volume, 337-370.

ČERNÝ, P., BRISBIN, W.C., 1982. The Osis Lake pegmatitic granite, Winnipeg River District, southeastern Manitoba. In: Cerný, P. (Ed.), Granitic Pegmatites in Science and Industry. Short Course Handbook 8. Mineralogical Association of Canada, 545-555.

ČERNÝ, P., ERCIT, T.S., 2005. The classification of granitic pegmatites revisited. Canadian Mineralogist 43, 2005-2026.

CHAPPEL, B.W., WHITE, A.J.R., 1974. Two contrasting granite types. Pacific Geology 8, 173-174.

CHAROY, B., LOTHE, F., DUSAUSOY, Y., NORONHA, F., 1992. The crystal chemistry of spodumene in some granitic aplite-pegmatite from Northern Portugal. Canadian Mineralogist 30, 639-651.

CHAROY, B., NORONHA, F., LIMA, A., 2001. Spodumene-Petalite-Eucryptite: mutual relationships and alteration style in pegmatite-aplite dykes from Northern Portugal. Canadian Mineralogist 39, 729-746.

CLARK, J.O.E., STEIGELER, S., 2000. The Facts on File Dictionary of Earth Science. Checkmark Books, New York, N.Y. 240p

CLARK, P.J., EVANS, F. C., 1954. Distance to nearest neighbor as a measure of spatial relationship in population. Ecology 35, 445-453.

CORSINI, A., CERVI, F., RONCHETTI, F., 2009. Weight of evidence and artificial neural networks for potential groundwater spring mapping: an application to the Mt. Modino area (northern Apennines, Italy) Geomorphology 111, 79-87.

CRITICAL RAW MATERIALS FOR THE EU, 2010. Report of the Ad-hoc Working Group on defining critical raw materials for the EU. RMSG, DGEI, EC.

DEMARTIS, M., PINOTTI, L.P., CONIGLIO, J.E., D'ERAMO, F.J., TUBIA, J.M., ARAGON, E., AGUILLEIRO INSUA, L.A., 2011. Ascent and emplacement of pegmatitic melts in a major reverse shear zone (Sierra de Cordoba, Argentina). Journal of Structural Geology 33, 1334-1346.

DEVEAUD, S., GUMIAUX, C., GLOAGUEN, E., BRANQUET, Y., 2013. Spatial statistical analysis applied to rare-element LCT-type pegmatite fields: an original to constrain faults-pegmatites-granites relationships. Journal of Geosciences 58, 163-182.

DIAS, G., LETERRIER, J., MENDES, A., SIMÕES, P., BERTRAND, J., 1998. U-PB zircon and monazite geochronology of post-collisional Hercynian granitoids from the Central Iberian Zone (Northern Portugal). Lithos 45, 349-369.

DIAS, R., RIBEIRO, A., 1995. The Ibero-Armorican Arc: A collision effect against an irregular continent? Tectonophysics 246, 113-128.

DIRECÇÃO GERAL ENERGIA E GEOLOGIA, 2014. *Estatística de recursos geológicos* (Statistic of geological resource) [Online]. Direcção Geral de Energia e Geologia. Available: www.dgeg.pt [Accessed April 2014].

DIXON, P.M., 2002. Riley's K function. In: El-Shaarawi, A.H., Piergorsch, W.W., Encyclopedia of Environmetrics.John Wiley & Sons, 1796-1803.

DRAJEM, M., HAMILTON, J., KAVANAGH, M.J., 2011. *A rule aimed at warlords upends African mines* [Online]. Bloomberg Businessweek Magazine. Available: www.businessweek.com [Accessed April 2014].

DUNCAN, R.P., 1993. Testing for life historical changes in spatial patterns of four tropical tree species in Westland, New Zealand. Journal of Ecology 81, 403-416.

FARINHA RAMOS, M., 2000. Prefácio. Estudos, notas e trabalhos. (Preface. Studies, notes and works) Instituto Geológico e Mineiro 42, 1-3.

FELTRIN, L., 2008. Predictive modeling of prospectivity for Pb-Zn deposits in the Lawn Hill Region, Queensland, Australia. Ore Geology Reviews 34, 399-427.

FERREIRA, N., IGLESIAS, M., NORONHA, F., PEREIRA, E., RIBEIRO, A., & RIBEIRO, M.L., 1987. Granitoides da Zona Centro Ibérica e o seu enquadramento geodinâmico. (Granitoids from the Central Iberian Zone and their geodynamical setting) In: Geologia de los Granitoides y Rocas Asociadas del Macizo (Bea F. et al., eds.). Libro Homenage a L.C. Garcia de Figuerola, 37- 51.

FRY, N., 1979. Random point distribution and strain measurement in rocks. Tectonophysics 60, 89-105.

GINSBURG, A.I., TIMOFEYEV, L.N., FELDMAN, L.G., 1979. Principles of geology of the granitic pegmatites. (in Russian) Nedra, Moscow.

GLOVER, A.S., ROGERS, W.Z., BARTON, J.E., 2012. Granitic pegmatites: storehouses of industrial minerals. Elements 8, 269–273.

GRANITIC PEGMATITES: THE STATE OF THE ART — FIELD TRIP GUIDEBOOK, 2007. Memórias Nº 9, Universidade do Porto, Faculdade de Ciências, Departamento de Geologia.

GUMIAUX, C., GAPAIS, D., BRUN, J.P., 2003, Geostatistics applied to best-fit interpolation of orientation data. Tectonophysics 376, 241–259.

HAASE, P., 1995. Spatial pattern analysis in ecology based on Ripley's *K*-function: Introduction and methods of edge correction. Journal of Vegetation Science 6, 575-582.

HEINRICH, E.W., 1953. Zoning in Pegmatite districts. American Mineralogist 38, 68-87.

HENDERSON, I.H.C., IHLEN, P.M., 2004. Emplacement of polygeneration pegmatites in relation to Sveco-Norwegian contractional tectonics: examples from southern Norway. Precambrian Research 133, 207-222.

IGLÉSIAS, M., RIBEIRO, M., RIBEIRO, A., 1983. La interpretacion aloctonista de la estrutura del Noroeste Peninsular. (Allochtonism interpretation of the northeastern Peninsular structure). Geol. Esp. Inst. Geol. Min 1, 459-467.

JACKSON, J.A., 1997. Gossary of Geology. 4t› Ed. American Geological Institute, Alexandria, Virginia. 472p

JAHNS, R.H., BURNHAM, C.W., 1969. Experimental studies of pegmatite genesis: I. A model for the derivation and crystallization of granitic pegmatites. Economic Geology 64, 843–864.

JULIVERT, M.; FONTBOTE, J.M.; RIBEIRO, A., CONDE, L.E., 1974. Mapa tectónico de la Península Ibérica Y Baleares E1: 1.000.000. Memoria explicativa. Publicación I.G.M.E. 101 p.

KESLER, S., GRUBER, P., MEDINA, P., KEOLEIAN, G., EVERSON, M., WALLINGTON, T., 2012 Global lithium resources: Relative importance of pegmatite, brine and other deposits. Ore Geology Reviews 48, 55–69.

KISKOWSKI, M.A., HANCOCK, J.F., KENWORTHY, A.K., 2009. On the use of Ripley´s K-function and its derivatives to analyze domain size. Biophysical Journal 97, 1095-1103.

KNOX-ROBINSON, C.M., GROVES, D.I., 1997. Gold prospectivity mapping using a Geographical Information System (GIS) with examples from Yilgrarn Block of Western Austalia. Chronique de la Recherche Minière 529, 127-138.

KNUDBY, A., LEDREW, E., BRENNING, A., 2010. Predictive mapping of reef fish species richness, diversity and biomass in Zanzibar using IKONOS imagery and machine-learning techniques. Remote Sensing of Environment 114, 1230-1241.

LANDES, K.K., 1933. Origin and classification of pegmatites. American Mineralogist 18, 33–56.

LIMA, A., 2000. Estrutura, mineralogia e génese dos filões aplitopegmatíticos com espodumena na região do Barroso-Alvão (Norte de Portugal). (Structure, mineralogy and genesis of the spodumene-rich aplite pegmatite bodies from Barroso-Alvão - Northern Portugal) Unpublished Ph.D. thesis, Universidade do Porto, 270 p.

LIMA, A., VIEIRA R., MARTINS, T., NORONHA, F., 2011. As fontes de lítio em Portugal. (Lithium sources in Portugal) Revista Portugal mineral. Edição especial indústria extractiva 3, 60-63.

LIMA, A., VIEIRA, R., MARTINS, T. C., NORONHA, F., CHAROY, B., 2003b. A ocorrência de petalite como fase litinífera dominante em numerosos filões do campo aplitopegmatítico do Barroso-Alvão (Norte de Portugal). (Petalite occurrence as a dominant lithium phase in numerous pegmatite bodies from the Barroso-Alvão pegmatite field - Northern Portugal) VI Congresso Nacional de Geologia. Costa da Caparica. Almada, CD-ROM, p. P 52-55.

LIMA, A., VIEIRA, R., MARTINS, T., FARINHA, J.A., NORONHA, F., CHAROY, B., 2003c. Os filões aplitopegmatíticos litiníferos da região Barroso-Alvão (Norte de Portugal). (Lithium-rich aplite pegmatite bodies from Barroso- Alvão region) Memórias e Notícias, nº 2 (Nova Série) Publi. Do Dep. Ciên. Terra do Mus. Mineral. Geol., Univ. Coimbra, 169-190.

LIMA, A., VIEIRA, R., MARTINS, T., NORONHA, F., CHAROY, B. 2003a. A ocorrência de petalite como fase litinífera dominante em numerosos filões do campo aplitopegmatítico do Barroso-Alvão (N. de Portugal). (Petalite occurrence as a dominant lithium phase in numerous pegmatite bodies from the Barroso-Alvão pegmatite field - Northern Portugal) CD-Rom Vol. Esp. V, P 52-55; VI CNG, Almada, Portugal.

LINDGREN, W., 1913. Mineral Deposits. Publisher unknown, New York, N.Y. 957 p.

LINNEN, R.L., VAN LICHTERVELDE, M., ČERNÝ, P., 2012. Granitic pegmatites as sources of strategic metals. Elements 8, 275–280.

LONDON, D., 1984. Experimental phase equilibria in the system LiAlSiO4–SiO2-H2O: a petrogenetic grid for lithium-rich pegmatites. American Mineralogist 69, 995–1004.

LONDON, D., 1986a. The magmatic–hydrothermal transition in the Tanco rare-element pegmatite: evidence from fluid inclusions and phase equilibrium experiments. American Mineralogist 71, 376–395.

LONDON, D., 1986b. Formation of tourmaline-rich gem pockets in miarolitic pegmatites. American Mineralogist 71, 396–405.

LONDON, D., 1998. Phosphorus-rich peraluminous granites. *Acta Universitatis Carolinae - Geologica,* 42 (1), 64-68.

LONDON, D., 2008. Pegmatites. Canadian Mineralogist, Special Publication 10, 347 p.

LONDON, D., 2013. Crystal-filled cavities in granitic pegmatites: bursting the bubble. Rocks and Minerals 88, 527–534

LONDON, D., 2014. A petrologic assessment of internal zonation in granitic pegmatites. Lithos 184–187, 74–104.

MARTIN, R.F., DE VITO, C., 2005. The patterns of enrichment in felsic pegmatites ultimately depend on tectonic setting. Canadian Mineralogist 43, 2027-2048.

MARTINS, H., 1998. Geoquímica e Petrogénese de Granitóides Biotíticos Tarditectónicos e Pós-téctonicos. Implicações metalogenéticas. (Geochemistry and petrogenesis of tardi-tectonic and post-tectonic biotite granitoids. Metalogenetic implication). Ph. D. thesis. University of Trás-os-Montes e Alto Douro, Vila Real, Portugal. 288 p.

MARTINS, H., SANT'OVAIA, H., NORONHA, F., 2009. Genesis and emplacement of felsic Variscan plutons within a deep crustal lineation, the Penacova-Régua-Verín fault: An integrated geophysics and geochemical study (NW Iberian Peninsula). Lithos 111, 142-155.

MARTINS, H., SANT'OVAIA, H., NORONHA, F., 2013. Late-Variscan emplacement and genesis of the Vieira do Minho composite pluton, Central Iberian Zone: Constraints from U–Pb zircon geochronology, AMS data and Sr–Nd–O isotope geochemistry. Lithos 162-163, 221-235.

MARTINS, J.A., NORONHA, F., 1982. Carta geológica de Portugal, escala 1:50000, 6-A (Montalegre) (Geological map of Portugal, scale 1:50000, 6-A - Montalegre) Instituto Geológico e Mineiro.

MARTINS, T., 2009. Multidisciplinary study of pegmatites and associated Li and Sn-Nb-Ta mineralisation from the Barroso-Alvão region. Unpublished Ph.D. thesis, Universidade do Porto, Portugal. 196 p.

MARTINS, T., LIMA, A., SIMMONS, W.B., FALSTER, A.U., NORONHA, F., 2011. Geochemical fractionation of Nb-Ta oxides in Li-bearing pegmatites from the Barroso-Alvão pegmatite field, Northern Portugal. Canadian Mineralogist 49, 777-791.

MARTINS, T., RODA-ROBLES, E., LIMA, A., PARSEVAL, P., 2012. Geochemistry and evolution of micas in the Barroso-Alvão pegmatite field, Northern Portugal. Canadian Mineralogist 50, 1117-1129.

MATHERON, G., 1962. Traité de Geostatistique Appliquée. (Treaty of Applied Geostatistics) Mémoire du Bureau de Recherche Géologique et Minières 24, 333p.

MIYASHIRO, A., 1961. Evolution of metamorphic belts. Journal of Petrology 2, 277-311.

NASA Landsat Program, 2000. Landsat ETM + scene P204R031_7K20000624, Ortho/GeoCover, EarthSat, Portugal/Spain, 24/06/2000.

NORONHA, F., 1983. Estudo metalogénico da área tungstífera da Borralha. (Metalogenetic study of the Borralha tungstiferous area) Unpublished Ph.D. thesis, Universidade do Porto, 413 p.

NORONHA, F., 1987. Nota sobre a ocorrência de filões com espodumena na folha de Dornelas. (Occurrence of pegmatite bodies with spodumene in the Dornelas geological map) Portuguese Geological Survey Internal report.

NORONHA, F., 1992. Carta geológica de Portugal, escala 1:50000, 6-C (Cabeceiras de Basto) (Geological map of Portugal, scale 1:50000, 6-C - Cabeceiras de Basto) Instituto Geológico e Mineiro.

NORONHA, F., RAMOS, J.M.F., REBELO, J., RIBEIRO, A., RIBEIRO, M.L., 1981. Essai de corrélation des phases de déformation hercyniennes dans le NW de la P.I.. (Correlation essay of the Hercynian deformation phases in the NW of Iberian Peninsula) Leid. Geol. Meded. 52 (1), 87-91.

NORONHA, F., RIBEIRO, M.A., ALMEIDA, A., DÓRIA, A., GUEDES, A., LIMA, A., MARTINS, H.C., SANT'OVAIA, H., NOGUEIRA, P., MARTINS, T., RAMOS, R., VIEIRA, R., 2013. Jazigos filonianos hidrotermais e aplitopegmatíticos espacialmente associados a granitos (Norte de Portugal). (Hydrothermal and aplitopegmatitic lodes spatially associated with granites) In: R.Dias, A. Araújo, P. Terrinha, J.C. Kullberg (Eds). Geologia de Portugal, Vol 1, Escolar Editora, 403-438.

NORONHA, F., RIBEIRO, M.A., MARTINS, H.C., LIMA, J., 1998. Carta geológica de Portugal, escala 1:50000, 6-D (Vila Pouca de Aguiar) (Geological map of Portugal, scale 1:50000, 6-D - Vila Pouca de Aguiar) Instituto Geológico e Mineiro.

NORONHA, F., RIBEIRO, M.L., 1983. Notícia explicativa da Carta geológica de Portugal na escala 1:50000. Folha 6A - Montalegre. (Explanatory notice of the geological map of Portugal, scale 1:50000, 6-A - Montalegre) Instituto Geológico e Mineiro, Lisboa, 30p.

NORTON, J.J., REDDEN, J.A., 1990. Relations of zoned pegmatites to other pegmatites, granite, and metamorphic rocks, in the southern Black Hills, South Dakota. American Mineralogist 75, 631-655.

PARTINGTON, G.A., 1990. Environment and structural controls on the intrusion of the giant rare metal greenbushes pegmatite, Western Australia. Economic Geology 85, 437-456.

PATTISON, D., 2001. Instability of Al_2SiO_5 "triple-point" assemblages in muscovite + biotite + quartz-bearing metapelites, with implications. American Mineralogist 86, 1414–1422.

PEREIRA, E., RIBEIRO, A., MARQUES, F., MUNHÁ, J., CASTRO, P., MEIRELES, C., RIBEIRO, M.A., PEREIRA, D., NORONHA, F., FERREIRA, N., 2001. Carta geológica de Portugal, escala 1:200000, folha nº2 (Geological map of Portugal, scale 1:200000, sheet nº2) Instituto Geológico e Mineiro.

PEREIRA, E., RIBEIRO, A., MEIRELES, C., 1993. Variscan shear zones and control of Sn-W, Au, U mineralizations in the Central-Iberian Zone in Portugal. Cuaderno Lab. Xeolóxico de Laxe 8, 89-119 (in Portuguese).

PORWAL, A.K., KREUZER, O.P., 2010. Introduction to the special issue: mineral prospectivity analysis and quantitative resource estimation. Ore Geology Reviews 38, 121-127.

PRIEM, H., DEN TEX, E., 1984. Tracing crustal evolution in the NW Iberian Peninsula through the Rb-Sr and U-Pb systematics of Palaeozoic granitoids: a review. Physics of the Earth and Planetary Interiors 35, 121-130

PROSPEG PROJECT - PEGMATITES REMOTE SENSING AND MAPPING. FINAL REPORT, 2013. Sinergeo, Lda. and Universidade do Minho.

RAMOS, R., 2012. Condicionamento tectono-estratigráficos e litogeoquímicos da evolução metamórfica Varisca, nas unidades parautóctones (Trás-os-Montes Ocidental). (Conditioning of the tectonostratigraphic and lithogeochemical Variscan metamorphic evolution in the parauthoctonous units - Occidental Trás-os-Montes) Unpublished Ph.D. thesis, Universidade do Porto, 168p

RIBEIRO, A., 1974. Contribution à l'étude tectonique de Trás-os-Montes Oriental. (Contribution for the tectonic studies of Oriental Trás-os-Montes). Memória dos Serviços Geológicos de Portugal 24, 168p.

RIBEIRO, A., 2013. Evolução geodinâmica de Portugal: os ciclos ante-mesozóicos. (Geodynamic evolution of Portugal: pre-Mesozoic cycles) In: R.Dias, A. Araújo, P. Terrinha, J.C. Kullberg (Eds). Geologia de Portugal, Vol 1, Escolar Editora, 15-57.

RIBEIRO, M.A., 1998. Estudo litogeoquímico das formações metassedimentares encaixantes de mineralizações em Trás-os-Montes Ocidental. Implicações metalogénicas. (Lithogeochemical study of the metasedimentary country rock hosting mineralization in Occidental Trás-os-Montes. Metalogenetic implication.) Ph. D. thesis. University of Porto, Portugal, 231 p.

RIBEIRO, M.A., 2000. Metamorfismo orogénico de sequências pelíticas: o exemplo da região de Vila Pouca de Aguiar. (Orogenic metamorphism of pelitic sequences: example of the Vila Pouca de Aguiar region) Geonovas 14, 21-26.

RIBEIRO, M.A., MARTINS, H.C., ALMEIDA, A., NORONHA, F., 2000. Carta geológica de Portugal, escala 1:50000, 6-C (Cabeceiras de Basto). (Geological map of Portugal, scale 1:50000, 6-C - Cabeceiras de Basto) Notícia Explicativa, Serviços Geológicos de Portugal. 48 p.

RIBEIRO, M.A., NORONHA, F., CUNEY, M., 2003. Importância do estudo litogeoquímico na caracterização das unidades tectono-estratigráficas do parautóctone da zona Galiza-Média.Trás-os-Montes. (Importance of the lithogeochemical study in the characterization of the parauthoctonous tectonostratigraphic units in Galiza-Média-Trás-os-Montes zone) Ciências da Terra (UNL), Lisboa, no esp. V, CD-ROM, B 89-B92.

RIBEIRO, M.A., RAMOS, R., NORONHA, F., 2007. Pegmatite-aplite veins of Barroso-Alvão field. Lithostratigraphy and metamorphism of host rocks. In: Granitic Pegmatites: the state of the art (A. Lima and E. Roda-Robles eds.), Fieldtrip guidebook, Memórias 9, 39-45.

RIEDEL, W., 1929. Zur Mechanik Geologischer Brucherscheinungen. (Geological mechanics of fracture phenomena). Zentralblatt für Mineralogie, Geologie und Paleontologie B, 354–368

RIPLEY, B.D., 1977. Modelling spatial patterns. Journal of the Royal Statistical Society, Series B 39, 172-192.

RODA-ROBLES, E., PESQUERA, A., GIL, P.P., TORRES-RUIZ, J., FONTAN, F., 2004. Tourmaline from the rare-element Pinilla pegmatite, (Central Iberian Zone, Zamora, Spain): chemical variation and implications for pegmatitic evolution. Mineralogy and Petrology 81, 249–263.

RODA, E., PESQUERA, A., VELASCO, F., FONTAN, F., 1999. The granitic pegmatites of the Fregeneda area (Salamanca, Spain): characteristics and petrogenesis. Mineralogical Magazine 63, 535-556.

RODRIGUES, J., COKE, C., DIAS, R., PEREIRA, E., RIBEIRO, A., 2005. Transition from autochthonous to parautochthonous deformation regimes in Murça-Marão sector (Central-Iberian Zone, northern Portugal). In: (eds.) Carosi, R., Dias, R., Iacopini, D., and Rosenbaum, G., The southern Variscan belt, Journal of the Virtual Explorer, Electronic Edition, ISSN 1441-8142, Volume 19, Paper 8.

ROZAS, V., ZAS, R., SOLLA, A., 2009. Spatial structure of deciduous forest stands with contrasting human influence in northwest Spain. European Journal of Forest Research 128, 273-285.

SANT'OVAIA, H., BOUCHEZ, J., NORONHA, F., LEBLANC, D., VIGNERESSE, J.L., 2000. Composite-laccolith emplacement of the post-tectonic Vila Pouca de Aguiar granite pluton (northern Portugal): a combined AMS and gravity study. Transactions of the Royal Society of Edinburgh: Earth Sciences 91,123-137.

SIMMONS W.B., FOORD, E.E., FALSTER, A.U., KING, V.T., 1995. Evidence for an anatectic origin of granitic pegmatites, western Maine, USA. Geological Society of America Annual Meeting, New Orleans, LA, Abstr. Prog. 27, A411.

SIMMONS, W.B., 2005. A look at pegmatite classifications. Crystallization Processes in Granitic Pegmatites - International Meeting Abstracts - 23rd-29th May 2005, Elba Island, Italy, Museo di Storia Naturale, Milan, Italy.

SIMMONS, W.B., WEBBER, K.L., 2008. Pegmatite genesis: state of the art. European Journal of Mineralogy 20 (4), 421-438.

STEWART, D.B., 1978. Petrogenesis of lithium-rich pegmatites. American Mineralogist 63, 970- 980.

STOYAN, D., AND PENTTINEN, A., 2000. Recent applications of point process methods in forestry statistics. Statistical Science 15, 61-78.

TEIXEIRA, C., MEDEIROS, A.C. 1969. Carta geológica de Portugal, escala 1:50000, 6-B (Chaves) (Geological map of Portugal, scale 1:50000, 6-B - Chaves) Instituto Geológico e Mineiro.

THIART, C., DE WIT, M., 2000. Linking spatial statistic to GIS: exploring potential gold and tin models of Africa. South African Journal of Geology 103, 215-230.

TRUEMAN, D.L., ČERNÝ, P., 1982. Exploration for rare-element granitic pegmatites in Granitic Pegmatites in Science and Industry. (P. Černý eds.) Mineralogical Association of Canada, Short Course Handbook 8, 463-494.

USGS/GLCF, 2000. Shuttle Radar Topography Mission, 3 Arc Second scene ID 159-595 Portugal/Spain, Filled Finished—A, Global Land Cover Facility, University of Maryland, Maryland, February 2000.

VAILLANT, M., JOUANY, J.M., DEVILLERS, J., 1995. A multicriteria estimation of the environmental risk of chemicals with the SIRIS method. Toxicol. Model. 1, 57-72.

VEARNCOMBE, J., VEARNCOMBE, S., 1999. The spatial distribution of mineralization: Applications of Fry analysis. Economic Geology 94, 475-486.

VEEN, A., SCHOENBERG, F.P., 2006. Assessing spatial point process models using weighted *K*-functions: Analysis of California earthquakes. Case Studies in Spatial Point Process Modeling, Lecture Notes in Statistics 185, 293-306.

VIEIRA, R., 2010. Rare-elements aplopegmatites from Almendra (V.N. de Foz-Côa) and Barca d'Alva (Figueira Castelo Rodrigo) regions. Aplitopegmatitic field of Fregeneda-Almendra. Unpublished Ph.D. thesis, Universidade do Porto, 274p

VLASOV, K.A., 1961. Principles of classifying granite pegmatites and their textural–paragenetic types. Transactions of the Academy of Sciences, U.S.S.R., Geologic Series 1, 5–20.

WILKINS, D.E., FORD, R.L., 2007. Nearest neighbor methods applied to dune field organization: the Coral Pink Sand Dune, Kane County, Utah, USA. Geomorphology 93, 48-57.

ZHAO, J., CHEN, S., ZUO, R., CARRANZA, E.J.M., 2011. Mapping complexity of spatial distribution of faults using fractal and multifractal models: vectoring towards exploration targets. Computers & Geosciences 37, 1958-1966.

ANNEXES

ANNEX 1

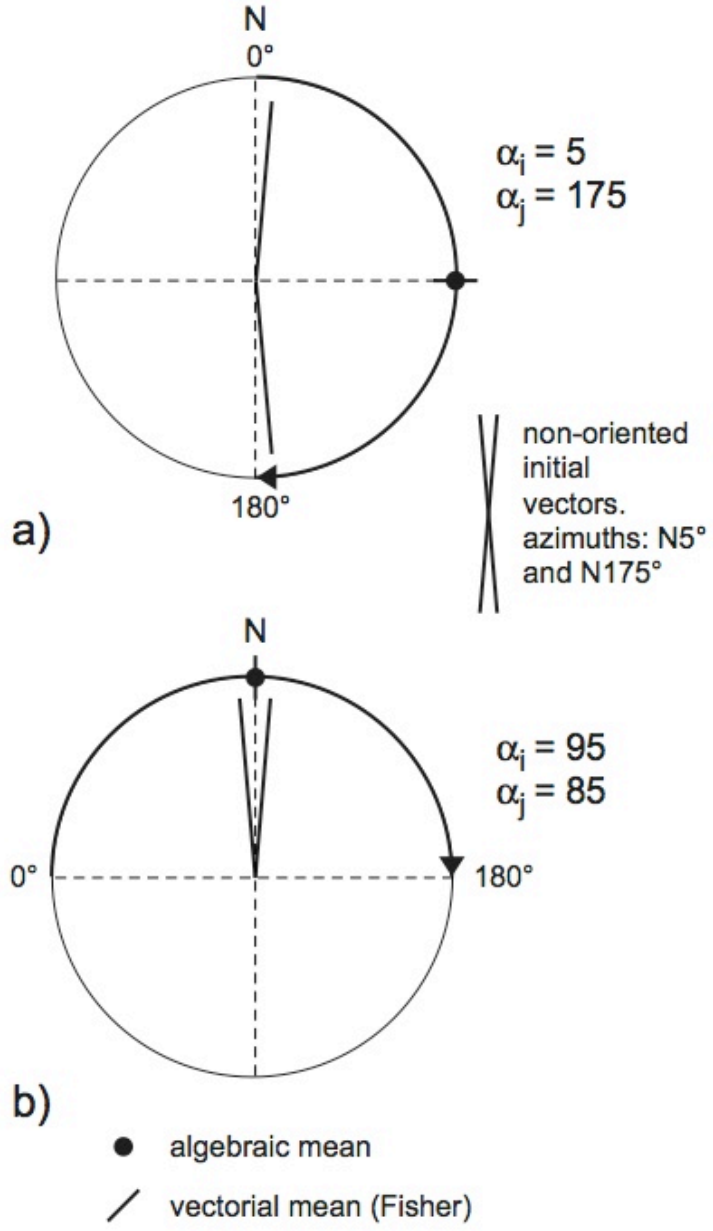

Illustration of problems attached to the calculation of mean values from circular angular data (From Gumiaux *et al.*, 2003).

ANNEX 2

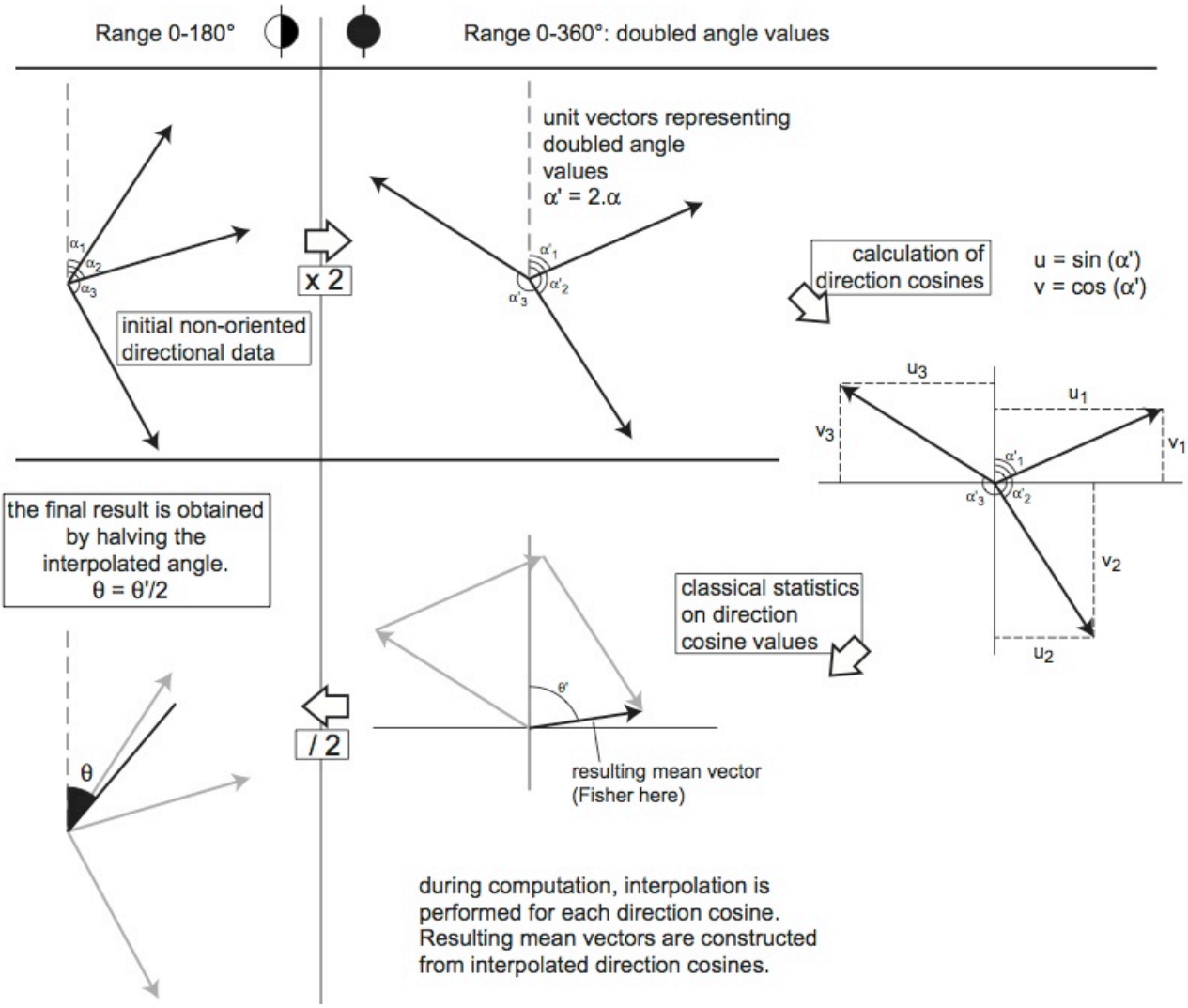

Illustration of the different steps followed during processing and interpolation of directional data (From Gumiaux *et al.*, 2003).

ANNEX 3

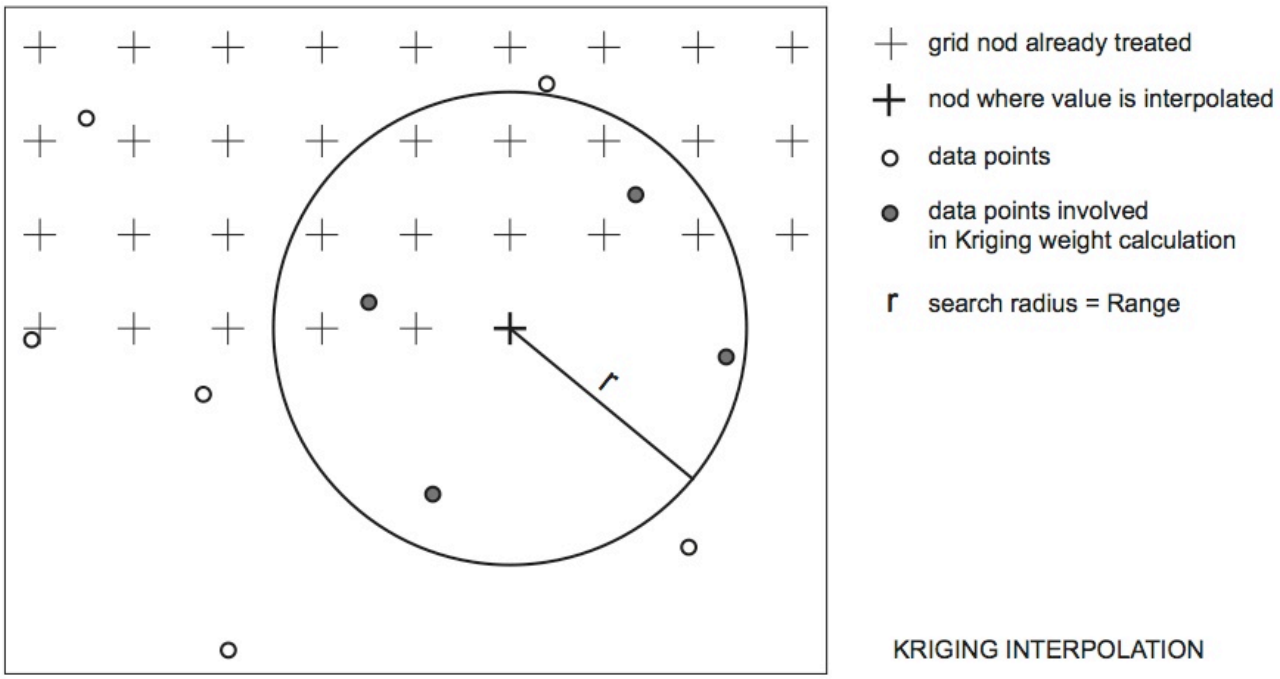

Illustration of data interpolation along a regular grid. For a given nod of the grid (thick cross), a circular neighbourhood is given around this point. The radius of the circle is defined by the range deduced from the variogram analysis. All data values located in the circle (black points) are implied in the calculation of the interpolated value attached to the given nod (From Gumiaux *et al.,* 2003).